UNIVERSITY OF CALIFORNIA,
IRVINE

Investigating Unusual Reduction Methods for the Generation of Low Oxidation State Rare-Earth Organometallic Complexes

DISSERTATION

submitted in partial satisfaction of the requirements
for the degree of

DOCTOR OF PHILOSOPHY

in Chemistry

by

William Nicholas Graham Moore

Dissertation Committee:
Distinguished Professor Emeritus William J. Evans, Chair
Professor Alan F. Heyduk
Distinguished Professor A. S. Borovik

2023

Dedication

To

My parents, Kent and Jana, my brother, Andrew, and my fiancée, DJ.

Thank you all for being a limitless source of love, peace, and friendship.

“Sometimes, the best way to solve your own problems is to help someone else.”

Uncle Iroh

Table of Contents

List of Figures

List of Tables

Acknowledgements

To Professor William J. Evans, thank you for accepting me into your group. Thank you for giving me consistent feedback through weekly individual meetings, group meetings, written draft edits, presentation practices, and emails at literally any time of the day or night. I became a better researcher, writer, chemist, presenter, conversationalist, and person because of that quantity and quality of feedback. Thank you for funding me and for funding the chemistry that I was lucky enough to get the chance to do. I do not take the grant money used for my salary and for purchasing lab equipment and chemicals lightly. Thank you for leading by example with your positive attitude, hard work, discipline, and willingness to talk about anything related to chemistry and beyond. That leadership was a major motivating factor when chemistry was not working or other distractions were present. Thank you for being understanding when life occasionally demanded my attention be shifted away from work. Your trust in me to get the work done before or after these times was tremendously empowering and remains an uncommon characteristic.

To Professor Alan F. Heyduk, thank you for chairing my candidacy exam, participating in my second year exam, and serving as one of my dissertation committee members. Your feedback has been helpful throughout this process. Thank you for teaching physical inorganic chemistry. I learned a lot in your class. Thank you as well for giving me constructive criticism when I needed it. You have a sharp eye for what makes high quality work and what qualifies as scientifically rigorous, and you are not afraid to give honest feedback in that arena, both positive and negative. Your comments have helped me to become a better scientist.

To Professor A. S. Borovik, thank you as well for participating in all three of my exams: second year exam, candidacy exam, and dissertation defense. Your feedback along the way has made me think about things on a deeper, more fundamental, level. Thank you for being an engaging speaker. I have learned to incorporate humor and involve my audiences better as a result of observing your presentation style. Thank you for connecting with me over shared experiences back at the University of Kansas (KU). Chatting

about KU hoops, football, early morning workouts at Memorial stadium, or even cheap golf spots around town always makes me smile.

To Professor James D. Blakemore, thank you for playing a big hand in my development as a scientist and for setting me up extremely well to succeed in graduate school. There is no doubt that I would not have been as successful in Bill's group (or possibly even gotten to graduate school at all) without your efforts to educate me (whether 1:1 during late night draft edits, as my professor during Inorganic Chemistry class, during group meetings, or showing me techniques in lab like spectroelectrochemistry). Thank you for working hard. I was motivated to work hard as well because of your work ethic. Thank you for getting excited about science. Your excitement is contagious! Thank you for devoting serious time to your undergraduate students, myself included. In particular, thank you for helping to get that *Molecules* manuscript ready for publication. I still remember the sense of pride and accomplishment I felt when I saw my work added to the literature for the first time.

To Wade Henke, Tyler Kerr, and Tener Jenkins, thank you all for being absolutely incredible mentors during different phases along my career as a chemist. Tyler, thank you for showing me how to use logic to design and run experiments. Some of the habits you taught me in that first week I spent with you still stick with me today. Wade, thank you for explaining complicated science, much of which I had zero knowledge of, in a way that I could grasp. Wade, thank you as well for teaching me how to execute a ton of synthetic techniques in a safe manner. Perhaps most importantly, thank you for being a quiet voice when the rest of the world likes to yell, and thank you for being an incredibly kind, relaxed human being. Your positive influence on me as a chemist, labmate, employee researcher, and mentor myself cannot be overstated. Tener, thank you similarly for your calm demeanor and enthusiasm for science in all of its aspects. Scientific conversations with you were some of the more enjoyable that I have had during graduate school. Also, thank you for your patience with me when I was chomping at the bit as a first year graduate student. You helped me to slow down just a little so as not to burn out.

To Emily Boyd, Zach Wood, Joseph Loomis, and Cara Loomis, thank you all for improving my academic performance at KU. Whenever I get asked the question about how I study best, I always give the

answer that I succeeded by studying with people smarter than me. Those people would be you. I feel extremely lucky that I got to be a part of a cohort with you all. I cannot wait to see what you all accomplish in the future, because I truly think there is no limit to what you all can achieve.

To Dr. Joseph W. Ziller, thank you for the work you put in to mount my early crystals and the work you put in to solve my structures and prepare the data for publication. The work you do is essential to not only my publications but most all other chemistry graduate students as well. Thank you for being a Bills fan. Someone's got to do it.

To Professor Filipp Furche, thank you for your willingness to take the time and help me conduct theoretical calculations correctly, particularly in regard to the thorium paper spearheaded by Joseph. Thank you for developing the software that allows these calculations to be done. I am not a computational chemist by training, but the program is quite intuitive as a result of your efforts and enjoyable to learn.

To my collaborators including Tro Babikian and John Keffer with the UCI Nuclear Reactor Facility, Alexandre Vincent in the Prof. Jeffrey Long group, TJ McSorley and Prof. Luis Jauregui in the UCI Physics Department, and Javier Fajardo Jr. and Prof. Harry Gray, thank you all for working with me at one time or another. Whether the projects were going well or not, you all supported me throughout the process. To anyone reading this, I highly recommend collaborating with these individuals if the opportunity ever arises. To Tro and John in specific, thank you very much for taking the time to help me irradiate my samples for relatively long periods of time and going the extra mile to fill the Dewar yourselves. It should also be noted that some of the text printed herein is drawn from several publications (DOI's: 10.1021/acs.organomet.1c00379, 10.1016/j.poly.2021.115493, 10.1021/acs.inorgchem.2c02857, 10.1021/acs.inorgchem.3c00689, and 10.1021/acsanm.3c00662) as is referenced in the text. Dr. Ming Fang is thanked for his contribution to the penultimate publication listed, and other coauthors mentioned throughout the text are also thanked for their individual contributions. We are grateful to the American Chemical Society and the Royal Society of Chemistry for their permission to include these works.

To my colleagues and friends over the years including Prof. Davide Lionetti, Dr. Keaton Prather, Dr. Amit Kumar, Ali Younis, and Griffin Barnes, I cannot thank you enough not only for your helpful

conversations, but your good friendship as well. Both contributions have played an equally important role in getting me to this point.

To the former Evans lab members I have gotten the chance to work with, including Dr. Austin J. Ryan, Dr. Tener F. Jenkins, Dr. Jessica R. White, Dr. Olaf Nachtigall, Michael Trinh, Dr. Justin C. Wedal, Dr. Amanda B. Chung, and Dr. Sierra R. Ciccone, thank you so much for passing along your expertise. Justin, thank you specifically for your guidance throughout the time we overlapped together. You taught me how to run calculations, how to run a gas reaction, how to take a lot of data and draw conclusions, and how to keep a level head. I am grateful for the influence you had on me.

To the current Evans lab members, including Dr. Cary R. Stennet, Dr. Joshua D. Queen, Lauren Anderson-Sanchez, Joseph Q. Nguyen, Kito Gilbert-Bass, Jonah P. Stiel, Gabriella (Gigi) Godinho, Brynn Turpin, and Allison K. Bernardo, thank you so, so much for making the lab an enjoyable place to work. I have always loved the chemistry that we do, but with this particular group I can also say that I love coming to work every day to spend time with you all. Cary, thank you for being the only other steadfast Taylor Swift megafan in the group. Hehe, in all reality, Cary, I could write a full essay on things that I am grateful to you for. Your "let's get it done… we can do anything" attitude, your lab work ethic, your vast chemistry knowledge, your direct communication, your consistency, and your ability to initiate and facilitate casual scientific or non-scientific conversation have all rubbed off on me. I am a better chemist and better person for having met you. Josh, thanks for your up front communication and for taking the metallocene project to heights I do not think I could have reached. Lauren, being able to bounce ideas back and forth and solve problems together over the last four years has been so much fun, and I want to thank you for being the one to make it fun. Your ability to make me laugh and stay positive has been a tremendous help to me throughout graduate school, and I would be a much less happy person without your presence. Joseph, thank you for your nonchalance and easy reliability. Your ability to relax and crack a broke whenever times were stressful helped me to relax as well, and for this I am incredibly grateful. Kito, thanks for accompanying me throughout ACS San Diego, and thank you as well for getting excited about science. There are a couple of people whose excitement is genuine and contagious, and you are one of them. Jonah, thank you for being

ambitious and working towards your goals. It is inspiring to see you work towards your objective of becoming a professor, and I wish you the best of luck in achieving that. Brynn, thanks for the advice on cat ownership and for being a fun presence whenever you come around the office. Gigi, thank you so much for asking the questions I never have the courage to ask. Also, thank you for laughing at my terrible jokes and generally being on the same page with me during random everyday arguments. Allison, thank you for bearing with my mentorship abilities (or lack thereof), for studying hard, and for being a quick learner. You have a massive amount of potential, and I cannot wait to see what you end up doing in the future.

To Dad, Mom, and Andrew, thank you all for supporting me throughout my life, but especially for your help and support over the last four years. Mom and Dad, all of the actions you took when raising me contributed to my natural intellect, which is a big reason why I have been successful in this PhD endeavor so far. Reading to me every day, encouraging me to go outside and play, talking me through the logic of how things work, showing me how to study effectively, how to write emails effectively, teaching me how to be polite and respectful of all… the list could go on. You deserve a large portion of the credit for this work (and hopefully this degree) simply for the outsized help you have given me throughout my life. Dad, thank you specifically for modeling well how to balance working for your employer and putting in work in your home life. Mom, thank you specifically for helping pick me up at my lowest points and showing enthusiasm and joy at my highest. Andrew, thank you for being my closest friend for a long, long time. Despite being younger than me, you are one of my role models. You are one of the most well-rounded and widely knowledgeable human beings I know despite your young age, and more importantly, you are incredibly kind, hard-working, disciplined, organized, and empathetic. You also deserve a large portion of the credit for this work, because I was succesful in part due to striving to meet the bar you have set.

To Donna Jean Vaughan, thank you for everything. I am more disciplined, more self-confident, harder-working overall, and more forthright since having met you, all of which have positively influenced my lab work. Thank you also for being a sounding board for me after long days, where I can decompress and share the good times and bad times unfiltered. You also deserve a large portion of the credit for this work.

Vita

Education

University of California, Irvine **October 2019 – August 2023**
Doctor of Philosophy in Chemistry (Graduation expected in Fall 2023)
- Advisor: William J. Evans

University of Kansas **August 2015 – June 2019**
Bachelor of Science in Chemistry
- Advisor: James D. Blakemore

Shawnee Mission East High School **August 2011 – May 2015**
High School Diploma
International Baccalaureate Diploma

Scholarships, Awards, and Certificates

2023 Graduate Dean's Dissertation Fellowship – *top 3 applicants in School of Physical Sciences nominated*
2022 Management Beyond the Classroom Certificate – *completed nine-session course on management*
2021 Inclusive Excellence Certificate – *completion of program on diversity, equity, and inclusion at UCI*
2019 Frank Newby Physical Science Award – *awarded to graduating seniors of exceptional merit*
2019 KU Center for Undergraduate Research Student Spotlight – *because research deemed of high-interest*
2018 Walter Gubar Scholarship – *awarded to a deserving chemistry student based on merit*
2018 Global Awareness Program Certificate – *awarded to students for local service and international study*
2017 Radioisotopes and Radiation Safety in Research Certificate – *lifetime certificate*
2017 Burton and Cherlye Mackenzie Scholarship – *awarded to undergraduate students with distinction*
2017 Research Experience Program Certificate – *given to those who demonstrate commitment to research*
2017 KU Undergraduate Research Award (2x) – *financial support for research via proposal competition*
2016 Owen W. Maloney Scholarship – *awarded to an outstanding freshman chemistry student*
2015 Chancellor's Scholarship – *distributed based on highest high school academic qualifications*

Volunteer and Extracurricular Activities

2023 Regional Science Olympiad Volunteer – *helped event run smoothly throughout the day*
2022 – 2023 Empowering Women through High School Engagement and STEM Research (EmpowHER) Mentor
2022 – 2023 Irvine Unified School District Science Fair Judge – *rated projects based on set criteria*
2022 – 2023 Laboratory Safety Representative – *liaison with EH&S and manage day-to-day lab safety*
2022 Discussion Leader – *facilitate ACS workshop: "The Graduate School Experience: What to Expect"*
2021 – 2022 Chemistry Teaching Assistant Mentor – *chosen to assist incoming cohort of graduate students*
2021 – 2022 Graduate Student Career Advisory Board – *involves advising Division of Career Pathways*
2020 – 2021 Graduate Safety Team Member – *chosen based on ability to guide safety protocol in department*
2018 Integrated Science Building Tour Guide – *involved showing prospective students chemistry facilities*
2018 KU Research Ambassador – *position given based on ability to encourage undergraduate research*

Publications

10. Nguyen, J. Q.; Moore, W. N. G.; Anderson-Sanchez, L. M.; Ziller, J. W. Furche, F.; Evans, W. J. Replacing Trimethylsilyl With Triisopropylsilyl Allows Isolation of Stable and Crystalline $(C_5H_4SiR_3)_3Th$ Complexes of Th(III) and Th(II). *Submitted.*

9. Wedal, J. W.; Moore, W. N. G.; Villareal, D.; Fu, W; Lukens, W. W.; Evans, W. J. Perplexing EPR Signals from $5f^3 6d^1$ U(II) Complexes. *Submitted*.

8. Moore, W. N. G.; McSorley, T. J.; Vincent, A.; Ziller, J. Z.; Jauregui, L. A.; Evans, W. J. Characterization and Exfoliation of a Layered Paramagnetic Tm(II) Compound Crystallized from Solution Phase. *ACS Appl. Nano Mater.* **2023**, *6*, 6461–6466. DOI: 10.1021/acsanm.3c00662

7. Chung, A. B.; Stennet, C. R.; Moore, W. N. G.; Fang, M.; Ziller, J. Z.; Evans, W. J. Reductive C–O Cleavage of Ethereal Solvents and 18-Crown-6 in $Ln(NR_2)_3/KC_8$ Reactions (R = $SiMe_3$). *Inorg. Chem.* **2023**, *62*, 5854–5862. DOI: 10.1021/acs.inorgchem.3c00689

6. Moore, W. N. G.; White, J. R. K.; Wedal, J. C.; Furche, F.; Evans, W. J. Reduction of Rare-Earth Metal Complexes Induced by γ Irradiation. *Inorg. Chem.* **2022**, *61*, 17713-17718. DOI: 10.1021/acs.inorgchem.2c02857

5. Huh, D. N.; Ciccone, S. R.; Moore, W. N. G.; Ziller, J. W.; Evans, W. J. Synthesis of Ba(II) Analogs of Ln(II)-in-(2.2.2-Cryptand) and Layered Hexagonal Net Ln(II) Complexes, $[(THF)Cs(\mu\text{–}\eta^5\text{:}\eta^5\text{–}C_5H_4SiMe_3)_3Ln^{II}]_n$. *Polyhedron*, **2021**, *210*, 115393. DOI: 10.1016/j.poly.2021.115493

4. Moore, W. N. G.; Ziller, J. W.; Evans, W. J. Optimizing Alkali Metal (M) and Chelate (L) Combinations for the Synthesis and Stability of $[M(L)][(C_5H_4SiMe_3)_3Y]$ Yttrium(II) Complexes. *Organometallics*, **2021**, *40*, 3170-3176. DOI: 10.1021/acs.organomet.1c00379

3. Henke, W. C.; Otolski, C. J.; Moore, W. N. G.; Elles, C. G.; and Blakemore, J. D. Ultrafast Spectroscopy of $[Mn(CO)_3]$ Complexes: Tuning the Kinetics of Light-Driven CO Release and Solvent Binding. *Inorg. Chem.*, **2020**, *59*, 2178-2187. DOI: 10.1021/acs.inorgchem.9b02758

2. Moore, W. N. G., Henke, W. C., Lionetti, D., Day, V. W., and Blakemore, J. D., Single-Electron Redox Chemistry on the [Cp*Rh] Platform Enabled by a Nitrated Bipyridyl Ligand. *Molecules*, **2018**, *23*, 2857. DOI: 10.3390/molecules23112857 *Selected to be on the journal Front Cover as Feature Article

1. Henke, W. C., Lionetti, D., Moore, W. N. G., Hopkins, J. A., Day, V. W., and Blakemore, J. D., Ligand Substituents Govern the Efficiency and Mechanistic Path of Hydrogen Production with [Cp*Rh] Catalysts. *ChemSusChem*, **2017**, *10*, 4589-4598. DOI: 10.1002/cssc.201701416

Presentations

12. Moore, W.N.G. *Using gamma irradiation to generate low oxidation state rare-earth species*, American Chemical Society (ACS) National Meeting, San Diego, CA, March 24, 2022 (Oral).

11. Moore, W.N.G. *Effects of Alkali Metals and Chelates on the Chemistry of Y(II) Ions in Tris(cyclopentadienyl) Complexes*. American Chemical Society (ACS) National Meeting, Virtual, April 8, 2021 (Oral).

10. Moore, W.N.G. *Tuning the redox properties of [Cp*Rh] catalysts with monosubstituted 2,2'-bipyridyl ligands*, American Chemical Society (ACS) National Meeting, Sci. Mix, Orlando, FL, April 1, 2019 (Poster).

9. Moore, W.N.G. *Tuning the redox properties of [Cp*Rh] catalysts with monosubstituted 2,2'-bipyridyl ligands*, American Chemical Society (ACS) National Meeting, Orlando, FL, April 2, 2019 (Oral).

8. Moore, W.N.G. *Driving Generation of Useful Chemical Fuels from Renewable Energy Sources*. Board of Regents Poster Presentation, April 18, 2019 (Poster).

7. Moore, W.N.G. *Driving Generation of Useful Chemical Fuels from Renewable Energy Sources*. Kansas Undergraduate Research Day at the Capitol, March 20, 2019 (Poster).
6. Moore, W.N.G. *Single-electron redox chemistry of [Cp*Rh] enabled by a nitrated bipyridine ligand*, American Chemical Society (ACS) National Meeting, New Orleans, LA, March 22, 2018 (Oral).
5. Moore, W.N.G. *Chemical and electrochemical properties of [Cp*Rh] complexes bearing nitrated bipyridine ligands,* ACS Regional Meeting, Ames, IA, October 23, 2018 (Oral).
4. Moore, W.N.G. *Multielectron Processes in a rhodium bipyridine complex relevant to hydrogen fuel production*, KU Spring Undergraduate Research Symposium, April 28, 2018 (Poster).
3. Moore, W.N.G. *Multielectron Processes in a rhodium bipyridine complex relevant to hydrogen fuel production*, ACS Regional Meeting, Lawrence, KS, October 20, 2017 (Oral).
2. Moore, W.N.G. *Rational Design in Storage of Renewable Energy: A Chemical Approach*, Rock Chalk Talks, Lawrence, KS, November 28, 2017 (Oral).
1. Moore W.N.G. *Multielectron Processes in a rhodium bipyridine complex relevant to hydrogen fuel production*, KU Summer Undergraduate Research Symposium, July 28, 2017 (Poster).

Abstract of the Dissertation

Investigating Unusual Reduction Methods for the Generation of Low Oxidation State Rare-Earth Organometallic Complexes

By

William Nicholas Graham Moore

Doctor of Philosophy in Chemistry

University of California, Irvine, 2023

Distinguished Professor Emeritus William J. Evans, Chair

This dissertation describes a variety of reduction techniques applied towards the synthesis and characterization of low oxidation state rare-earth metal compounds in order to determine the techniques' efficacy and the ability of these methods to yield species with interesting properties different from those generated from the widely used potassium-based reduction systems. The research results described herein add to the fundamental knowledge base on the coordination and redox chemistry of the rare-earth metals, which are scandium, yttrium, and the lanthanides.

In Chapter 1, an array of alkali metal (M) and organic chelate (L) combinations were used to generate nine $[M(L)][Cp'_3Y^{II}]$ ($Cp' = C_5H_4SiMe_3$) complexes in order to determine whether K/crypt (crypt = 2.2.2-cryptand) is indeed the most suitable for reducing Cp'_3Y^{III} and isolating Y(II) complexes. During the process, two new Y(II) complexes were crystallographically characterized, namely $[(THF)Na_2(18c6)_2][Cp'_3Y^{II}]_2$ and $[Na(crypt)][Cp'_3Y^{II}]$. EPR, UV-visible absorbance, and IR spectroscopies revealed minimal differences in the spectroscopic characeristics of these complexes. Interestingly, the decomposition profiles of these species at room temperature show marked differences. This Chapter initiates a discussion of the factors that determine the stability of these low oxidation state-complexes.

In Chapter 2, cesium metal smears were used to reduce Cp'_3Yb^{III} and Cp'_3Tm^{III} and generate a series of ytterbium(II) and thulium(II) complexes that display an extended structure by single crystal X-ray

diffraction (XRD). The structures are composed of layers of hexagonal nets with alternating vertices of Cs(I) and Ln(II) ions. This structure is robust with respect to the level of THF-solvation, as compounds with 0, 1, and 2 bound THF molecules per monomer unit were characterized. The Tm-containing species, $[(THF)Cs(\mu\text{–}\eta^5\text{:}\eta^5\text{–}Cp')_3Tm^{II}]_n$, was synthesized in order to investigate whether the trigonal arrangement of S = ½ Tm(II) ions yielded spin frustration at low temperatures and whether single crystals were exfoliatable. By collaborating with Alexandre Vincent from the lab of Professor Jeffrey R. Long at the University of California, Berkeley, SQUID measurements were collected to show that the thulium ions are in the +2 oxidation state and non-interacting. And by collaborating with TJ McSorley from the lab of Professor Luis A. Jauregui in the Department of Physics at the University of California, Irvine, exfoliation of single crystals was successful down to approximately 50 layers.

In Chapter 3, a method was adapted to induce the reduction of Ln(III) organometallic complexes (Ln = Sc, Y, La) by exposing them to γ-irradiation in a glassy matrix. The method was first utilized to reduce Ln(III) complexes to known $[Ln(II)]^{1-}$ anions, which were identified by EPR and UV-visible spectroscopies. That γ-irradiation method was extended to generate and characterize a new anion, namely $[La^{II}(NR_2)_3]^{1-}$ (R = $SiMe_3$). Furthermore, the formation of $[Cp'_3Y^{II}]^{1-}$ was monitored over time to show the low conversion rate of the method (<1% over 6.5 hours). This method may have broader implications for the generation and characerization of low oxidation state species otherwise unisolable by chemical means.

In Chapter 4, an attempt to generate a bridging $[C\equiv C]^{2-}$ unit for reduction to the magnetically interesting, previously unknown $[C\equiv C]^{3-}$ bridge is described. The reaction of $(C_5Me_5)_2Y(\mu\text{–}Ph)_2BPh_2$ with $NaC\equiv CH$ did not yield the desired $(C_5Me_5)_2Y(CC)Y(C_5Me_5)_2$ and instead forms an interesting C–C coupled product, namely $(C_5Me_5)_2Y(\mu\text{–}\eta^3\text{:}\eta^1\text{–}CCCCH_2)Y(C_5Me_5)_2$. This represents the second crystallographically characterized butatrienylidene dianion. The product was characterized by ^1H, ^{13}C, and HMQC NMR, UV-visible absorbance, and IR spectroscopies. Theoretical calculations were conducted to investigate the nature of the C–C bonding in the butatrienylidene bridge.

In Chapter 5, results are reported on separate approaches to reduce organometallic rare-earth metal complexes using photoredox reactions and using barium powder. The photoredox approach focused on

reducing Cp'_3Y^{III} in collaboration with Professor Harry B. Gray and his graduate student Dr. Javier Fajardo Jr. at the California Institute of Technology using a powerful photoreductant developed in their lab, namely $W(CN_{dipp})_6$. Upon excitation with UV-visible light, the reduction potential is shifted approximately 2.3 V more negative {$E_{1/2}$ of $W(CN_{dipp})_6 = -0.72$ V vs $Fc^{+/0}$, $E_{1/2}$ of $[W(CN_{dipp})_6]^* \approx -3.0$ V vs $Fc^{+/0}$}. The reduction of Cp'_3Y^{III} by this species was attempted in toluene with the inclusion of a suite of sacrificial reductants. No isolation or characterization of Y(II) product was observed. Regarding the use of barium as a reductant, barium powder was generated in order to maximize its surface area and improve the speed at which a reduction reaction would occur. Reductions were attempted in the presence of crypt with Cp'_3Ln (Ln = Y, Tm, Yb). Reductions were observed for thulium and ytterbium. Crystals isolated from a sample dissolved in wet acetonitrile demonstrate the electrostatic attraction of Ba(II) and anionic ligands, yielding the structure $[Ba(crypt)Cp][Cp_2Yb(\mu\text{–}OSiMe_3)_2YbCp_2]$.

Introduction

Rare-earth metals are composed of scandium, yttrium, and the lanthanide elements, see Figure 0.1. These elements are grouped together because they tend to share similar physical and chemical properties. For instance, they all form primarily ionic bonds that do not involve significant metal-ligand orbital mixing.

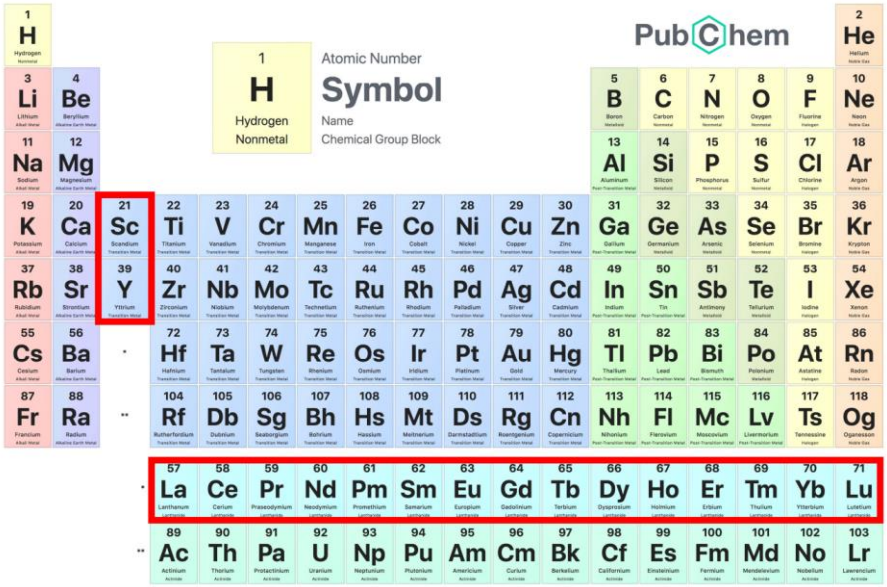

Figure 0.1. Periodic table with rare-earth elements denoted in red boxes.[1]

Furthermore, all of these elements are most commonly isolated in the +3 oxidation state.[2-6] In fact, for a long time it was thought that they were only isolable in the +3 oxidation state, with the exceptions of Sm, Eu, and Yb, which can form stable +2 oxidation state compounds as a result of their resulting electron configurations being at or near half or fully filled 4f shells: $4f^6$ Sm(II), $4f^7$ Eu(II), and $4f^{14}$ Yb(II). Similarly, Ce could be isolated in the +4 oxidation state due to stabilization from its $4f^0$ electron configuration, see Figure 0.2, top, for summary of available oxidation states up to 1997.

1997

	La	Ce	Pr	Nd	Pm	Sm	Eu	Gd	Tb	Dy	Ho	Er	Tm	Yb	Lu
Valence Electrons	3	4	5	6	7	8	9	10	11	12	13	14	15	16	17
Oxidation States	3	4 3	3	3	3	3 2	3 2	3	3	3	3	3	3	3 2	3

2023

	La	Ce	Pr	Nd	Pm	Sm	Eu	Gd	Tb	Dy	Ho	Er	Tm	Yb	Lu
Valence Electrons	3	4	5	6	7	8	9	10	11	12	13	14	15	16	17
Oxidation States	3 2	4 3 2	4 3 2	3 2	3	3 2	3 2	3 2	4 3 2	3 2	3 2	3 2	3 2	3 2	3 2

Figure 0.2. Isolated oxidation states, aside from the zero oxidation state available to all metals in their elemental form.

Early synthetic explorations focused on isolating elements beyond Sm, Eu, and Yb in the +2 oxidation state were geared towards the synthesis of LnI_2 species (Ln = rare-earth metal).[7-9] By heating a finely ground mixture of the rare-earth metal and the triiodide (LnI_3) in a sealed tungsten tube under inert conditions, a comproportionation reaction occurs, and several of these species were isolated and characterized crystallographically (Ln = La, Ce, Pr, Nd, Sm, Gd, Dy, Tm, Yb). Interestingly, most of these species were determined to contain Ln(III) with a free electron in the lattice, rather than Ln(III) ions. Only the diiodides of Nd, Sm, Dy, Tm, and Yb were determined to contain legitimate +2 ions. Subsequently, efforts by Bochkarev and coworkers in collaboration with the Evans group were able to generate the first crystalline Tm(II) compound, $TmI_2(MeOCH_2CH_2OMe)_3$, by heating thulium metal with TmI_3 in dimethoxyethane (DME) at reflux in another example of a comproportionation reaction.[10] In addition, crystalline $DyI_2(DME)_3$[11] and $NdI_2(THF)_5$[12] were isolated soon thereafter.

Only in 2008 was another rare-earth element isolated in the +2 oxidation state by Lappert and coworkers.[13] Using potassium graphite as a reductant, an organometallic lanthanum complex in a trigonal ligand environment, Cp''_3La ($Cp'' = C_5H_3(SiMe_3)_2$), was reduced in the presence of an organic chelate, 18-crown-6 or 2.2.2-cryptand, to yield $[K(18c6)(OEt_2][Cp''_3La]$ (18c6 = 18-crown-6) and [K(crypt)][Cp''_3La]

(crypt = 2.2.2-cryptand). The La(II) ions in these complexes were characterized by EPR spectroscopy and Superconducting Quantum Interference Device (SQUID) magnetometry. A $4f^05d^1$ electron configuration was proposed for La(II) based the small (< 0.05 Å) changes in metal-ligand bond distances upon reduction, which was very different from the 0.1-0.2 Å increase in distances observed for $4f^n$ Ln(III) to $4f^{n+1}$ Ln(II) reductions.

The use of similar reduction procedures incorporating potassium-based reductants and organic chelates enabled isolation of the entire rare-earth metal series in the +2 oxidation state using the tris Cp′ (Cp′ = $C_5H_4SiMe_3$) ligand system by MacDonald et al.[14-16] Figure 0.2, bottom, shows a compilation of elements isololated in the new +2 oxidation state and Figure 0.3 shows the synthetic scheme by which they were obtained. Upon reduction of the $4f^n$ Ln(III) precursors, most of the complexes adopt a "non-traditional" electron configuration of $4f^n5d^1$, while Sm, Eu, Tm, and Yb adopt a "traditional" $4f^{n+1}$ electron configuration.[17] These mixed principal quantum number complexes exhibit interesting properties, notably producing record high monometallic single molecule effective magnetic moments,[18-21] room temperature quantum bits,[22] and a suite of reductive reactivity.[23-29]

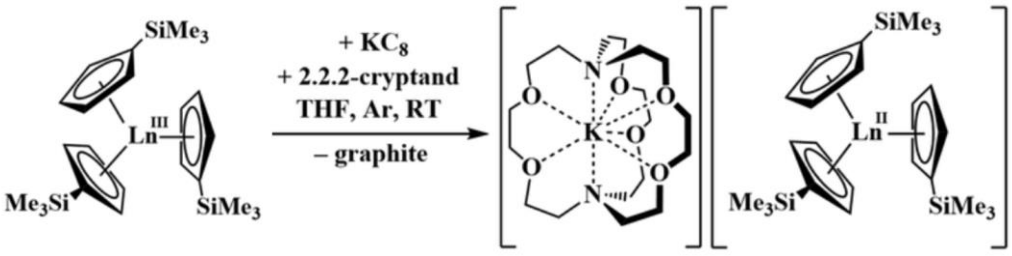

Figure 0.3. Synthesis of [K(crypt)][Cp′$_3$Ln] species (Ln = Sc, Y, La, Ce, Pr, Nd, Sm, Eu, Gd, Tb, Dy, Ho, Er, Tm, Yb, Lu).

All of the non-traditional $4f^n5d^1$ Ln(II) complexes decompose at room temperature. As a result, an important aspect of most of their syntheses is keeping them at low temperatures (<35 °C). Syntheses attempted at room temperature often led to transient formation of the Ln(II) complex followed by rapid decomposition. Some decomposition products isolated during the early stages of these explorations from $Ln^{III}A_3/K$ (A = anion) reactions that form transient "$(Ln^{II}A_3)^{1-}$" products include the potassium salt of the

free ligand (i.e. KA where A = anionic ligand),[13] the tetrakis salt (i.e. [K(chelate)][$Ln^{III}A_4$]),[30,31] cyclometallated products (i.e. [K(chelate)][A_2Ln^{III}(A-κ_1,κ_2)],[32] and solvent-activation products (i.e. THF ring-opening or DME C–O bond cleavage products, where THF = tetrahydrofuran and DME = dimethoxyethane).[33]

Variation in the synthetic method was mainly limited to sporadic use of alternate alkali metals or chelates. For instance, the use of rubidium and sodium as reductants in combination with 18c6 as a chelate enabled crystallographic characterization of the $[Y(NR_2)_3]^{1-}$ anion.[28] Additionally, it has been found that some Ln(II) complexes are isolable using alkali metals such as lithium and cesium in the absence of an organic chelate.[34]

In an effort to characterize and isolate low oxidation state rare-earth metal ions and compounds, some other techniques have been employed as well (see Figure 0.4 for abbreviated chronology). In 1966, Fong et al subjected a KCl matrix doped with Sm^{2+} to increasing amounts of γ irradiation.[34] Characterization of the resulting crystals via UV-visible absorbance spectroscopy and magnetic studies was consistent with the formation of $4f^6 6s^1$ Sm^{1+} ions. Around the same time, it was discovered that doping Ln^{3+} ions into CaF_2 matrices and subjecting them to γ irradiation yielded spectra of the corresponding Ln^{2+} ions.[36] A couple decades later in the 1980's and 1990's, Cloke and coworkers found that employing metal-vapor chemistry to co-condense Ln(0) atoms with 1,3,5-tri-t-butylbenzene (Bz*) was successful in yielding a series of $Ln^0(Bz^*)_2$ (Ln = Y, Pr, Nd, Gd, Tb, Dy, Ho, Er, Lu) sandwich complexes, several of which were crystallographically characterized, including those containing Gd and Ho.[37] Similar co-condensation methods also yielded a Sc(0) complex, $Sc^0(\eta\text{–}C_6{}^tBu_3MeH_2)_2$ and a Sc(I) complex, $[\{\eta^5\text{–}P_3C_2{}^tBu_2)Sc^I\}_2(\mu\text{–}\eta^6\text{:}\eta^6\text{–}P_3C_3{}^tBu_3)]$.[38]

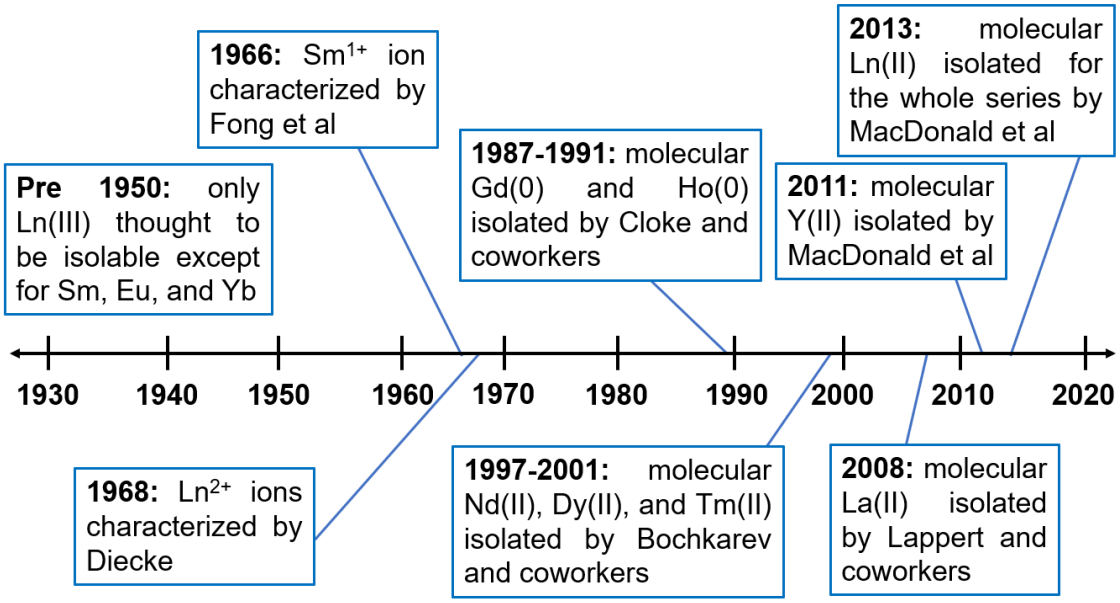

Figure 0.4. A chronology showing selected events in the history of generating and characterizing low oxidation state rare-earth metal ions.

This dissertation describes efforts to expand upon reduction methods used to generate and characterize organometallic complexes of the rare-earth metals. The foundational and exploratory work described above served as a reference point throughout the work described herein as well as the construction of this thesis.

References

(1) Public Domain. PubChem from the National Institutes of Health. Accessed **2023**.

(2) Morss, L. R. Thermochemical Properties of Yttrium, Lanthanum, and the Lanthanide Elements and Ions. *Chem. Rev.* **1976**, *76*, 827–841. DOI: 10.1021/cr60304a007.

(3) Meyer, G. Reduced Halides of the Rare-Earth Elements. *Chem. Rev.* **1988**, *88*, 93–107. DOI: 10.1021/cr00083a005.

(4) Meyer, G.; Meyer, H. J. Unusual Valences in Rare-Earth Halides. *Chem. Mater.* **1992**, *4*, 1157–1168. DOI: 10.1021/cm00024a012.

(5) Bochkarev, M. N. Molecular Compounds of "New" Divalent Lanthanides. *Coord. Chem. Rev.* **2004**, *248*, 835–851. DOI: 10.1016/j.ccr.2004.04.004.

(6) Nief, F. In *Handbook on the Physics and Chemistry of Rare Earths*; Gschneidner, K. A., Jr., Bunzli, J.-C. G., Pecharsky, V. K., Eds.; North-Holland: Amsterdam, **2010**, *40*, Chapter 246.

(7) Drudino, L. F.; Corbett, J. D. Rare Earth Metal-Metal Halide Systems. The Preparation of Neodymium(II) Halides. *J. Am. Chem. Soc.* **1959**, *81*, 5512. DOI: 10.1021/ja01529a067.

(8) Corbett, J. D. Conproportionation Routes to Reduced Lanthanide Halides. In *Synthesis of Lanthanide and Actinide Compounds*; **2011**, 159–173. DOI: 10.1007/978-94-011-3758-4_6.

(9) Sallach, R. A.; Corbett, J. D. Magnetic Susceptibilities of Neodymium(II) Chloride and Iodide. *Inorg. Chem.* **1964**, *3*, 993–995. DOI: 10.1021/ic50017a015.

(10) Bochkarev, M. N.; Fedushkin, I. L.; Fagin, A. A.; Petrovskaya, T. V.; Ziller, J. W.; Broomhall-Dillard, R. N. R.; Evans, W. J. Synthesis and Structure of the First Molecular Thulium(II) Complex: $[TmI_2(MeOCH_2CH_2OMe)_2]$. *Angew. Chem. Int. Ed. Eng.* **1997**, *36*, 133–135. DOI: 10.1002/anie.199701331.

(11) Bochkarev, M. N.; Fedushkin, I. L.; Dechert, S.; Fagin, A. A.; Schumann, H. $[NdI_2(thf)_5]$, the First Crystallographically Authenticated Neodymium(II) Complex. *Angew. Chem. Int. Ed.* **2001**, *40*, 3176–3178. DOI: 10.1002/1521-3773(20010903)40:17<3176::aid-anie3176>3.0.co;2-y.

(12) Evans, W. J.; Allen, N. T.; Ziller, J. W. The Availability of Dysprosium Diiodide as a Powerful Reducing Agent in Organic Synthesis: Reactivity Studies and Structural Analysis of $DyI_2((DME)_3$ and Its Naphthalene Reduction Product. *J. Am. Chem. Soc.* **2000**, *122*, 11749–11750. DOI: 10.1021/ja0034949.

(13) Hitchcock, P. B.; Lappert, M. F.; Maron, L.; Protchenko, A. V. Lanthanum Does Form Stable Molecular Compounds in the +2 Oxidation State. *Angew. Chem. Int. Ed.* **2008**, *47*, 1488–1491. DOI: 10.1002/anie.200704887.

(14) MacDonald, M. R.; Ziller, J. W.; Evans, W. J. Synthesis of a Crystalline Molecular Complex of Y^{2+}, $[(18\text{-Crown-6})K][(C_5H_4SiMe_3)_3Y]$. *J. Am. Chem. Soc.* **2011**, *133*, 15914–15917. DOI: 10.1021/ja207151y.

(15) MacDonald, M. R.; Bates, J. E.; Fieser, M. E.; Ziller, J. W.; Furche, F.; Evans, W. J. Expanding Rare-Earth Oxidation State Chemistry to Molecular Complexes of Holmium(II) and Erbium(II). *J. Am. Chem. Soc.* **2012**, *134*, 8420–8423. DOI: 10.1021/ja303357w.

(16) MacDonald, M.; Bates, J. E.; Ziller, J. W.; Furche, F.; Evans, W. J. Completing the Series of +2 Ions for the Lanthanide Elements: Synthesis of Molecular Complexes of Pr^{2+}, Gd^{2+}, Tb^{2+}, and Lu^{2+}. *J. Am. Chem. Soc.* **2013**, *135*, 9857–9868. DOI: 10.1021/ja403753j.

(17) Fieser, M. E.; Macdonald, M. R.; Krull, B. T.; Bates, J. E.; Ziller, J. W.; Furche, F.; Evans, W. J. Structural, Spectroscopic, and Theoretical Comparison of Traditional vs Recently Discovered Ln^{2+} Ions in the [K(2.2.2-Cryptand)][$(C_5H_4SiMe_3)_3Ln$] Complexes: The Variable Nature of Dy^{2+} and Nd^{2+}. *J. Am. Chem. Soc.* **2015**, *137*, 369–382. DOI: 10.1021/ja510831n.

(18) Meihaus, K. R.; Fieser, M. E.; Corbey, J. F.; Evans, W. J.; Long, J. R. Record High Single-Ion Magnetic Moments Through $4f^n5d^1$ Electron Configurations in the Divalent Lanthanide Complexes $[(C_5H_4SiMe_3)_3Ln]^-$. *J. Am. Chem. Soc.* **2015**, *137*, 9855–9860. DOI: 10.1021/jacs.5b03710.

(19) Ryan, A. J.; Darago, L. E.; Balasubramani, S. G.; Chen, G. P.; Ziller, J. W.; Furche, F.; Long, J. R.; Evans, W. J. Synthesis, Structure, and Magnetism of Tris(Amide) $[Ln\{N(SiMe_3)_2\}_3]^{1-}$ Complexes of the Non-Traditional +2 Lanthanide Ions. *Chem. Eur. J.* **2018**, *24*, 7702–7709. DOI: 10.1002/chem.201800610.

(20) Anderson, D. M.; Cloke, F. G. N.; Cox, P. A.; Edelstein, N.; Green, J. C.; Pang, T.; Sameh, A. A.; Shalimoff, G. On the Stability and Bonding in Bis(η-Arene)Ianthanide Complexes. *J. Chem. Soc. Chem. Commun.* **1989**, *1*, 53–55. DOI: 10.1039/C39890000053.

(21) M. E. Fieser, Ph.D. Dissertation, University of California–Irvine **2015**.

(22) Ariciu, A. M.; Woen, D. H.; Huh, D. N.; Nodaraki, L. E.; Kostopoulos, A. K.; Goodwin, C. A. P.; Chilton, N. F.; McInnes, E. J. L.; Winpenny, R. E. P.; Evans, W. J.; Tuna, F. Engineering Electronic Structure to Prolong Relaxation Times in Molecular Qubits by Minimising Orbital Angular Momentum. *Nat. Commun.* **2019**, *10*, 1–8. DOI: 10.1038/s41467-019-11309-3.

(23) Palumbo, C. T.; Darago, L. E.; Windorff, C. J.; Ziller, J. W.; Evans, W. J. Trimethylsilyl versus Bis(Trimethylsilyl) Substitution in Tris(Cyclopentadienyl) Complexes of La, Ce, and Pr: Comparison of Structure, Magnetic Properties, and Reactivity. *Organometallics* **2018**, *37*, 900–905. DOI: 10.1021/acs.organomet.7b00881.

(24) Palumbo, C. T.; Fieser, M. E.; Ziller, J. W.; Evans, W. J. Reactivity of Complexes of $4f^n5d^1$ and $4f^{n+1}$ Ln^{2+} Ions with Cyclooctatetraene. *Organometallics* **2017**, *36*, 3721–3728. DOI: 10.1021/acs.organomet.7b00498.

(25) Woen, D. H.; Chen, G. P.; Ziller, J. W.; Boyle, T. J.; Furche, F.; Evans, W. J. Solution Synthesis, Structure, and CO2Reduction Reactivity of a Scandium(II) Complex, $\{Sc[N(SiMe_3)_2]_3\}^-$. *Angew. Chem. Int. Ed.* **2017**, *56*, 2050–2053. DOI: 10.1002/anie.201611758.

(26) Kotyk, C. M.; MacDonald, M. R.; Ziller, J. W.; Evans, W. J. Reactivity of the Ln^{2+} Complexes [K(2.2.2-Cryptand)][$(C_5H_4SiMe_3)_3Ln$]: Reduction of Naphthalene and Biphenyl. *Organometallics* **2015**, *34*, 2287–2295. DOI: 10.1021/om501063h.

(27) Woen, D. H.; Huh, D. N.; Ziller, J. W.; Evans, W. J. Reactivity of Ln(II) Complexes Supported by $(C_5H_4Me)^{1-}$ Ligands with THF and $PhSiH_3$: Isolation of Ring-Opened, Bridging Alkoxyalkyl, Hydride, and Silyl Products. *Organometallics* **2018**, *37*, 3055–3063. DOI: 10.1021/acs.organomet.8b00419.

(28) Ryan, A. J.; Ziller, J. W.; Evans, W. J. The Importance of the Counter-Cation in Reductive Rare-Earth Metal Chemistry: 18-Crown-6 Instead of 2,2,2-Cryptand Allows Isolation of $[Y^{II}(NR_2)_3]^{1-}$ and Ynediolate and Enediolate Complexes from CO Reactions. *Chem. Sci.* **2020**, *11*, 2006–2014. DOI: 10.1039/c9sc05794c.

(29) Chung, A. B.; Ryan, A. J.; Fang, M.; Ziller, J. W.; Evans, W. J. Reductive Reactivity of the $4f^75d^1$ Gd(II) Ion in $\{Gd^{II}[N(SiMe_3)_2]_3\}^-$: Structural Characterization of Products of Coupling, Bond Cleavage, Insertion, and Radical Reactions. *Inorg. Chem.* **2021**, *60*, 15635–15645. DOI: 10.1021/acs.inorgchem.1c02241.

(30) Ryan, A. J.; Ziller, J. W.; Evans, W. J. The Importance of the Counter-Cation in Reductive Rare-Earth Metal Chemistry: 18-Crown-6 Instead of 2,2,2-Cryptand Allows Isolation of $[Y^{II}(NR_2)_3]^{1-}$ and Ynediolate and Enediolate Complexes from CO Reactions. *Chem. Sci.* **2020**, *11*, 2006–2014. DOI: 10.1039/c9sc05794c.

(31) Evans, W. J.; Lee, D. S.; Rego, D. B.; Perotti, J. M.; Kozimor, S. A.; Moore, E. K.; Ziller, J. W. Expanding Dinitrogen Reduction Chemistry to Trivalent Lanthanides via the LnZ_3/Alkali Metal Reduction

System: Evaluation of the Generality of Forming $Ln_2(\mu\text{-}\eta_2\text{:}\eta_2\text{-}N_2)$ Complexes via LnZ_3/K. *J. Am. Chem. Soc.* **2004**, *126*, 14574–14582. DOI: 10.1021/ja046047s.

(32) Fang, M.; Bates, J. E.; Lorenz, S. E.; Lee, D. S.; Rego, D. B.; Ziller, J. W.; Furche, F.; Evans, W. J. (N2)3- Radical Chemistry via Trivalent Lanthanide Salt/Alkali Metal Reduction of Dinitrogen: New Syntheses and Examples of $(N_2)^{2-}$ and $(N_2)^{3-}$ Complexes and Density Functional Theory Comparisons of Closed Shell Sc^{3+}, Y^{3+}, and Lu^{3+} versus $4f^9$ Dy^{3+}. *Inorg. Chem.* **2011**, *50*, 1459–1469. DOI: 10.1021/ic102016k.

(33) Fang, M.; Lee, D. S.; Ziller, J. W.; Doedens, R. J.; Bates, J. E.; Furche, F.; Evans, W. J. Synthesis of the $(N_2)^{3-}$ Radical from Y 2+ and Its Protonolysis Reactivity To Form $(N_2H_2)^{2-}$ via the $Y[N(SiMe_3)_2]_3/KC_8$ Reduction System. *J. Am. Chem. Soc.* **2011**, 133, 3784–3787. DOI: 10.1021/ja1116827.

(34) Huh, D. N.; Ziller, J. W.; Evans, W. J. Chelate-Free Synthesis of the U(II) Complex, $[(C_5H_3(SiMe_3)_2)_3U]^{1-}$, Using Li and Cs Reductants and Comparative Studies of La(II) and Ce(II) Analogs. *Inorg. Chem.* **2018**, *57*, 11809–11814. DOI: 10.1021/acs.inorgchem.8b01966.

(35) Fong, F. K.; Cape, J. A.; Wong, E. Y. Monovalent Samarium in Potassium Chloride. *Phys. Rev.* **1966**, *151*, 299–303. DOI: 10.1103/PhysRev.151.299.

(36) Dieke, G. H. Chapter 12. Divalent Rare Earth Ions in Crystals. In *Spectra and Energy Levels of Rare Earth Ions in Crystals*; Interscience Publishers, **1968**; pp 177–188.

(37) Cloke, F. G. N. Zero Oxidation State Compounds of Scandium, Yttrium, and the Lanthanides. *Chem. Soc. Rev.* **1993**, *22*, 17–24. DOI: 10.1039/CS9932200017.

(38) Arnold, P. L.; Cloke, F. G. N.; Hitchcock, P. B.; Nixon, J. F. The First Example of a Formal Scandium(I) Complex: Synthesis and Molecular Structure of the 22-Electron Scandium Triple Decker Incorporating the Novel 1,3,5-Triphosphabenzene Ring. *J. Am. Chem. Soc.* **1996**, *118*, 7630–7631. DOI: 10.1021/ja961253o.

Chapter 1:

Optimizing Alkali Metal (M) and Chelate (L) Combinations for the Synthesis and Stability of [M(L)][$(C_5H_4SiMe_3)_3Y$] Yttrium(II) Complexes

INTRODUCTION[†]

As described in the introduction, historically, the rare-earth elements, i.e. scandium, yttrium, and the lanthanides, have had a limited number of oxidation states. The +3 oxidation state is the most stable for all these elements and, for many years, the only lower oxidation states accessible in molecular species were Eu(II), Yb(II) and Sm(II).[1] By 2001, Tm(II), Dy(II), Nd(II),[2,3] and Sc(II)[4] had been added to this list, but at that time, +2 ions of the other rare earth metals were not expected to be stable in solution.[5,6]

It was a surprise when the first crystallographically characterized complexes of La(II), namely [K(crypt)][Cp''_3La] and [K(18c6)Et_2O][Cp''_3La], were isolated in 2008.[7] These syntheses were accomplished by reducing Cp''_3La^{III} ($Cp'' = C_5H_3(SiMe_3)_2$) with potassium in the presence of a chelate. A similar method was used to isolate the first Y(II) complex: [(18c6)K(μ–Cp′)$Y^{II}Cp'_2$].[8] In the crystal structure of this complex, the potassium cation interacts with one of the Cp′ rings in an η^5 fashion. It was later found that by using crypt as the chelate, a more stable Y(II) complex was obtained, namely [K(crypt)][Cp'_3Y^{II}].[9] In this crystal structure, no interaction is observed between the K^+ cation and the Cp′ rings. Decomposition measurements on these two Y(II) species at 3 mM concentrations indicated that the 18c6 complex undergoes a first order decomposition process in THF at room temperature with $t_{1/2} \approx 8$ min and the crypt complex follows a second order decomposition process with $t_{1/2} \approx 140$ min.[9]

Subsequently, the K/crypt combination has been used extensively to generate other Y(II) complexes. Although many were characterized by EPR spectroscopy, e.g. from reduction of the Y(III) complexes $(C_5H_5)_3Y$,[10] $(C_5H_4Me)_3Y$,[10] $[C_5H_3(SiMe_3)_2]_3Y$,[10] $(C_5Me_4H)_3Y$,[10] and $Y(OC_6H_2\text{-}2,6\text{-}^tBu_2\text{-}4\text{-}Me)_3$,[11]

[†] Portions of this Chapter have been published: Moore, W. N. G.; Ziller, J. W.; Evans, W. J. Optimizing Alkali Metal (M) and Chelate (L) Combinations for the Synthesis and Stability of [M(L)][$(C_5H_4SiMe_3)_3Y$] Yttrium(II) Complexes. *Organometallics*, **2021**, *40*, 3170-3176. DOI: 10.1021/acs.organomet.1c00379

crystallographic characterization of an Y(II) product was possible in only two cases, both with the $[K(crypt)]^{1+}$ countercation: $[K(crypt)][Y(OC_6H_2\text{-}2,6\text{-}Ad_2\text{-}4\text{-}^tBu)_3]$[12] and $[K(crypt)]\{[C_5H_3(SiMe_3)_2]_2Y(C_5H_5)\}$[10]. With an amide-based ligand set, it was found that 18c6 facilitated more rapid crystallization and therefore isolation of $[K(18\text{-crown-}6)_2]\{Y[N(SiMe_3)_2]_3\}$.[13,14] These Y(II) systems are of considerable interest because $[K(crypt)][Cp'_3Y^{II}]$ was found to behave as a qubit at room temperature.[15]

Although the combination of potassium as a reductant and crypt as a chelate for the potassium ion was successful in these cases, it was unclear whether this was the optimum M/L combination (M = alkali metal, L = organic chelating agent) for the synthesis and isolation of $[M(L)][Cp'_3Y^{II}]$ complexes. The reduction of $4f^n$ Ln(III) complexes to $4f^n5d^1$ Ln(II) complexes was extensively studied with K/crypt,[9,16-23] but a comprehensive comparative study of different M/L combinations had not been done with either the lanthanides, yttrium, or scandium.

To evaluate the effect of M and L on the generation and stability of $[M(L)][Cp'_3Y^{II}]$ complexes, eight other combinations of reducing metal and chelating ligand were examined for comparison with K/crypt. In addition, chemical evidence of the putative Y(II) species was sought in the form of a clean oxidation to reform Cp'_3Y^{III}. This was achieved using Hg, which previously has been shown to react with $\{[(Me_3Si)_2N]_2Y(THF)\}_2(\mu\text{–}\eta^2\text{:}\eta^2\text{–}N_2)[K(THF)_6]$ to cleanly generate its precursor, $\{[(Me_3Si)_2N]_2Y(THF)\}_2(\mu\text{–}\eta^2\text{:}\eta^2\text{–}N_2)$.[24]

RESULTS

Spectroscopic Characterization. Nine alkali metal (M)/chelate (L) combinations were investigated for the generation of $[M(L)][Cp'_3Y]$ complexes following the synthetic reaction shown in Figure 1.1. All of the products were characterized by IR, UV-visible absorption, and EPR spectroscopies. For EPR data collection, the dark purple solutions formed according to the reduction reactions shown in Scheme 1 in an argon glovebox were pipetted (using glassware pre-cooled to −35 °C) into EPR tubes also pre-cooled to −35 °C, the tubes were capped, and the tubes were inserted into a liquid nitrogen bath outside of the box. In frozen THF solutions at 77 K, the X-band EPR spectra for all products showed an axial signal

split by the ^{89}Y nucleus (I = ½, 100% abundance), with $g_x = g_y = 1.99$ ($g_\perp = 1.99$) and $g_z = 2.00$ ($g_\parallel = 2.00$). The hyperfine coupling constants are also identical for all products with A_{iso} = 36 G (100.9 MHz). The consistency of these data indicates that the countercation is not interacting with the yttrium metal center or any of the Cp′ ligands in the frozen THF solutions.

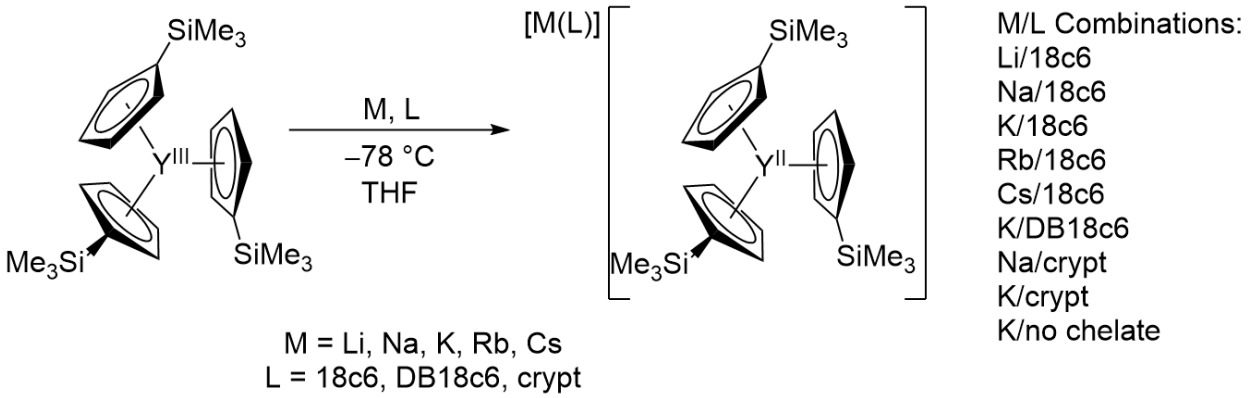

Figure 1.1. Synthesis of [M(L)][Cp′$_3$Y^{II}] species from Cp′$_3$Y^{III}.

The UV-visible absorbance profiles of the [M(L)][Cp′$_3$Y^{II}] complexes showed similar characteristics. Each spectrum has three absorption maxima near 390 nm ($\varepsilon \approx 1100$ M^{-1}cm^{-1}), 530 nm ($\varepsilon \approx 1300$ M^{-1}cm^{-1}), and 700 nm ($\varepsilon \approx 450$ M^{-1}cm^{-1}), which have previously been assigned by TDDFT studies as d→d and d→p* metal-to-ligand charge transfer bands.[9] The high energy shoulder is most variable with λ_{max} ranging from 380-400 nm and molar absorptivities ranging from 1000-2000 M^{-1} cm^{-1}. It is unknown whether this variability is inherent to the molecules or a result of minor decomposition. The lack of variability in the lower energy peaks is also indicative of negligible interactions between the countercation and [Cp′$_3$Y^{II}]$^{1-}$ unit in THF solutions.

IR characterization was obtained for all complexes except the Li/18c6 and K/none pairings. Both of these decomposed in the solid state before reliable IR data could be obtained. The remaining complexes exhibit spectra similar within chelate groupings, i.e. all of the M/18c6 pairings yield near identical IR spectra.

Crystallographic Characterization. Four of the M/L combinations provided crystallographically characterizable complexes. Two of these are the previously reported structures, [(18c6)K(μ–Cp′)Y^{II}Cp′$_2$],[8] **1-Y**, and [K(crypt)][Cp′$_3Y^{II}$], **2-Y**,[9] which were identified by unit cell determination, and two are new structures, [(THF)Na_2(18c6)$_2$][Cp′$_3Y^{II}$]$_2$, **3-Y**, and [Na(crypt)][Cp′$_3Y^{II}$], **4-Y**.

Crystals of the Na/18c6 reduction product, **3-Y,** differ from those of the K/18c6 product, **1-Y**, in that the alkali metal is not located near any cyclopentadienyl ring. In **1-Y** there are K-C(μ–Cp′) distances of 3.055(2) – 3.079(2) Å, whereas in **3-Y** the closest Na-C(Cp′) distance is 5.809(3) Å. The structure of **3-Y** is further unusual in that the unit cell contains two $(Cp'_3Y^{II})^{1-}$ anions with the charge balanced by a $[(THF)Na_2(18c6)_2]^{2+}$ dication that has two different types of Na^{1+} coordination environments. The $[Na_2(18c6)_2]^{2+}$ dication has previously been observed in several structures,[25-27] but never with a single additional THF molecule. Hence, this structure adds another example to the many variations of countercations comprised of alkali metal cations and 18c6.[13] Each sodium in $[(THF)Na_2(18c6)_2]^{2+}$ is coordinated to the 6 oxygen atoms of an 18c6 ring as well as one oxygen of the other 18c6 ring. One of the sodium atoms also has a THF attached trans to the single oxygen of the other ring (see crystal structure of **3-Y** in Figure 1.2).

The crystalline product of the Na/crypt reduction, **4-Y**, is similar to that of the potassium analog, **2-Y**. The Na^{1+} cation is bound only by crypt and does not interact with any cyclopentadienyl rings or solvent molecules. The bond distances and angles in the $(Cp'_3Y^{II})^{1-}$ components of **(1-Y)-(4-Y)** are all very similar.

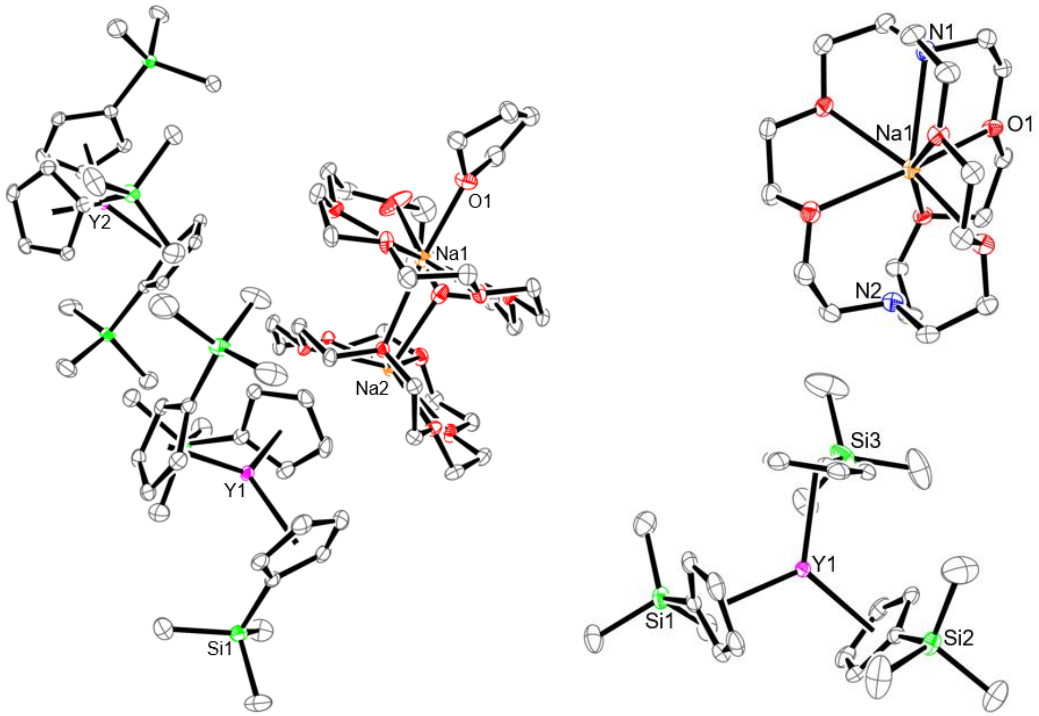

Figure 1.2. Crystal structures of **3-Y** (left) and **4-Y** (right) with displacement ellipsoids drawn at 50% and hydrogen atoms omitted for clarity.

Decomposition Studies. In solution, all of the reduction products begin to decompose upon warming to room temperature from −78 °C. No decomposition is observed if the temperature is maintained at −40 °C. Analysis of the K/18c6 product after 5 minutes at room temperature yields a ^{1}H NMR spectrum in THF-d_8 which shows more than 9 peaks between 5.5-7.0 ppm and more than 4 peaks between 0.0-1.0 ppm. These are attributed to Cp'_{ring} protons and Cp'_{methyl} protons, respectively, in different chemical environments. However, none of these peaks correspond to the yttrium starting material, Cp'_3Y^{III}, or KCp′ and remain unidentified. This suggests that a number of decomposition pathways may be occurring, and mechanistic analysis would be complicated given that the identity of the products is unknown. A mechanistic analysis is further complicated by the observation of an EPR signal in agreement with the presence of an electride, [K(chelate)][e$^-$], in the decomposed samples. For example, leaving [K(DB18c6)][Cp'_3Y^{II}] in THF solution at room temperature for 1 minute and then freezing the sample to 77 K yields an EPR spectrum containing an isotropic signal (g_{iso} = 2.00) consistent with [K(DB18c6)][e$^-$],

in addition to the Y(II) signal.[28] The observation of EPR signals that look like [K(chelate)][e$^-$] in the spectra of reduced rare-earth complexes is not uncommon,[29,30] and this electride may contribute to the formation of many different decomposition products. After one week, all solutions shift from dark purple to colorless with no absorptions in the UV-visible region. The attenuation of the absorptions was used to monitor the decreasing concentrations of the Y(II) species during decomposition.

The relative stabilities of the nine M/L combinations were quantitatively analyzed using the following standardized method. First, a solution of Cp'_3Y (40 mg, 0.08 mmol) and chelate (0.08 mmol) in 1.00 mL THF was cooled to −78 °C in a scintillation vial. A vial with excess reductant and a pipette were similarly cooled. A 0.1 cm Schlenk cuvette was cooled to −35 °C. The solution of the Cp'_3Y and chelate was added to the cooled vial containing the reductant using the cooled pipette. The reduced solution was then placed in the Schlenk cuvette. This cuvette was immediately removed from the argon glovebox and inserted into a UV-visible spectrometer. The absorbance at 700 nm was monitored for $t > 3 \times t_{1/2}$ (for the species that yielded reliable half-life data), or until less than 5% of the Y(II) material was remaining (for the species that decomposed too rapidly for effective half-life data). Assuming complete conversion to $[M(L)][Cp'_3Y^{II}]$ during reduction which is consistent with the lack of decomposition observed when the samples are kept at −40 °C, the initial concentration is about 80 mM for these reduced species. These conditions and concentrations are similar to previously-reported syntheses of Ln(II) complexes[9–16,18–23] and yield observable decomposition data for all complexes. Decomposition profiles for all complexes are shown in Figure 1.3. By conducting the decomposition measurements in triplicate, effective $t_{1/2}$ values at this 80 mM starting concentration were determined for three complexes: 71 ± 7 min for K/crypt, 23 ± 3 min for Na/crypt, and 16 ± 2 min for K/18c6. Clearly, the K/crypt combination yields the most stable Y(II) species. For the other M/L combinations, the products decomposed significantly during the transfer process and did not yield reliable $t_{1/2}$ values.

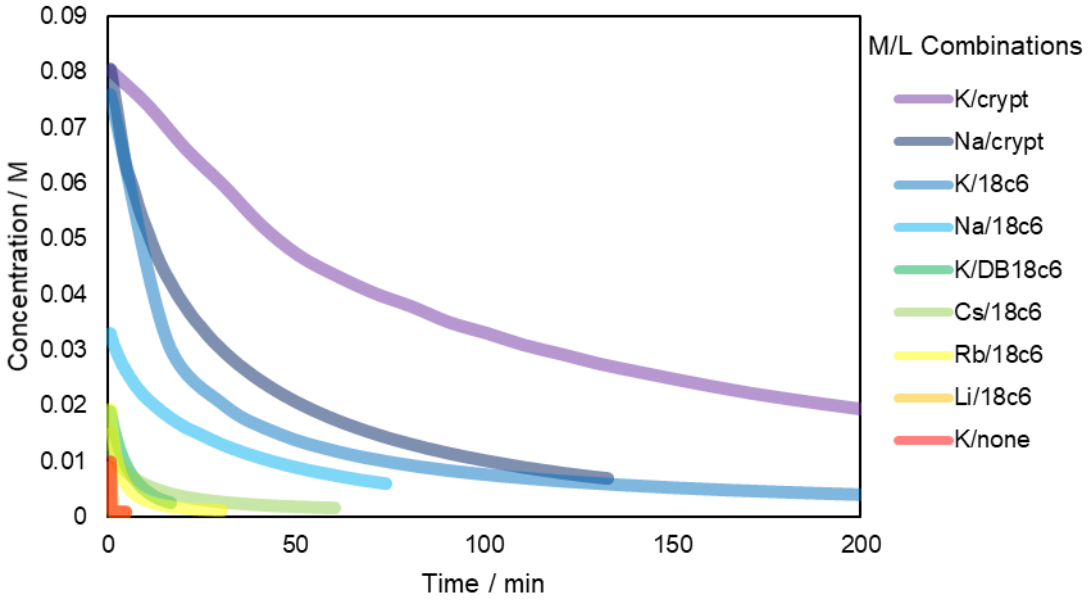

Figure 1.3. Plots of the concentration of [M(L)][Cp′$_3$Y] species as a function of time, obtained by monitoring the 700 nm absorption in their UV-visible spectra.

Oxidation Studies. A reaction was sought that would provide a clean one-electron oxidation of these Y(II) species to regenerate the starting material, Cp′$_3$Y^{III}, which would be useful in chemically characterizing the Y(III)/Y(II) redox couples in general. Mercury was tried since it was found to affect a clean oxidation of an $(N_2)^{3-}$ complex, {[(Me$_3$Si)$_2$N]$_2$Y(THF)}$_2$(μ–η^2:η^2–N$_2$)[K(THF)$_6$], to its $(N_2)^{2-}$ precursor, {[(Me$_3$Si)$_2$N]$_2$Y(THF)}$_2$(μ–η^2:η^2–N$_2$).[24] A freshly prepared solution of [K(18c6)][Cp′$_3$Y^{II}] in THF was reacted with a drop of Hg. No reaction occurred immediately, but upon vigorous agitation, the solution converted from dark purple to a faint yellow, consistent with the color of Cp′$_3$Y^{III}. A ^{1}H NMR spectrum taken in situ during an analogous reaction in a THF-d_8 solution showed growth of peaks associated with a single diamagnetic, Cp′-containing species and free 18c6 (see Figure 1.4 below). The ^{1}H NMR spectrum taken after filtration confirmed the reformation of Cp′$_3$Y^{III} and free 18c6. The initially shiny Hg drop dulled in color to a light grey and broke into small clumps, which is consistent with the presence of potassium mercury amalgam, K(Hg). This suggested that K(Hg) is not a powerful enough reductant to reduce Cp′$_3$Y^{III}. This process was independently confirmed when no reaction was observed between K(Hg) and Cp′$_3$Y^{III} in

the presence of 18c6 in a THF solution. The Y(II) sample without a chelate, i.e. $[K(THF)_n][Cp'_3Y^{II}]$, readily went colorless with Hg, but the reaction of Hg with $[K(crypt)][Cp'_3Y^{II}]$ took one day to discolor.

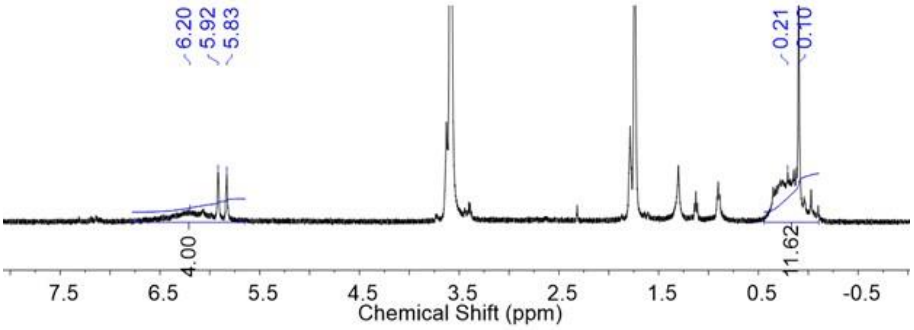

Figure 1.4. ^{1}H NMR taken in situ during reaction between $[K(18c6)][Cp'_3Y^{II}]$ and Hg(0).

A similar oxidation was attempted with the trityl radical since $[K(crypt)][CPh_3]$ is an isolable red crystalline product.[31] Reactions of $[K(18c6)][Cp'_3Y^{II}]$ with freshly synthesized $\cdot CPh_3$ gave a red product in some cases with absorbance maxima at about 430 nm and 500 nm, characteristic of the $[CPh_3]^{1-}$ anion.[32] Additionally, the ^{1}H NMR spectra of these red solutions showed the three resonances associated with Cp'_3Y^{III}. The reaction was not reliably reproducible, and the ^{1}H NMR spectrum also contained other species. It is plausible that even a small amount of $[K(18c6)][CPh_3]$ could account for the color due to its high molar absorptivity ($\varepsilon \approx 20{,}000\ M^{-1}\ cm^{-1}$).[32]

DISCUSSION

The choice of alkali metal reductant and chelating agent has a significant effect on the generation and stability of $[M(L)][Cp'_3Y]$ products. The K/crypt, Na/crypt, K/18c6, and Na/18c6 combinations give crystallographically-characterizable Y(II) products, however, the Li/18c6 combination and K without any chelate do not yield isolable solids. In these cases, only EPR and UV-visible absorbance spectroscopies show the presence of an Y(II) ion. The combination that gives the product with the longest stability in THF solution is K/crypt. This is consistent with the isolation of many Ln(II) and An(II) (An = actinide) complexes with $[K(crypt)]^{1+}$ as the countercation.[9,33-37]

The factors that lead to K/crypt as the optimum combination for this complex are not easily discerned. Since the decompositions do not cleanly go to Cp'_3Y and multiple unidentified decomposition

products are observed, mechanistic analysis is complicated. The data suggest that there may be multiple reaction pathways. Comparison of the M/18c6 combinations indicates that the Lewis acidity of the alkali metal cannot be the primary factor. Potassium yields the most stable complex of these combinations, but its Lewis acidity, as gauged by the pK_a = 16.06 of $[K(H_2O)_n]^{1+}$,[38] is intermediate compared to lithium ($[Li(H_2O)_n]^{1+}$ pK_a = 13.8)[39] and cesium ($[Cs(H_2O)_n]^{1+}$ pK_a = 16.34),[38] both of which decompose much more readily.

Interestingly, the equilibrium constants for the association of $[M(L)]^+$ complexes in solution, which take into account solvation effects, are also inadequate to explain the trends observed. The $[K(crypt)]^{1+}$ cation does have the highest equilibrium constant for complexation (log K_{eq} = 5.3)[40,41] of all cation/chelate combinations investigated in this study as well as the longest $t_{1/2}$ at room temperature. This suggests that the encapsulation of the alkali metal cation may be an important factor in the solution stability of these complexes. However, this argument does not hold true for the less stable complexes. For instance, the $[Na(18c6)]^{1+}$ cation has the lowest equilibrium constant (log K_{eq} = 0.8)[40,42] aside from $[K(THF)_n]^{1+}$, but the Y(II) decomposition $t_{1/2}$ is not the shortest. Furthermore, isolation of the $[(THF)Na_2(18c6)_2]^{2+}$ dication in crystals of **3-Y** indicates that simple $[M(chelate)]^{1+}$ species are not the only cations accessible in this system. The fact that 18c6 allows for more M^+ binding modes[13] may help explain the discrepancies between equilibrium constant and $t_{1/2}$ observed for the 18c6 complexes.

Options for increasing stability by using other metals for the reductions or other solvents that give higher $[M(L)]^{n+}$ formation constants are limited. For instance, although barium ions have a much higher equilibrium constant (log K_{eq} = 9.5)[40,41,43] in crypt and could generate a more stable cation, it typically needs activation to effect reduction. No reaction was observed between Cp'_3Y^{III} and Ba metal shavings over the course of 72 h at −78 °C. Solvents such as acetonitrile or DMF would also increase this equilibrium constant (log K_{eq} = 10.46 for K/crypt in MeCN),[34,39] but $[M(L)][Cp'_3Y]$ complexes decompose rapidly in both.

CONCLUSION

Nine M/L combinations have been used to generate $[M(L)][Cp'_3Y^{II}]$ complexes at −78 °C. Their EPR and UV-visible spectra indicate that the countercation is not interacting with the $[Cp'_3Y^{II}]^{1-}$ anion in

THF solution. Two new Y(II) crystal structures with the Na/crypt and Na/18c6 pairings were obtained and revealed an unusual $[(THF)Na_2(18c6)_2]^{2+}$ dication which crystallizes with two $[Cp'_3Y^{II}]^{1-}$ anions. Decomposition studies show that all complexes decompose in THF solution at room temperature, with the K/crypt complex providing the most stable Y(II) complex. The three other crystallographically characterized variations (Na/crypt, K/18c6, Na/18c6) were also the next three most stable according to the decomposition data. No single countercation characteristic yet appears to explain the entire stability order observed.

EXPERIMENTAL

All manipulations and syntheses described below were conducted with the rigorous exclusion of air and water using standard Schlenk line and glovebox techniques under an argon atmosphere. Solvents were sparged with UHP argon and dried by passage through columns containing Q-5 and molecular sieves prior to use. Deuterated NMR solvents were dried for one week over NaK alloy or molecular sieves, degassed by three freeze-pump-thaw cycles, and vacuum transferred before use. ^{1}H NMR spectra were recorded on Bruker AVANCE600, GN500, or CRYO500 MHz spectrometers. All spectra were collected at 298 K, unless otherwise stated, and referenced internally to residual protio-solvent resonances. Infrared spectra were collected on an Agilent Cary 630 equipped with a diamond ATR attachment. UV-visible absorbance spectra were collected on an Agilent Cary 60 UV-vis. EPR spectra were collected using the X-band frequency (9.3−9.8 GHz) on a Bruker EMX spectrometer equipped with an ER4119HS-W1 microwave bridge. 2.2.2-Cryptand (Aldrich) was placed under high vacuum (10^{-5} Torr) overnight before use. 18-Crown-6 (Alfa Aesar) was sublimed before use. Dibenzo-18-crown-6 (Fisher) was placed under high vacuum (10^{-5} Torr) at 40 °C overnight before use. Alkali metals (lithium, sodium, potassium, rubidium, and cesium) were purchased from Aldrich, washed with hexanes, and scraped to yield fresh surfaces before use. Gomberg's dimer,[46] Cp'_3Y,[8] [K(crypt)][Cp'_3Y],[9] and [K(18c6)][Cp'_3Y][8] were synthesized via literature procedures.

[Li(18c6)][Cp′$_3$Y]: A vial containing Cp'_3Y (43 mg, 0.090 mmol) and 18c6 (23 mg, 0.090 mmol) dissolved in 1 mL THF and a separate vial with a lithium smear were each cooled to −78 °C. The solution

of 18c6 and Cp'_3Y was pipetted onto the Li smear, and an immediate color change from light yellow to dark purple was observed. Removal of the solvent in vacuo resulted in a dark purple microcrystalline material (64 mg, 96%) consistent with [Li(18c6)][Cp'_3Y] based on UV-visible and EPR spectroscopies. UV-vis λ_{max}, nm (ε, M^{-1} cm^{-1}): 400 (1300), 530 (1000), 700 (500). EPR: $g_\perp$ = 1.99, $g_\parallel$ = 2.00, A = 36 G (100.9 MHz).

[Na(18c6)][Cp′$_3$Y]: Cp'_3Y (43 mg, 0.090 mmol) was reacted with a sodium smear in the presence of 18c6 (23 mg, 0.090 mmol) as described above for [Li(18c6)][Cp'_3Y] to yield a dark purple microcrystalline material (60. mg, 89%) consistent with [Na(18c6)][Cp'_3Y] based on UV-visible, IR, and EPR spectroscopies. Black, X-ray quality crystals of [(THF)Na_2(18c6)$_2$][Cp'_3Y]$_2$, **3-Y**, were grown from a concentrated solution in THF left at −35 °C over two nights. IR ῡ, cm^{-1}: 3054w, 2946w, 2889w, 1444w, 1400w, 1352m, 1295w, 1240m, 1181w, 1109s, 1037s, 959m, 905m, 825s, 748s, 718m, 684m. UV-vis λ_{max}, nm (ε, M^{-1} cm^{-1}): 390 (1100), 530 (1400), 700 (4500). EPR: $g_\perp$ = 1.99, $g_\parallel$ = 2.00, A = 36 G (100.9 MHz). *Anal. Calc.* for [Na(18c6)][Cp'_3Y] $C_{36}H_{63}NaO_6Si_3Y$: C, 54.87; H, 8.06. Found: C, 40.98; H, 5.69; N, 2.34. The low percentage values and found CH ratio ($C_{36}H_{60}$) close to the calculated ratio are consistent with incomplete combustion, as sometimes is the case with silicon-containing rare-earth complexes.[47-53]

[Rb(18c6)][Cp′$_3$Y]: Cp'_3Y (42 mg, 0.090 mmol) was reacted with a rubidium smear in the presence of 18c6 (23 mg, 0.090 mmol) as described above for [Li(18c6)][Cp'_3Y] to yield a dark purple microcrystalline material (68 mg, 95%) consistent with [Rb(18c6)][Cp'_3Y] based on UV-visible, IR, and EPR spectroscopies. IR ῡ, cm^{-1}: 3054w, 2946w, 2884m, 1471w, 1444w, 1401w, 1350m, 1284w, 1241m, 1181w, 1109s, 1037s, 959m, 905m, 825s, 748s, 718m, 684m. UV-vis λ_{max}, nm (ε, M^{-1} cm^{-1}): 390 (1600), 530 (1300), 700 (450). EPR: $g_\perp$ = 1.99, $g_\parallel$ = 2.00, A = 36 G (100.9 MHz).

[Cs(18c6)][Cp′$_3$Y]: Cp'_3Y(39 mg, 0.090 mmol) was reacted with a cesium smear in the presence of 18c6 (22 mg, 0.090 mmol) as described above for [Li(18c6)][Cp'_3Y] to yield a dark purple microcrystalline material (64 mg, 92%) consistent with [Cs(18c6)][Cp'_3Y] based on UV-visible, IR, and EPR spectroscopies. IR ῡ, cm^{-1}: 3044w, 2946w, 2884m, 1471w, 1444w, 1401w, 1350m, 1283w, 1241m, 1181w, 1109s, 1037s, 959m, 905m, 825s, 748s, 718m, 684m. UV-vis λ_{max}, nm (ε, M^{-1} cm^{-1}): 380 (2000), 530 (1400), 700 (450). EPR: $g_\perp$ = 1.99, $g_\parallel$ = 2.00, A = 36 G (100.9 MHz).

[K(DB18c6)][Cp′$_3$Y]: Cp′$_3$Y (46 mg, 0.090 mmol) was reacted with a potassium smear in the presence of DB18c6 (35 mg, 0.090 mmol) as described above for [Li(18c6)][Cp′$_3$Y] to yield a dark purple microcrystalline material (0.070, 85%) consistent with [K(DB18c6)][Cp′$_3$Y] based on UV-visible, IR, and EPR spectroscopies. IR ῡ, cm^{-1} (*I*): 3067w, 2948w, 2890w, 1595w, 1504m, 1453w, 1360w, 1324w, 1244s, 1213m, 1178m, 1126m, 1039m, 992w, 946m, 903m, 827s, 773s, 739s, 685m. UV-vis λ_{max}, nm (ε, M^{-1} cm^{-1}): 373 (1000), 530 (1200), 690 (500). EPR: $g_{\perp}$ = 1.99, $g_{\parallel}$ = 2.00, A = 36 G (100.9 MHz).

[K(THF)$_n$][Cp′$_3$Y]: Cp′$_3$Y (35 mg, 0.090 mmol) was reacted with a potassium smear in THF as described above for [Li(18c6)][Cp′$_3$Y], except without chelate, to yield a dark purple microcrystalline material (48 mg, 71% assuming n = 6) consistent with [K(THF)$_n$][Cp′$_3$Y] based on UV-visible and EPR spectroscopies. UV-vis λ_{max}, nm (ε, M^{-1} cm^{-1}): 391 (1400), 530 (1300), 700 (500). EPR: $g_{\perp}$ = 1.99, $g_{\parallel}$ = 2.00, A = 36 G (100.9 MHz).

[Na(crypt)][Cp′$_3$Y], 4-Y: Cp′$_3$Y (41 mg, 0.090 mmol) was reacted with a sodium smear in the presence of crypt (35 mg, 0.090 mmol) as described above for [Li(18c6)][Cp′$_3$Y] to yield a dark purple microcrystalline material (69 mg, 94%) consistent with [Na(crypt)][Cp′$_3$Y] based on UV-visible, IR, and EPR spectroscopies. Slow diffusion of pentane into a concentrated THF solution resulted in dark black X-ray quality crystals of **4-Y**. IR ῡ, cm^{-1}: 3075w, 2948w, 2865m, 2714w, 1444w, 1398w, 1360m, 1298w, 1242m, 1177w, 1104s, 1038s, 980w, 904m, 825s, 752s, 686m. UV-vis λ_{max}, nm (ε, M^{-1} cm^{-1}): 380 (1100), 530 (1300), 700 (500). EPR: $g_{\perp}$ = 1.99, $g_{\parallel}$ = 2.00, A = 36 G (100.9 MHz). *Anal. Calc.* for [Na(crypt)][Cp′$_3$Y] $C_{42}H_{75}N_2NaO_6Si_3Y$: C, 56.04; H, 8.04; N, 3.11. Found: C, 39.83; H, 6.14; N, 2.47. The low percentage values and found CHN ratio ($C_{42}H_{77}N_2$) close to the calculated ratio are consistent with incomplete combustion, as sometimes is the case with silicon-containing rare-earth complexes.[47-53]

X-ray Data Collection, Structure Solution, and Refinement for [(THF)Na$_2$(18c6)$_2$][Cp′$_3$Y^{II}]$_2$, 3-Y. A purple crystal of approximate dimensions 0.142 x 0.251 x 0.417 mm was mounted in a cryoloop and transferred to a Bruker SMART APEX II diffractometer system. The APEX2[54] program package was used to determine the unit-cell parameters and for data collection (40 sec/frame scan time). The raw frame data was processed using SAINT[55] and SADABS[56] to yield the reflection data file. Subsequent calculations

were carried out using the SHELXTL[57] program package. The diffraction symmetry was 2/*m* and the systematic absences were consistent with the monoclinic space group $P2_1/n$ that was later determined to be correct. The structure was solved by direct methods and refined on F^2 by full-matrix least-squares techniques. The analytical scattering factors[58] for neutral atoms were used throughout the analysis. Hydrogen atoms were included using a riding model. Least-squares analysis yielded wR2 = 0.0830 and Goof = 1.032 for 910 variables refined against 19528 data (0.78 Å), R1 = 0.0345 for those 16111 data with $I > 2.0\sigma(I)$.

X-ray Data Collection, Structure Solution, and Refinement for [Na(crypt)][Cp′$_3$Y], 4-Y. A black crystal of approximate dimensions 0.246 x 0.350 x 0.393 mm was mounted in a cryoloop and transferred to a Bruker SMART APEX II diffractometer system. The APEX2[54] program package was used to determine the unit-cell parameters and for data collection (30 sec/frame scan time). The raw frame data was processed using SAINT[55] and SADABS[56] to yield the reflection data file. Subsequent calculations were carried out using the SHELXTL[57] program package. The diffraction symmetry was 2/*m* and the systematic absences were consistent with the monoclinic space group $P2_1/n$ that was later determined to be correct. The structure was solved by direct methods and refined on F^2 by full-matrix least-squares techniques. The analytical scattering factors[58] for neutral atoms were used throughout the analysis. Hydrogen atoms were included using a riding model. Least-squares analysis yielded wR2 = 0.0816 and Goof = 1.009 for 505 variables refined against 13634 data (0.75 Å), R1 = 0.0347 for those 10924 data with $I > 2.0\sigma(I)$. There were several high residuals present in the final difference-Fourier map. It was probable that the residuals were due to disordered pentane solvent. The SQUEEZE[59] routine in the PLATON[60] program package was used to account for the electrons in the solvent accessible voids.

References

(1) Morss, L. R. Thermochemical Properties of Yttrium, Lanthanum, and the Lanthanide Elements and Ions. *Chem. Rev.* **1976**, *76*, 827–841. DOI: 10.1021/cr60304a007.

(2) Bochkarev, M. N. Molecular Compounds of "New" Divalent Lanthanides. *Coord. Chem. Rev.* **2004**, *248*, 835–851. DOI: 10.1016/j.ccr.2004.04.004.

(3) Nief, F. Non-classical Divalent Lanthanide Complexes. *Dalton Trans.* **2010**, *39*, 6589–6598. DOI: 10.1039/c001280g.

(4) Arnold, P. L.; Cloke, F. G. N.; Nixon, J. F. The First Stable Scandocene: Synthesis and Characterisation of bis(η-2,4,5-tri-*tert*-butyl-1,3-diphosphacyclopentadienyl)scandium(II). *Chem. Commun.* **1998**, *1*, 797–798. DOI: 10.1039/a800089a.

(5) Woen D. H. Evans W. J. Expanding the +2 Oxidation State to the Rare-Earth Metals, Uranium, and Thorium in Molecular Complexes. *Handbook on the Physics and Chemistry of the Rare Earths Including Actinides* **2016**, *50*, 337-394. DOI: 10.1016/bs.hpcre.2016.08.00

(6) Evans, W. J. Tutorial on the Role of Cyclopentadienyl Ligands in the Discovery of Molecular Complexes of the Rare-Earth and Actinide Metals in New Oxidation States. *Organometallics* **2016**, *35*, 3088–3100. DOI: 10.1021/acs.organomet.6b00466

(7) Hitchcock, P. B.; Lappert, M. F.; Maron, L.; Protchenko, A. V. Lanthanum Does Form Stable Molecular Compounds in the +2 Oxidation State. *Angew. Chem. Int. Ed.* **2008**, *47*, 1488–1491. DOI: 10.1002/anie.200704887.

(8) MacDonald M. R.; Ziller, J. W.; Evans, W. J. Synthesis of a Crystalline Molecular Complex of Y^{2+}, [(18-crown-6)K][$(C_5H_4SiMe_3)_3Y$]. *J. Am. Chem. Soc.* **2011**, *133*, 15914–15917. DOI: 10.1021/ja207151y.

(9) MacDonald, M. R.; Bates, J. E.; Ziller, J. W.; Furche, F.; Evans, W. J. Completing the Series of +2 Ions for the Lanthanide Elements: Synthesis of Molecular Complexes of Pr^{2+}, Gd^{2+}, Tb^{2+}, and Lu^{2+}. *J. Am. Chem. Soc.* **2013**, *135*, 9857−9868. DOI: 10.1021/ja403753j.

(10) Corbey, J. F.; Woen, D. H.; Palumbo, C. T.; Fieser, M. E.; Ziller, J. W.; Furche, F.; Evans, W. J. Ligand Effects in the Synthesis of Ln^{2+} Complexes by Reduction of Tris(cyclopentadienyl) Precursors Including C–H Bond Activation of an Indenyl Anion. *Organometallics* **2015**, *34*, 3909-3921. DOI: acs.organomet.5b00500.

(11) Moehring, S. A.; Beltrán-Leiva, M. J.; Arratia-Pérez, R.; Ziller, J. W.; Evans, W. J. Rare-Earth Metal(II) Aryloxides: Structure, Synthesis, and EPR Spectroscopy of [K(2.2.2-cryptand)][Sc(OC_6H_2-*t*Bu_2-2,6-Me-4)$_3$]. *Chem. Eur. J.* **2018**, *24*, 18059-18067. DOI: 10.1002/chem.201803807.

(12) Moehring, S. A.; Miehlich, M.; Hoerger, C. J.; Meyer, K.; Ziller, J. W.; Evans, W. J. A Room-Temperature Stable Y(II) Aryloxide: Using Steric Saturation to Kinetically Stabilize Y(II) Complexes. *Inorg. Chem.* **2020**, *59*, 3207–3214. DOI: 10.1021/acs.inorgchem.9b03587.

(13) Fang, M.; Lee, D. S.; Ziller, J. W.; Doedens, R. J.; Bates, J. E.; Furche, F.; Evans, W. J. Synthesis of the $(N_2)^{3-}$ Radical from Y^{2+} and Its Protonolysis Reactivity To Form $(N_2H_2)^{2-}$ via the Y[$N(SiMe_3)_2$]$_3$/KC_8 Reduction System. *J. Am. Chem. Soc.* **2011**, *133*, 3784–3787. DOI: 10.1021/ja1116827.

(14) Ryan, A. J.; Ziller, J. W.; Evans, W. J. The Importance of the Counter-Cation in Reductive Rare-Earth Metal Chemistry: 18-Crown-6 Instead of 2.2.2-Cryptand Allows Isolation of $[Y^{II}(NR_2)_3]^{1-}$ and Ynediolate and Enediolate Complexes from CO Reactions. *Chem. Sci.* **2020**, *11*, 2006–2014. DOI: 10.1039/c9sc05794c.

(15) Ariciu, A. M.; Woen, D. H.; Huh, D. N.; Nodaraki, L. E.; Kostopoulos, A. K.; Goodwin, C. A. P.; Chilton, N. F.; McInnes, E. J. L.; Winpenny, R. E. P.; Evans, W. J.; Tuna, F. Engineering Electronic Structure to Prolong Relaxation Times in Molecular Qubits by Minimising Orbital Angular Momentum. *Nat. Commun.* **2019**, *10*, 1–8. DOI: 10.1038/s41467-019-11309-3.

(16) Kotyk, C. M.; Fieser, M. E.; Palumbo, C. T.; Ziller, J. W.; Darago, L. E.; Long, J. R.; Furche, F.; Evans, W. J. Isolation of +2 Rare Earth Metal Ions with Three Anionic Carbocyclic Rings: Bimetallic Bis(Cyclopentadienyl) Reduced Arene Complexes of La^{2+} and Ce^{2+} Are Four Electron Reductants. *Chem. Sci.* **2015**, *6*, 7267–7273. DOI: 10.1039/c5sc02486b.

(17) Evans, W. J. Tutorial on the Role of Cyclopentadienyl Ligands in the Discovery of Molecular Complexes of the Rare-Earth and Actinide Metals in New Oxidation States. *Organometallics* **2016**, *35*, 3088–3100. DOI: 10.1021/acs.organomet.6b00466.

(18) Woen, D. H.; Chen, G. P.; Ziller, J. W.; Boyle, T. J.; Furche, F.; Evans, W. J. Solution Synthesis, Structure, and CO_2 Reduction Reactivity of a Scandium(II) Complex, $\{Sc[N(SiMe_3)_2]_3\}^-$. *Angew. Chem. Int. Ed.* **2017**, *56*, 2050–2053. DOI: 10.1002/anie.201611758.

(19) Fieser, M. E.; Palumbo, C. T.; La Pierre, H. S.; Halter, D. P.; Voora, V. K.; Ziller, J. W.; Furche, F.; Meyer, K.; Evans, W. J. Comparisons of Lanthanide/Actinide +2 Ions in a Tris(Aryloxide)Arene Coordination Environment. *Chem. Sci.* **2017**, *8*, 7424–7433. DOI: 10.1039/c7sc02337e.

(20) Palumbo, C. T.; Darago, L. E.; Windorff, C. J.; Ziller, J. W.; Evans, W. J. Trimethylsilyl versus Bis(Trimethylsilyl) Substitution in Tris(Cyclopentadienyl) Complexes of La, Ce, and Pr: Comparison of Structure, Magnetic Properties, and Reactivity. *Organometallics* **2018**, *37*, 900–905. DOI: 10.1021/acs.organomet.7b00881.

(21) Palumbo, C. T.; Halter, D. P.; Voora, V. K.; Chen, G. P.; Chan, A. K.; Fieser, M. E.; Ziller, J. W.; Hieringer, W.; Furche, F.; Meyer, K.; Evans, W. J. Metal versus Ligand Reduction in Ln^{3+} Complexes of a Mesitylene-Anchored Tris(Aryloxide) Ligand. *Inorg. Chem.* **2018**, *57*, 2823–2833. DOI: 10.1021/acs.inorgchem.7b03236.

(22) Ryan, A. J.; Darago, L. E.; Balasubramani, S. G.; Chen, G. P.; Ziller, J. W.; Furche, F.; Long, J. R.; Evans, W. J. Synthesis, Structure, and Magnetism of Tris(Amide) $[Ln\{N(SiMe_3)_2\}_3]^{1-}$ Complexes of the Non-Traditional +2 Lanthanide Ions. *Chem. Eur. J.* **2018**, *24*, 7702–7709. DOI: 10.1002/chem.201800610.

(23) Kelly, R. P.; Maron, L.; Scopelliti, R.; Mazzanti, M. Reduction of a Cerium(III) Siloxide Complex To Afford a Quadruple-Decker Arene-Bridged Cerium(II) Sandwich. *Angew. Chem. Int. Ed.* **2017**, *56*, 15663–15666. DOI: 10.1002/anie.201709769.

(24) Fang, M.; Bates, J. E.; Lorenz, S. E.; Lee, D. S.; Rego, D. B.; Ziller, J. W.; Furche, F.; Evans, W. J. $(N_2)^{3-}$ Radical Chemistry via Trivalent Lanthanide Salt/Alkali Metal Reduction of Dinitrogen: New Syntheses and Examples of $(N_2)^{2-}$ and $(N_2)^{3-}$ Complexes and Density Functional Theory Comparisons of Closed Shell Sc^{3+}, Y^{3+}, and Lu^{3+} versus $4f^9$ Dy^{3+}. *Inorg. Chem.* **2011**, *50*, 1459–1469. DOI: 10.1021/ic102016k.

(25) Bjorklund, J. L.; Pyrch, M. M.; Basile, M. C.; Mason, S. E.; Forbes, T. Z. Actinyl-Cation Interactions: Experimental and Theoretical Assessment of $[Np(vi)O_2Cl_4]^{2-}$ and $[U(vi)O_2Cl_4]^{2-}$ Systems. *Dalton Trans.* **2019**, *48*, 8861–8871. DOI: 10.1039/c9dt01753d.

(26) Zhang, H.; Wang, X.; Teo, B. K. Molecular Design and Crystal Engineering of a New Series of Inorganic Polymers Separated by Organic Spacers: Structures of [(18C6)K][$Cd(SCN)_3$] and $[(18C6)_2Na_2(H_2O)_2]_{1/2}[Cd(SCN)_3]$. *J. Am. Chem. Soc.* **1996**, *118*, 11813–11821. DOI: 10.1021/ja9605230.

(27) Toumi, H.; Amiri, N.; Belkhiria, M. S.; Daran, J. C.; Nasri, H. Di-μ-Azido-Bis(μ-1,4,7,10,13,16-Hexaoxacyclooctadecane)Bis(5,10,15, 20-Tetraphenylporphyrinato)Dicadmiumdisodium. *Acta Crystallogr. Sect. E Struct. Reports Online* **2012**, *E68*, m1557-m1558. DOI: 10.1107/S1600536812048052.

(28) Saenko, E. V.; Takahashi, K.; Feldman, V. I. EPR Evidence for a Physically Trapped Excess Electron in a Glassy Ionic Liquid. *J. Phys. Chem. Lett.* **2013**, *4*, 2896–2899. DOI: 10.1021/jz401292e.

(29) Kundu, K.; White, J. R. K.; Moehring, S. A.; Yu, J. M.; Ziller, J. W.; Furche, F.; Evans, W. J.; Hill, S. A 9.2-GHz Clock Transition in a Lu(II) Molecular Spin Qubit Arising from a 3,467-MHz Hyperfine Interaction. *Nat. Chem.* **2022**, *14*, 392–397. DOI: 10.1038/s41557-022-00894-4. (29)

(30) Moehring, S. A.; Evans, W. J. Evaluating Electron Transfer Reactivity of Rare-Earth Metal(II) Complexes Using EPR Spectroscopy. *Organometallics* **2020**, 39, 1187–1194. DOI: 10.1021/acs.organomet.9b00837.

(31) Smiles, D. E.; Wu, G.; Hayton, T. W. Synthesis of Uranium-Ligand Multiple Bonds by Cleavage of a Trityl Protecting Group. *J. Am. Chem. Soc.* **2014**, *136*, 96–99. DOI: 10.1021/ja411423a.

(32) Häfelinger G.; Streitwieser Jr. A.; Berechnungen Nach Dem Hiickelschen LCAO-MO-Verfahren Und Bandenzuordnungen. *Chem. Ber.* **1968**, *101*, 2785–2799. DOI: 10.1002/cber.19681010824.

(33) Langeslay, R. R.; Fieser, M. E.; Ziller, J. W.; Furche, F.; Evans, W. J. Synthesis, Structure, and Reactivity of Crystalline Molecular Complexes of the $\{[C_5H_3(SiMe_3)_2]_3Th\}^{1-}$ Anion Containing Thorium in the Formal +2 Oxidation State. *Chem. Sci.* **2015**, *6*, 517–521. DOI: 10.1039/c4sc03033h.

(34) La Pierre, H. S.; Scheurer, A.; Heinemann, F. W.; Hieringer, W.; Meyer, K. Synthesis and Characterization of a Uranium(II) Monoarene Complex Supported by δ Backbonding. *Angew. Chem. Int. Ed.* **2014**, *53*, 7158–7162. DOI: 10.1002/anie.201402050.

(35) Ryan, A. J.; Angadol, M. A.; Ziller, J. W.; Evans, W. J. Isolation of U(II) Compounds Using Strong Donor Ligands, C_5Me_4H and $N(SiMe_3)_2$, Including a Three-Coordinate U(II) Complex. *Chem. Commun.* **2019**, *55*, 2325–2327. DOI: 10.1039/c8cc08767a.

(36) Goodwin, C. A. P.; Chilton, N. F.; Natrajan, L. S.; Boulon, M. E.; Ziller, J. W.; Evans, W. J.; Mills, D. P. Investigation into the Effects of a Trigonal-Planar Ligand Field on the Electronic Properties of Lanthanide(II) Tris(Silylamide) Complexes (Ln = Sm, Eu, Tm, Yb). *Inorg. Chem.* **2017**, *56*, 5959–5970. DOI: 10.1021/acs.inorgchem.7b00664.

(37) Su, J.; Windorff, C. J.; Batista, E. R.; Evans, W. J.; Gaunt, A. J.; Janicke, M. T.; Kozimor, S. A.; Scott, B. L.; Woen, D. H.; Yang, P. Identification of the Formal +2 Oxidation State of Neptunium: Synthesis and Structural Characterization of $\{Np^{II}[C_5H_3(SiMe_3)_2]_3\}^{1-}$. *J. Am. Chem. Soc.* **2018**, *140*, 7425–7428. DOI: 10.1021/jacs.8b03907.

(38) Kumar, A.; Blakemore, J. D. On the Use of Aqueous Metal-Aqua pK_a Values as a Descriptor of Lewis Acidity. *Inorg. Chem.* **2021**, *60*, 1107–1115. DOI: 10.1021/acs.inorgchem.0c03239.

(39) Perrin, D. D.; Ionisation Constants of Inorganic Acids and Bases in Aqueous Solution. Pergamon: **1982**.

(40) Izatt, R. M.; Bradshaw, J. S.; Nielsen, S. A.; Lamb, J. D.; Christensen, J. J.; Sen, D. Thermodynamic and Kinetic Data for Cation-Macrocycle Interaction. *Chem. Rev.* **1985**, *85*, 271–339. DOI: 10.1021/cr00068a003.

(41) Kauffmann, E.; Lehn, J. -M.; Sauvage, J. -P. Enthalpy and Entropy of Formation of Alkali and Alkaline-Earth Macrobicyclic Cryptate Complexes. *Helv. Chim. Acta* **1976**, *59*, 1099–1111. DOI: 10.1002/hlca.19760590414.

(42) Izatt, R. M.; Terry, R. E.; Haymore, B. L.; Hansen, L. D.; Dallev, N. K.; Avondet, A. G.; Christensen, J. J. Calorimetric Titration Study of the Interaction of Several Uni- and Bivalent Cations with

15-Crown-5, 18-Crown-6, and Two Isomers of Dicyclohexo-18-crown-6 in Aqueous Solution at 25 °C and μ = 0.1. *J. Am. Chem. Soc.* **1976**, *98*, 7620–7626. DOI: 10.1021/ja00440a028.

(43) Lehn, J.-M.; Sauvage, J. P. Cryptates. XVI. [2]-Cryptates. Stability and selectivity of alkali and alkaline-earth macrobicyclic complexes. *J. Am. Chem. Soc.* **1975**, *97*, 6700–6707. DOI: 10.1021/ja00856a018.

(44) Wedal, J. C.; Barlow, J. M.; Ziller, J. W.; Yang, J. Y.; Evans, W. J. Electrochemical studies of tris(cyclopentadienyl)thorium and uranium complexes in the +2, +3, and +4 oxidation states. *Chem. Sci.* **2021**, *12*, 8501-8511. DOI: 10.1039/D1SC01906F.

(45) Kolthoff, I. M.; Chantooni, M. K., Jr. Relationship between transfer activity coefficients, ${}^{S1}\gamma^{S2}$, of cryptate 2.2.2 complexes and their stability constant in various solvents. *Proc. Natl. Acad. Sci. U.S.A.* **1980**, *77*, 5040–5042. DOI: 10.1073/pnas.77.9.5040.

(46) Neumann, W. P.; Uzick, W.; Zarkadis, A. K. Sterically hindered free radicals. 14. Substituent-dependent stabilization of para-substituted triphenylmethyl radicals. *J. Am. Chem. Soc.* **1986**, *108*, 3762. DOI: 10.1021/ja00273a034.

(47) Jenkins, T. F.; Woen, D. H.; Mohanam, L. N.; Ziller, J. W.; Furche, F.; Evans, W. J. Tetramethylcyclopentadienyl Ligands Allow Isolation of Ln(II) Ions across the Lanthanide Series in [K(2.2.2-cryptand)][$(C_5Me_4H)_3Ln$] Complexes. *Organometallics* **2018**, *37*, 3863–3873. DOI: 10.1021/acs.organomet.8b00557.

(48) Chilton, N. F.; Goodwin, C. A. P.; Mills, D. P.; Winpenny, R. E. P. The first near-linear bis(amide) f-block complex: A blueprint for a high temperature single molecule magnet. *Chem. Commun.* **2015**, *51*, 101–103. DOI: 10.1039/c4cc08312a.

(49) Goodwin, C. A. P.; Chilton, N. F.; Vettese, G. F.; Pineda, E. M.; Crowe, I. F.; Ziller, J. W.; Winpenny, R. E. P.; Evans, W. J.; Mills, D. P. Physicochemical Properties of Near-Linear Lanthanide(II) Bis(silylamide) Complexes (Ln = Sm, Eu, Tm, Yb). *Inorg. Chem.* **2016**, *55*, 10057–10067. DOI: 10.1021/acs.inorgchem.6b00808.

(50) Goodwin, C. A. P.; Reta, D.; Ortu, F.; Chilton, N. F.; Mills, D. P. Synthesis and Electronic Structures of Heavy Lanthanide Metallocenium Cations. *J. Am. Chem. Soc.* **2017**, *139*, 18714–18724. DOI: 10.1021/jacs.7b11535.

(51) Ortu, F.; Packer, D.; Liu, J.; Burton, M.; Formanuik, A.; Mills, D. P. Synthesis and structural characterization of lanthanum and cerium substituted cyclopentadienyl borohydride complexes. *J. Organomet. Chem.* **2018**, *857*, 45–51. DOI: 10.1016/j.jorganchem.2017.09.010.

(52) Huh, D. N.; Roy, S.; Ziller, J. W.; Furche, F.; Evans, W. J. Isolation of a Square-Planar Th(III) Complex: Synthesis and Structure of $[Th(OC_6H_2tBu_2\text{-}2,6\text{-}Me\text{-}4)_4]^{1-}$. *J. Am. Chem. Soc.* **2019**, *141*, 12458–12463. DOI: 10.1021/jacs.9b04399.

(53) Gabbaï, F. P.; Chirik, P. J.; Fogg, D. E.; Meyer, K.; Mindiola, D. J.; Schafer, L. L.; You, S. L. An Editorial about Elemental Analysis. *Organometallics* **2016**, *35*, 3255–3256. DOI: 10.1021/acs.organomet.6b00720.

(54) APEX2 Version 2014.11-0, Bruker AXS, Inc.; Madison, WI 2014.

(55) SAINT Version 8.34a, Bruker AXS, Inc.; Madison, WI 2013.

(56) Sheldrick, G. M. SADABS, Version 2014/5, Bruker AXS, Inc.; Madison, WI 2014.

(57) Sheldrick, G. M. SHELXTL, Version 2014/7, Bruker AXS, Inc.; Madison, WI 2014.

(58) International Tables for Crystallography 1992, Vol. C., Dordrecht: Kluwer Academic Publishers.

(59) Spek, A.L. PLATON SQUEEZE: a tool for the calculation of the disordered solvent contribution to the calculated structure factors, *Acta Cryst.* **2015**, *C71*, 9-19. DOI: 10.1107/S2053229614024929.

(60) Spek, A. L. Structure validation in chemical crystallography, *Acta. Cryst.* **2009**, *D65*, 148-155. DOI: 10.1107/S090744490804362X.

Chapter 2:

Synthesis and Characterization of Lanthanide-Containing Thin Films for the Construction of van der Waals Heterostructures

INTRODUCTION[†,§]

As part of an effort to expand upon alkali metal reductions conducted in the absence of organic chelates and to investigate the generation of layered structures, cesium-based reductions of rare-earth organometallic precursors were conducted. The results, including the synthesis of extended structures containing layered hexagonal nets and a collaboration aimed at determining if these crystals could be exfoliated to form thin film heterostructures, are described in this Chapter.

Thin films have garnered significant interest as they have been shown to exhibit unusual emergent properties.[1-6] The range of synthetic methods used to generate these materials includes chemical vapor deposition (CVD),[7] liquid exfoliation,[5,8] chemical growth,[9] spin-coating techniques (SCT),[10] layer-by-layer (LbL) assembly deposition,[11] and mechanical exfoliation of available layered solid-state materials.[12,13] Exfoliation is advantageous in that the bulk properties of a material can be elucidated prior to generation of thin films.

The materials most suitable for exfoliation to thin films are classified as van der Waals (vdW) materials, which are characterized as having layered solid-state structures in which there are strong bonds in two dimensions, but only weak interlayer interactions at distances greater than or equal to 3 Å in the third dimension.[14] Interest in this class of materials was sparked with the initial exfoliation of graphene,[12] and

---

† Portions of this chapter have been published: Moore, W. N. G.; McSorley, T. J.; Vincent, A.; Ziller, J. Z.; Jauregui, L. A.; Evans, W. J. Characterization and Exfoliation of a Layered Paramagnetic Tm(II) Compound Crystallized from Solution Phase. *ACS Appl. Nano Mater.* **2023**, *in press*. DOI: 10.1021/acsanm.3c00662.

§ Portions of this chapter have been published: Huh, D. N.; Ciccone, S. R.; Moore, W. N. G.; Ziller, J. W.; Evans, W. J. Synthesis of Ba(II) Analogs of Ln(II)-in-(2.2.2-Cryptand) and Layered Hexagonal Net Ln(II) Complexes, $[(THF)Cs(\mu\text{–}\eta^5\text{:}\eta^5\text{–}C_5H_4SiMe_3)_3Ln^{II}]_n$. *Polyhedron*, **2021**, *210*, 115393. DOI: 10.1016/j.poly.2021.115493.

subsequent studies of atomically thin layers increased significantly.[15] Several exfoliation methods have been developed, including micromechanical exfoliation with Scotch or Nitto low residue tape,[16] sonication,[17] and commercial blending.[18]

Solid-state compounds with layered structures like graphite, boron nitride, and transition-metal dichalcogenides (TMDs) are well-studied vdW materials, but the variety available is limited.[14] One way used to generate new layered materials is by stacking films of these precursor materials on top of each other.[19] The construction of thin film heterostructures from molecular precursors synthesized in solution is a less-explored area that has the potential to dramatically increase the array of possible compositions for thin films.[8] In addition, solution-phase chemistry could be used to rationally design the specific components of the thin films. This has some precedent for these known vdW materials[8] and would be beneficial to extend to new systems such as those that contain rare-earth metal ions. Rare-earth metal containing thin films synthesized via other methods are garnering interest as molecular sensors,[20] luminescent materials,[21] and spin liquid candidates.[22]

As part of a general effort to expand Ln(II) chemistry, an organometallic rare-earth compound, $[(THF)Cs(\mu\text{–}\eta^5\text{:}\eta^5\text{–}Cp')_3Yb^{II}]_n$, **5a-Yb** ($Cp' = C_5H_4SiMe_3$), was synthesized and found to have a layered structure (see Figure 2.3) that could potentially be exfoliated to form thin films.[23] Compound **5a-Yb** is one of several recent structures that crystallize with layers of hexagonal networks comprised of three M(II) ions (M = Ba, Yb, and U) and three Cs(I) ions connected by bridging Cp′ ligands.[24,25] The trimethylsilyl groups of the Cp′ ligand and the methylene groups of the bound THF molecules extend outwards perpendicular to the layer plane but do not form covalent bonds with other layers. The interlayer distance of approximately 1.8 Å between these functional groups is on the shorter side for a vdW material, but this crystal system seemed promising for exfoliation studies.

An initial investigation was undertaken to determine if this layered structure was robust in the face of differing solvation levels. As such, the results of subjecting **5a-Yb** to vacuum and crystallizing from a different solvent matrix are described herein. The resulting structure, $[Cs(\mu\text{–}\eta^5\text{:}\eta^5\text{–}Cp')_3Yb^{II}]_n$, **5b-Yb**, is reported here and compared with $[(THF)Cs(\mu\text{–}\eta^5\text{:}\eta^5\text{–}Cp')_3Ba^{II}(THF)]_n$[25] (**5-Ba**) and **5a-Yb**.

A subsequent investigation focused on adapting the synthesis to a paramagnetic Ln(II) metal center. Substituting diamagnetic Yb(II) with a paramagnetic analog was of interest because the hexagonal network incorporates these ions in a triangular orientation that offers the potential for spin frustration at low temperatures. In order to explore the exfoliation of this type of structure with an S = $^1/_2$ paramagnetic compound, rather than diamagnetic **5a-Yb**, the $4f^{13}$ Tm(II) analog, $[(THF)Cs(\mu\text{–}\eta^5\text{:}\eta^5\text{–}Cp')_3Tm^{II}]_n$, **5-Tm**, was synthesized. Reported here are the synthesis and X-ray crystal structure of **5-Tm**, its characterization by SQUID magnetometry as a $^2F_{7/2}$ Tm(II) compound, and its successful exfoliation to make a heterostructure with hexagonal boron nitride. Synthesizing otherwise inaccessible crystal lattices (heavy elements/rare earths/more complex geometries) that can be incorporated into a nanodevice/heterostructure with other two-dimensional layered materials inherently creates opportunities to study new materials.

RESULTS AND DISCUSSION

Solvation Level Investigation. $[(THF)Cs(\mu\text{–}\eta^5\text{:}\eta^5\text{–}Cp')_3Ba(THF)]_n$, **5-Ba**, was synthesized directly from BaI_2, KCp′, and excess Cs metal as shown in Figure 2.1. A THF suspension of BaI_2 was added to a THF solution of two equivalents of KCp′, stirred overnight, and then filtered into a vial containing a Cs metal smear. The colorless mixture was stored in a –35 °C freezer overnight and subsequently filtered into a layer of Et_2O. Colorless single crystals obtained the next day were structurally characterized as $[(THF)Cs(\mu\text{–}\eta^5\text{:}\eta^5\text{–}Cp')_3Ba(THF)]_n$. Since no net reduction by Cs was observed with barium, the reaction constitutes an unusual method to introduce a cesium cation to this complex. The reaction mechanism remains unknown.

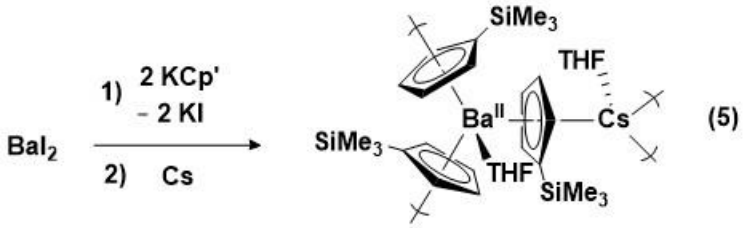

Figure 2.1. Synthetic scheme for the isolation of $[(THF)Cs(\mu\text{–}\eta^5\text{:}\eta^5\text{–}Cp')_3Ba(THF)]_n$ where curved brackets indicate the bounderies of the monomer unit.

The structure of $[(THF)Cs(\mu–\eta^5:\eta^5–Cp')_3Ba(THF)]_n$, **5-Ba**, is very similar to that of $[(THF)Cs(\mu–\eta^5:\eta^5–Cp')_3Yb^{II}]$,[23] **5a-Yb**, except that in **5-Ba** both Cs(I) and the Ba(II) ion have coordinated THF molecules. Both structures are composed of layers of hexagonal nets containing three Cs(I) ions and three M(II) ions.

Examination of the variable temperature ^{1}H NMR spectra of the Yb(II) complex $[(THF)Cs(\mu–\eta^5:\eta^5–Cp')_3Yb^{II}]_n$, **5a-Yb**, in THF suggested that an equilibrium exists between **5a-Yb** and $Cp'_2Yb^{II}(THF)_2$ and CsCp′. When **5a-Yb** was recrystallized from acetonitrile/diethyl ether, a solvent-free analog of the mono-THF **5a-Yb** and bis-THF **5-Ba** complexes was formed: $[Cs(\mu–\eta^5:\eta^5–Cp')_3Yb^{II}]_n$, **5b-Yb**, Figure 2.2. This crystal structure demonstrated that the layered motif could be accessed using solvent-based crystallization methods in three levels of solvation (0, 1, and 2 THF molecules present per formula unit) and that neither acetonitrile nor diethyl ether readily coordinated in the THF locations of **5a-Yb** and **5-Ba**.

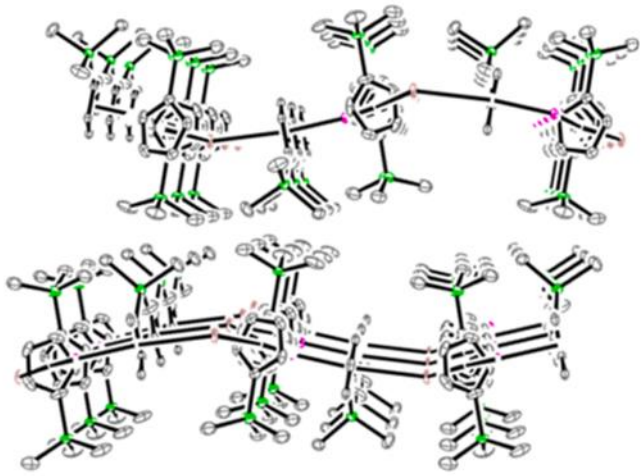

Figure. 2.2. Side view of the extended structure $[Cs(\mu–\eta^5:\eta^5–Cp')_3Yb^{II}]_n$, **5b-Yb**, where Cs = brown and Yb = magenta.

Metrical data on **5a-Yb**, **5b-Yb**, and **5-Ba** are presented in Table 2.1. The Yb-Cp'_{cent} (Cp'_{cent} = Cp′ ring centroid) distances in **5a-Yb** and **5b-Yb** are similar as expected for the similar coordination environments for Yb in each species. The Cs–Cp'_{cent} distances in **5a-Yb** and **5b-Yb** overlap, but the higher coordinated **5-Ba** has some longer distances as expected for a higher coordinate metal atom. The Ba–Cp'_{cent} distances are about 0.35 Å longer than the Yb–Cp'_{cent} distances in **5a-Yb** and **5b-Yb** which is a difference

close to the 0.28 Å larger size of Ba(II) and the 0.05 Å increase in bond distances that accompanies an increase by one of coordination number according to Shannon radii.[26]

Table 2.1. Summary of bond length (Å) ranges of select $[Cs(\mu–\eta^5:\eta^5–Cp')_3M]_n$ oligomeric complexes, **5a-Yb**, **5b-Yb**, and **5-Ba**, RMSD calculations (ω_{hex}, Å) for Cs(I)/M(II) hexagons, and dihedral angles (°).

	M(II)–Cp′$_{cent}$	Cs(I)–Cp′$_{cent}$	ω_{hex} (Å)	Dihedral Angle
$[(THF)Cs(\mu–\eta^5:\eta^5–Cp')_3Ba(THF)]_n$ **5-Ba**	2.852-2.875	3.202-3.244	0.697	29.70
$[(THF)Cs(\mu–\eta^5:\eta^5–Cp')_3Yb]_n$ **5a-Yb**	2.503-2.510	3.159-3.268	0.671	20.26
$[Cs(\mu–\eta^5:\eta^5–Cp')_3Yb]_n$ **5b-Yb**	2.510-2.523	3.141-3.183	0.500	12.89

To determine how the degree of THF solvation affected the planarity of the hexagonal rings, the root-mean-square deviations (RMSD) of the six metal vertices from the mean plane of their positions for **5a-Yb**, **5a-Yb** and **5-Ba** were calculated. The ω_{hex} = 0.697 Å value for the bis-THF **5-Ba** is remarkably similar to the ω_{hex} = 0.671 Å value for mono-THF **5a-Yb**. However, the ω_{hex} = 0.500 Å value for THF-free **5b-Yb** is much smaller, indicating a more planar structure.

To further assess the effect of THF on the corrugated nature of these structures, the dihedral angles between adjacent planes of six metal atom hexagons were measured. The solvent-free Yb structure **5b-Yb** yields a dihedral angle of 12.89°, and the mono-THF Yb structure **5a-Yb** yields a dihedral angle of 20.26°, consistent with the difference seen in the RMSD value. Interestingly, complex **5-Ba** shows a marked difference with respect to **5a-Yb**, in this case, with a greater dihedral angle of 29.70°. Together, these three structures demonstrate that the hexagonal layers can be reliably replicated with zero, one, and two coordinated THF molecules in the repeat units.

The structures can also be compared with $[Na(\mu–\eta^5:\eta^5–C_5H_5)_3Yb^{II}]_n$,[27] **6-Yb**, which can be generated by reduction of $(C_5H_5)_3Yb$ with sodium naphthalenide or by reaction of $(C_5H_5)_2Yb$ with $Na(C_5H_5)$. Complex **6-Yb** is an analog of **5b-Yb**, but with Na in place of Cs and unsubstituted C_5H_5 instead

of $C_5H_4SiMe_3$. Complex **6-Yb** differs from **5a-Yb**, **5b-Yb**, and **5-Ba** in that crystals were obtained by sublimation at 400 °C. Although **6-Yb** has an extended structure, it is a 3-dimensional structure and does not exist in layers. The difference in structure could be due to the different size of the alkali metal, the different method of crystallization, or the fact that **6-Yb** does not have the $SiMe_3$ groups that are found between the layers in **5a-Yb**, **5b-Yb**, and **5-Ba**. All of these differences provide bases upon which to test crystal engineering in this system in the future.

Synthesis and X-ray Crystal Structure of a Layered Tm(II) Complex. $[(THF)Cs(\mu\text{–}\eta^5\text{:}\eta^5\text{–}Cp')_3Tm^{II}]_n$, **5-Tm**, was synthesized by reduction of Cp'_3Tm^{III} with a cesium smear in THF at −35 °C (Figure 2.3), resulting in a color change from lime green to dark green/black. Crystallization by slow diffusion of Et_2O into a concentrated THF solution of **5-Tm** at −35 °C yielded dark green/black hexagonal blocks approximately 0.276 × 0.288 × 0.628 mm in size. Single crystal X-ray diffraction studies revealed that compound **5-Tm** (Figure 2.4) is isomorphous with compound **5a-Yb**.

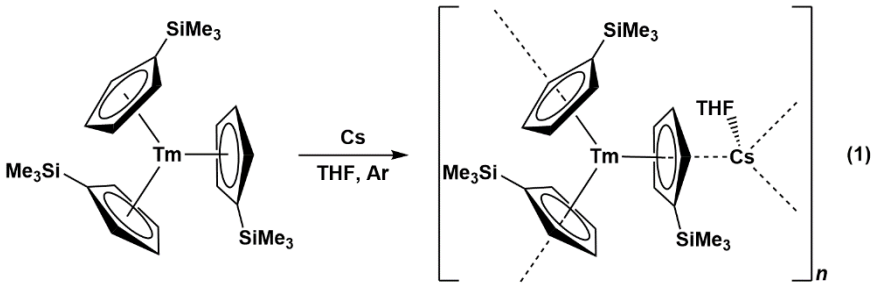

Figure 2.3. Synthesic scheme for the isolation of $[(THF)Cs(\mu\text{–}\eta^5\text{:}\eta^5\text{–}Cp')_3Tm]_n$, **5-Tm**.

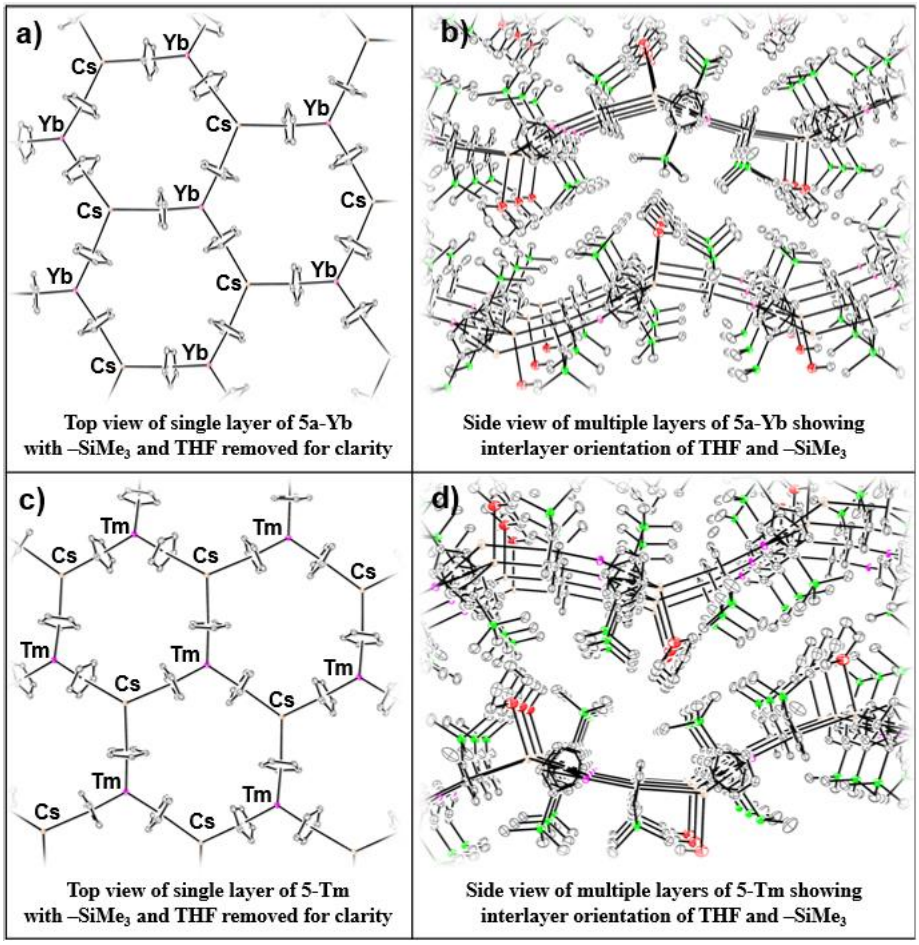

Figure 2.4. ORTEP of extended structures of both ([(THF)Cs(μ–η^5:η^5–Cp′)$_3$Yb^{II}]$_n$), **5a-Yb**, and ([(THF)Cs(μ–η^5:η^5–Cp′)$_3$Tm^{II}]$_n$), **5-Tm**. All displacement ellipsoids are drawn at the 50% probability level (magenta = Tm, pink = Yb, tan = Cs, green = Si, red = O).

The bond distances and angles in **5-Tm** are similar to those in **5a-Yb**, which is consistent with the similar radial size of Tm(II) and Yb(II). There are also metrical similarities between **2** and the closely related non-layered complex, [K(crypt)][Cp′$_3$Tm^{II}], **7-Tm**.[28] For example, the 2.501 Å Tm–Cp′$_{cnt}$ (Cp′$_{cnt}$ = centroid of Cp′) distance in **5-Tm** is similar to the Tm–Cp′$_{cnt}$ distances of 2.509 Å and 2.502 Å observed in **5a-Yb** and **7-Tm**, respectively. The layers in **5-Tm** are corrugated, as shown by the 20.17° dihedral angle between adjacent mean planes of six metal ions. Furthermore, the root-mean-square deviations (RMSD, ω_{hex}) of the six metal ions from the mean plane of their positions is ω_{hex} = 0.669 Å, versus ω_{hex} = 0 for a completely planar structure. These data are similar to those for the Yb(II) analog, **1**: ω_{hex} = 0.671 and

dihedral angle = 20.26°.[23] This observed consistency between **5a-Yb** and **5-Tm** demonstrates that the corrugated nature of the individual layers is not impacted by changing the M(II) center from Yb(II) to Tm(II).

Spectroscopic and Magnetic Properties. The solution-phase characterization of **5-Tm** via multinuclear NMR and UV-visible absorption spectroscopies was conducted in THF since **5-Tm** is insoluble in solvents such as diethyl ether, toluene, and hexanes and it is reactive towards other solvents such as acetonitrile and dimethylformamide. The UV-visible absorption spectrum of **5-Tm** features bands centered at 430 nm (ε = 600 $M^{-1}cm^{-1}$) and 645 nm (ε = 300 $M^{-1}cm^{-1}$), as well as a shoulder at 340 nm (ε = 700 $M^{-1}cm^{-1}$). The molar absorptivities are consistent with f→d Laporte allowed transitions typical for Tm(II) complexes.[28] The spectrum of **5-Tm** is quite similar to the spectrum of **7-Tm**, which displays absorbances at 416, 550, and 634 nm.[28] The Raman spectrum of **5-Tm** is silent from 0-2500 cm^{-1} using 405, 532, and 785 nm lasers.

The variable temperature magnetic susceptibility of **5-Tm** (Figure 2.4) was measured under applied fields of 0.1 T, 0.5 T, and 1 T to establish the ground state electron configuration of the thulium ions and to evaluate the exchange interactions present (Figure 2.4). The room temperature $\chi_M T$ product was found to be approximately 3.4 K·emu/mol under each of the three applied fields. Upon fitting these data sets in PHI,[29] the results were found to be consistent with a single unique ion in a $^2F_{7/2}$ electronic ground state possessing temperature-independent paramagnetism (TIP) along with weak intermolecular exchange on the order of 10^{-2} cm^{-1} (Figure 2.5). These results are consistent with a $4f^{13}$ thulium electron configuration, which is typical for other Tm(II)-containing complexes.[30] The vanishingly weak magnetic exchange observed was in line with expectations since the Tm(II) ions are spatially isolated from their nearest neighbors by two closed-shell Cp cyclopentadienyl ligands and a bridging Cs(I) ion.

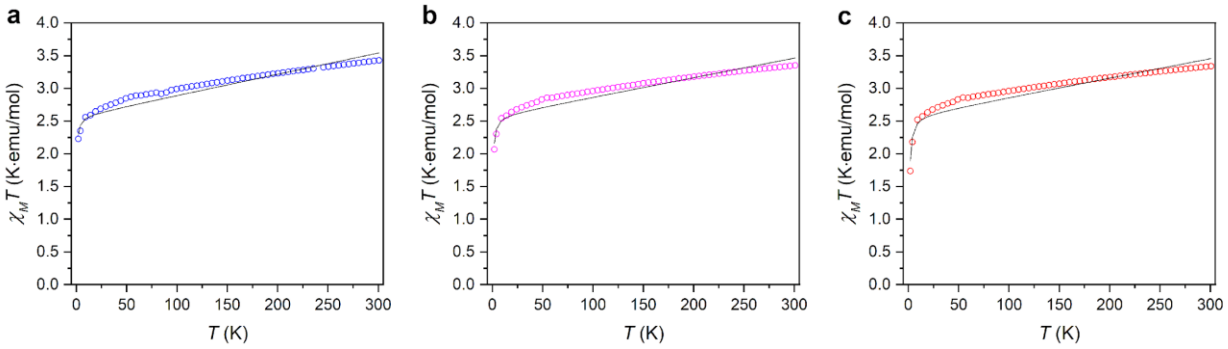

Figure 2.5. Variable temperature magnetic susceptibility of **5-Tm** from 2 to 300 K. Fitted curves are shown as black traces. Fits were obtained in a |J, M_J⟩ basis using Hamiltonian given in Figure 2.6. Open circles correspond to experimental data. Applied fields and fit parameters with their parenthesized uncertainties are reported. **a.** H = 0.1 T, zJ = −0.024(4) cm^{-1}, TIP = 0.00323(4) K·emu/mol; **b.** H = 0.5 T, zJ = −0.0312(4) cm^{-1}, TIP = 0.00297(4) K·emu/mol; **c.** H = 1 T, zJ = −0.043(6) cm^{-1}, TIP = 0.00295(4) K·emu/mol. The intermolecular interaction (zJ) between spins was modelled using the mean-field approximation as implemented in PHI.[29]

$$\hat{H} = g_l \mu_B \hat{J}_{Tm} \cdot \vec{B}$$

Figure 2.6. Hamiltonian used with the |J, M_J⟩ basis.

Despite the paramagnetic nature of **5-Tm**, ^{1}H and ^{133}Cs NMR spectra were observable. Resonances in the ^{1}H NMR spectrum of **5-Tm** are broadened with a full width half maximum (FWHM) of 230 Hz that is consistent with its paramagnetism. A single ^{133}Cs resonance is observed for **5-Tm** at −218.62 ppm, and it is nearly identical to that of the previously characterized Yb(II) analog (δ = −218.18 ppm).[24] This suggests that the cesium cations have similar chemical environments in solution. No signal was observed in the X-band CW EPR spectrum of **5-Tm** taken in perpendicular mode at 77 K which is consistent with the strong spin-orbit coupling associated with the anisotropic 4f^{13} electron configuration that induces relatively fast electron relaxation.

Exfoliation. In order to obtain thin layers of **5-Tm**, a sample of **5-Tm** was mechanically exfoliated using blue Nitto low residue tape under an argon atmosphere inside a glovebox. The tape was then adhered to a small slab of polydimethylsiloxane (PDMS) that was pre-cooled to −35 °C. Lowering the temperature

of the PDMS closer to its glass transition temperature has been shown to improve its adhesion properties.[31] After removing the tape from the cold PDMS, thin layers of **5-Tm** deposited on the surface of the PDMS. These layers were then transferred onto a SiO_2/Si substrate for further studies. After imaging several thin layers, films containing steps of different thicknesses were observed, demonstrating the layered nature of **5-Tm**, Figure 2.7.a. In order to protect the samples from exposure to water or oxygen, the exfoliated flakes were covered with hexagonal boron nitride (hBN) as shown in Figure 2.7.b. The Raman spectrum of the sample collected with a 532 nm laser displayed no absorbances between 100-2500 cm^{-1}, consistent with the spectrum of the bulk crystals.

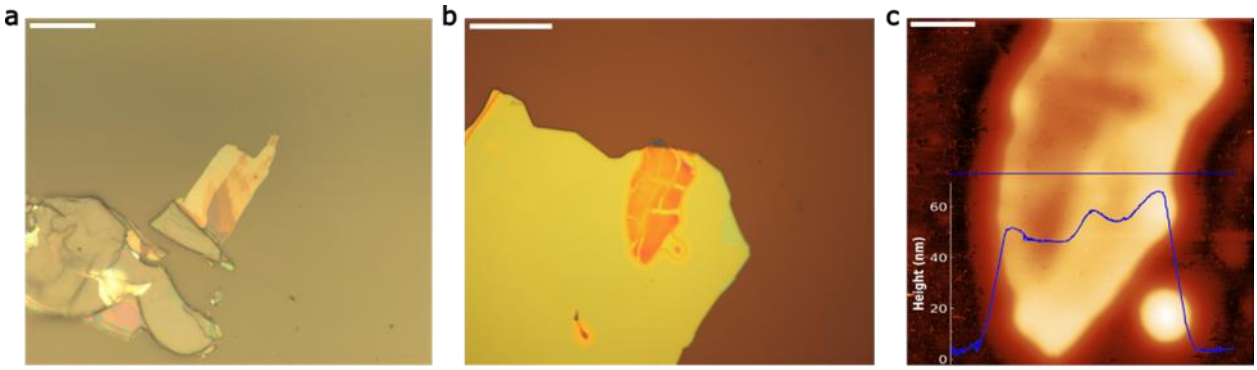

Figure 2.7. Characterization of thin layers of **5-Tm**. a. Optical image of a sample of exfoliated thin flakes of **5-Tm** on PDMS (sample a). Scale bar is 20 μm. b. Optical image of sample b encapsulated by hBN. Scale bar is 25 μm. c. AFM image of sample b. Inset shows step height along blue trace. Scale bar is 5 μm.

Atomic Force Microscopy (AFM). Topographical characterization of the sample in Figure 3b was performed using an atomic force microscope. This allowed an estimate of the number of layers within the hBN encapsulated flake. From the optical microscope images, differences in contrast indicated that the sample was composed of regions of varying thicknesses. In Figure 2.7.c, two plateaus of relatively constant thickness can be observed, one at 50 nm and another at 58 nm. With a single layer thickness of approximately 10 Å, this suggests that sample in Figure 3b is approximately 50 layers thick.

CONCLUSION

The synthesis of a layered paramagnetic Tm(II) compound, $[(THF)Cs(\mu–\eta^5:\eta^5–Cp'_3Tm^{II}]_n$, **5-Tm**, from the reduction of Cp'_3Tm^{III} with cesium in THF provided an opportunity to determine if heterostructures could be constructed from molecular species generated in solution. Compound **5-Tm** was fully characterized by single crystal X-ray crystallography, UV-visible and NMR spectroscopy, and magnetic measurements that show **5-Tm** is a $4f^{13}\ ^2F_{7/2}$ Tm(II) compound. Air- and moisture- sensitive single crystals of **5-Tm** were exfoliated to thin films (approximately 50 layers in thickness) and successfully covered with hexagonal boron nitride to make a heterostructure. This demonstrates the viability of using molecularly designed compounds of this type for the construction of heterostructures. Given the robust nature of complex **5-Tm** and the synthetic capability to tailor the lanthanide starting material, it is of interest to incorporate more magnetically interesting lanthanides into this system in the future.

EXPERIMENTAL

All manipulations and syntheses described below were conducted with the rigorous exclusion of air and water using standard Schlenk line and glovebox techniques under an argon atmosphere. Solvents were sparged with UHP argon and dried by passage through columns containing Q-5 and molecular sieves prior to use. Deuterated THF was dried for 1 week over NaK alloy, degassed by three freeze-pump-thaw cycles, and vacuum-transferred before use. ^1H and ^{133}Cs NMR spectra were recorded on a GN500 MHz spectrometer. The ^1H NMR spectrum was collected at 298 K and referenced internally to residual protio-solvent resonances. The ^{133}Cs spectrum was collected at 298 K and referenced to $CsNO_3$ following the recommended scale based on ratios of absolute frequencies.[32] UV−visible absorbance spectra were collected on an Agilent Cary 60 UV−vis spectrometer. Infrared spectra were collected on an Agilent Cary 630 spectrometer equipped with a diamond ATR attachment. EPR spectra were collected using the X-band frequency (9.3−9.8 GHz) on a Bruker EMX spectrometer equipped with an ER4119HS-W1 microwave bridge. Cesium (>99.5%, Aldrich) was used as received in the ampule sealed under argon. Cp'_3Tm and Cp'_3Yb were synthesized via literature procedures.[28]

All magnetic measurements were carried out on a Quantum Design MPMS-XL SQUID magnetometer. Under an atmosphere of argon, crystals of **5-Tm** were mechanically ground into a fine

powder, 12.0 mg of which was loaded into a quartz tube (inner diameter 5 mm, outer diameter 7 mm). The powder was covered with a solid layer of eicosane (50.3 mg) and flame-sealed under vacuum. The eicosane was subsequently melted at 45 °C in order to restrain the sample (prevent crystallite torquing) and to improve thermal conductivity between the sample and the environment. Diamagnetic corrections were calculated using Pascal's constants[33] and were applied to all reported magnetic susceptibility values unless otherwise noted.

[Cs(μ–η^5:η^5–Cp′)$_3$Yb]$_n$, 5b-Yb. Crystals of **5a-Yb** (50 mg, 0.06 mmol) were evacuated at room temperature for 30 min and subsequently dissolved in cold acetonitrile. Light blue crystals of **5b-Yb** (21 mg, 46%) were grown from slow vapor diffusion of Et_2O into the acetonitrile solution at − 35 ◦C over the course of 1 day. IR $\tilde{\upsilon}$, cm^{-1} : 3073w, 2947w, 2893w, 1438w, 1400w, 1353w, 1306w, 1242 m, 1176 m, 1035 m, 903 m, 824 s, 742 s, 680 m. UV–vis λ_{max}, nm (ε, $M^{-1}cm^{-1}$): 375 (950) and 610 (300). ^{1}H NMR δ, ppm (500 MHz, CD_3CN): 5.91 (s, 6H) , 5.79 (s, 6H), 0.12 (s, 27H). ^{133}Cs NMR δ, ppm (65 MHz, CD_3CN): −106.55 (s). Anal. Calcd. for [Cs(μ–η^5:η^5–Cp′)$_3$Yb]$_n$, $C_{24}H_{39}CsSi_3Yb$: C, 40.16; H, 5.48. Found: C, 38.57; H, 5.17. The incomplete combustion observed with this sample sometimes occurs with silicon-containing complexes,[34] but the observed CH ratio, $C_{24}H_{38}$, is close to the calculated.

[(THF)Cs(μ–η^5:η^5–Cp′)$_3$Tm]$_n$, 5-Tm. Under an argon atmosphere, a vial with Cp′$_3$Tm (45 mg, 0.080 mmol) dissolved in THF (1.5 mL) and a vial with a cesium smear were precooled to −35 °C. The light green THF solution of Cp′$_3$Tm was transferred by pipet into the vial containing the cesium smear, and the heterogeneous mixture was stirred for 5 min at room temperature, over which time the color changed to dark black/green. The solvent was removed in vacuo, and the remaining solids were washed with cold hexanes. Extraction with THF and removal of the solvent under reduced pressure yielded a black microcrystalline material (42 mg, 69%). Black crystals of [(THF)Cs(μ–η^5:η^5–Cp′)$_3$Tm]$_n$ that were suitable for study by single crystal X-ray crystallography were grown by slow vapor diffusion of Et_2O into a concentrated THF solution at −35 °C. ^{1}H NMR (500 MHz, THF-d_8): δ 19.81 (s, 6H), δ 5.51 (s, 6H), δ −0.05 (s, 27H). ^{133}Cs NMR (65 MHz, THF-d_8): δ −218.62 (s). IR ν, cm^{-1}: 3073w, 2947w, 2893w, 1438w, 1400w, 1353w, 1306w, 1242m, 1176m, 1035m, 903m, 824s, 742s, 680m. UV−visible λ_{max}, nm (ε,

$M^{-1}cm^{-1}$): 340 (700), 430 (600), 645 (300). Anal. Calcd for [(THF)Cs(μ–η^5:η^5–Cp′)$_3$Tm]$_n$, [$C_{28}H_{47}CsOSi_3Tm$]: C, 42.80; H, 6.03. Found: C, 35.65; H, 5.698. Incomplete combustion was observed as has been found in the past with complexes of this type,[35] but the observed CH ratio was $C_{28}H_{53}$.

Heterostructure Formation. h-BN crystals exfoliated via thermal release tape were transferred onto a stamp of PDMS by applying the tape to the surface of the stamp and peeling it off. A large uniform flake of hBN was optically located on the PDMS and subsequently transferred to a SiO_2/Si chip with recently exfoliated Tm(II) material. This was achieved by aligning both hBN and Tm(II) flakes, using a robotic transfer stage with 12 degrees of freedom inside an argon-filled glovebox. Once the flakes were aligned, the stamp was slowly lowered until the BN was in contact with the Tm(II) flakes. The system was heated to 80 °C, and the stamp was slowly lifted until out of contact. The hBN flake was left behind on top of the Tm(II) flake, encapsulating it.

X-ray Data Collection, Structure Solution, and Refinement for [Cs(μ–η^5:η^5–Cp′)$_3$Yb^{II}]$_n$. A blue crystal of approximate dimensions 0.078 x 0.169 x 0.214 mm was mounted in a cryoloop and transferred to a Bruker SMART APEX II diffractometer system. The APEX2[35] program package was used to determine the unit-cell parameters and for data collection (45 sec/frame scan time). The raw frame data was processed using SAINT[36] and SADABS[37] to yield the reflection data file. Subsequent calculations were carried out using the SHELXTL[38] program package. The diffraction symmetry was 2/*m* and the systematic absences were consistent with the monoclinic space group $P2_1/n$ that was later determined to be correct. The structure was solved by direct methods and refined on F^2 by full-matrix least-squares techniques. The analytical scattering factors[39] for neutral atoms were used throughout the analysis. Hydrogen atoms were included using a riding model. Disordered atoms were included using multiple components with partial site-occupancy-factors. Disordered carbon atoms C(6), C(7) and C(24) were refined with equivalent anisotropic displacement parameters (EADP)[38]. Least-squares analysis yielded wR2 = 0.0709 and Goof = 1.018 for 284 variables refined against 7928 data (0.75 Å), R1 = 0.0302 for those 6282 data with $I > 2.0\sigma(I)$. There were several high residuals present in the final difference-Fourier map. It was not possible to determine the nature of the residuals although it was probable that diethylether solvent

was present. The SQUEEZE[40] routine in the PLATON[41] program package was used to account for the electrons in the solvent accessible voids.

X-ray Data Collection, Structure Solution, and Refinement for [(THF)Cs(μ–η^5:η^5–Cp′)$_3$Tm^{II}]$_n$. A black crystal of approximate dimensions 0.276 x 0.288 x 0.628 mm was mounted in a cryoloop and transferred to a Bruker SMART APEX II diffractometer system. The APEX2[35] program package was used to determine the unit-cell parameters and for data collection (15 sec/frame scan time). The raw frame data was processed using SAINT[36] and SADABS[37] to yield the reflection data file. Subsequent calculations were carried out using the SHELXTL[38] program package. The diffraction symmetry was 2/*m* and the systematic absences were consistent with the monoclinic space group $P2_1/n$ that was later determined to be correct. The structure was solved by direct methods and refined on F^2 by full-matrix least-squares techniques. The analytical scattering factors[39] for neutral atoms were used throughout the analysis. Hydrogen atoms were included using a riding model. The structure was polymeric. Least-squares analysis yielded wR2 = 0.0647 and Goof = 1.141 for 316 variables refined against 9526 data (0.72 Å), R1 = 0.0279 for those 8548 data with I > 2.0σ(I).

References

(1) Novoselov, K. S.; Jiang, D.; Schedin, F.; Booth, T. J.; Khotkevich, V. V.; Morozov, S. V.; Geim, A. K. Two-Dimensional Atomic Crystals. *Proc. Natl. Acad. Sci. U. S. A.* **2005**, *102*, 10451–10453. DOI: 10.1073/pnas.0502848102.

(2) Novoselov, K. S.; Fal'Ko, V. I.; Colombo, L.; Gellert, P. R.; Schwab, M. G.; Kim, K. A Roadmap for Graphene. *Nature* **2012**, *490*, 192–200. DOI: 10.1038/nature11458.

(3) Lee, C.; Wei, X.; Kysar, J. W.; Hone, J. Measurement of the Elastic Properties and Intrinsic Strength of Monolayer Graphene. *Science* **2008**, *321*, 385–388. DOI: 10.1126/science.1157996.

(4) Peng, Y.; Li, Y.; Ban, Y.; Jin, H.; Jiao, W.; Liu, X.; Yang, W. Metal-Organic Framework Nanosheets as Building Blocks for Molecular Sieving Membranes. *Science* **2014**, *346*, 1356–1359. DOI: 10.1126/science.1254227.

(5) Nicolosi, V.; Chhowalla, M.; Kanatzidis, M. G.; Strano, M. S.; Coleman, J. N. Liquid Exfoliation of Layered Materials. *Science* **2013**, *340*, 72–75. DOI: 10.1126/science.1226419.

(6) Bradshaw, D.; Garai, A.; Huo, J. Metal–Organic Framework Growth at Functional Interfaces: Thin Films and Composites for Diverse Applications. *Chem. Soc. Rev.* **2012**, *41*, 2344–2381. DOI: 10.1039/c1cs15276a.

(6) Ajayan, P.; Kim, P.; Banerjee, K. Two-Dimensional van Der Waals Materials. *Phys. Today* **2016**, *69*, 38–44. DOI: 10.1063/PT.3.3297.

(7) Tang, L.; Tan, J.; Nong, H.; Liu, B.; Cheng, H. M. Chemical Vapor Deposition Growth of Two-Dimensional Compound Materials: Controllability, Material Quality, and Growth Mechanism. *Acc. Mater. Res.* **2021**, *2*, 36–47. DOI: 10.1021/accountsmr.0c00063.

(8) Han, J. H.; Kwak, M.; Kim, Y.; Cheon, J. Recent Advances in the Solution-Based Preparation of Two- Dimensional Layered Transition Metal Chalcogenide Nanostructures. *Chem. Rev.* **2018**, *118*, 6151–6188. DOI: 10.1021/acs.chemrev.8b00264.

(9) Bonilla, M.; Kolekar, S.; Ma, Y.; Diaz, H. C.; Kalappattil, V.; Das, R.; Eggers, T.; Gutierrez, H. R.; Phan, M. H.; Batzill, M. Strong Roomerature Ferromagnetism in VSe_2 Monolayers on van Der Waals Substrates. *Nat. Nanotechnol.* **2018**, *13*, 289–293. DOI: 10.1038/s41565-018-0063-9.

(10) Polai, B.; Satpathy, B. K.; Jena, B. K.; Nayak, S. K. An Overview of Coating Processes on Metal Substrates Based on Graphene-Related Materials for Multifarious Applications. *Ind. Eng. Chem. Res*. **2022**, *61*, 13763–13786. DOI: 10.1021/acs.iecr.2c02147.

(11) Santos, J. C. C.; Pramudya, Y.; Krstić, M.; Chen, D. H.; Neumeier, B. L.; Feldmann, C.; Wenzel, W.; Redel, E. Halogenated Terephthalic Acid “Antenna Effects” in Lanthanide-SURMOF Thin Films. *ACS Appl. Mater.* **2020**, *12*, 52166–52174. DOI: 10.1021/acsami.0c15392.

(12) Novoselov, K. S.; Geim, A. K.; Morozov, S. V.; Jiang, D.; Zhang, Y.; Dubonos, S. V.; Grigorieva, I. V.; Firsov, A. A. Electric Field in Atomically Thin Carbon Films. *Science* **2004**, *306*, 666–669. DOI: 10.1126/science.1102896.

(13) Wang, Y.; Ziebel, M. E.; Sun, L.; Gish, J. T.; Pearson, T. J.; Lu, X. Z.; Thorarinsdottir, A. E.; Hersam, M. C.; Long, J. R.; Freedman, D. E.; Rondinelli, J. M.; Puggioni, D.; Harris, T. D. Strong Magnetocrystalline Anisotropy Arising from Metal-Ligand Covalency in a Metal-Organic Candidate for 2D Magnetic Order. *Chem. Mater.* **2021**, *33*, 8712–8721. DOI: 10.1021/acs.chemmater.1c02670.

(14) Duong, D. L.; Yun, S. J.; Lee, Y. H. Van Der Waals Layered Materials: Opportunities and Challenges. *ACS Nano* **2017**, *11*, 11803–11830. DOI: 10.1021/acsnano.7b07436.

(15) Bhimanapati, G. R.; Lin, Z.; Meunier, V.; Jung, Y.; Cha, J.; Das, S.; Xiao, D.; Son, Y.; Strano, M. S.; Cooper, V. R.; Liang, L.; Louie, S. G.; Ringe, E.; Zhou, W.; Kim, S. S.; Naik, R. R.; Sumpter, B. G.; Terrones, H.; Xia, F.; Wang, Y.; Zhu, J.; Akinwande, D.; Alem, N.; Schuller, J. A.; Schaak, R. E.; Terrones, M.; Robinson, J. A. Recent Advances in Two-Dimensional Materials beyond Graphene. *ACS Nano* **2015**, *9*, 11509–11539. DOI: 10.1021/acsnano.5b05556.

(16) Chahal, S.; Ranjan, P.; Motlag, M.; Yamijala, S. S. R. K. C.; Late, D. J.; Sadki, E. H. S.; Cheng, G. J.; Kumar, P. Borophene via Micromechanical Exfoliation. *Adv. Mater.* **2021**, *33*, 1–13. DOI: 10.1002/adma.202102039.

(17) Gosch, J.; Synnatschke, K.; Stock, N.; Backes, C. Comparative Study of Sonication-Assisted Liquid Phase Exfoliation of Six Layered Coordination Polymers. *Chem. Commun.* **2022**, *11*, 55–58. DOI: 10.1039/d2cc03366f.

(18) Ng, K. L.; Maciejewska, B. M.; Qin, L.; Johnston, C.; Barrio, J.; Titirici, M.-M.; Tzanakis, I.; Eskin, D. G.; Porfyrakis, K.; Mi, J.; Grobert, N. Direct Evidence of Exfoliation Efficiency and Graphene Dispersibility of Green Solvents towards Sustainable Graphene Production. *ACS Sustainable Chem. Eng.* **2023**, 11, 58–66. DOI: acssuschemeng.2c03594.

(19) Meng, J.; Wang, D.; Cheng, L.; Gao, M.; Zhang, X. Recent Progress in Synthesis, Properties, and Applications of Hexagonal Boron Nitride-Based Heterostructures. *Nanotechnology* **2019**, *30*. DOI: 10.1088/1361-6528/aaf301.

(20) Qu, X. L.; Yan, B. Ln(III)-Functionalized Metal-Organic Frameworks Hybrid System: Luminescence Properties and Sensor for Trans, Trans-Muconic Acid as a Biomarker of Benzene. *Inorg. Chem.* **2018**, *57*, 7815–7824. DOI: 10.1021/acs.inorgchem.8b00912.

(21) Chen, P.; Xu, X.; Li, D.; Li, Z.; Wang, H.; Pi, L.; Zhou, X.; Zhai, T. 2D Van Der Waals Rare Earth Material Based Ratiometric Luminescence Thermography Integrated on Micro–Nano Devices Vertically. *Adv. Opt. Mater.* **2022**, *10*, 1–8. DOI: 10.1002/adom.202102102.

(22) Chamorro, J. R.; McQueen, T. M.; Tran, T. T. Chemistry of Quantum Spin Liquids. *Chem. Rev.* **2021**, *121*, 2898–2934. DOI: 10.1021/acs.chemrev.0c00641.

(23) Huh, D. N.; Ziller, J. W.; Evans, W. J. Crystal Structure of the $[(THF)Cs(\mu\text{-}\eta^5\text{:}\eta^5\text{-}Cp')_3Yb]_n$ Oligomer. *Acta Crystallogr. Sect. E Crystallogr. Commun.* **2020**, *76*, 1131–1135. DOI: 10.1107/S2056989020008051.

(24) Huh, D. N.; Ciccone, S. R.; Moore, W. N. G.; Ziller, J. W.; Evans, W. J. Synthesis of Ba(II) Analogs of Ln(II)-in-(2.2.2-Cryptand) and Layered Hexagonal Net Ln(II) Complexes, $[(THF)Cs(\mu\text{–}\eta^5\text{:}\eta^5\text{–}C_5H_4SiMe_3)_3Ln^{II}]_n$. *Polyhedron* **2021**, *210*, 115493. DOI: 10.1016/j.poly.2021.115493.

(25) Huh, D. N.; Ziller, J. W.; Evans, W. J. Chelate-Free Synthesis of the U(II) Complex, $[(C_5H_3(SiMe_3)_2)_3U]^{1-}$, Using Li and Cs Reductants and Comparative Studies of La(II) and Ce(II) Analogs. *Inorg. Chem.* **2018**, *57*, 11809–11814. DOI: 10.1021/acs.inorgchem.8b01966.

(26) Shannon, R. D. Revised effective ionic radii and systematic studies of interatomic distances in halides and chalcogenides, *Acta Cryst.*, **1976**, *A32*, 751-767. DOI: 10.1107/S0567739476001551.

(27) Apostolidis, C.; Deacon, G. B.; Dornberger, E.; Edelmann, F. T.; Kanellakopulos, B.; MacKinnon, P.; Stalke, D. Crystallization and X-Ray Structures of $[NaYb(C_5H_5)_3]$ and $Yb(C_5H_5)_2$. *Chem. Commun.* **1997**, *94*, 1047–1048. DOI: 10.1039/a700531h.

(28) Fieser, M. E.; Macdonald, M. R.; Krull, B. T.; Bates, J. E.; Ziller, J. W.; Furche, F.; Evans, W. J. Structural, Spectroscopic, and Theoretical Comparison of Traditional vs Recently Discovered Ln^{2+} Ions in the $[K(2.2.2\text{-Cryptand})][(C_5H_4SiMe_3)_3Ln]$ Complexes: The Variable Nature of Dy^{2+} and Nd^{2+}. *J. Am. Chem. Soc.* **2015**, *137*, 369–382. DOI: 10.1021/ja510831n.

(29) Chilton, N. F.; Anderson, R. P.; Turner, L. D.; Soncini, A.; Murray, K. S. PHI: A Powerful New Program for the Analysis of Anisotropic Monomeric and Exchange-Coupled Polynuclear d- and f-Block Complexes. *J. Comput. Chem.* **2013**, *34*, 1164–1175. DOI: 10.1002/jcc.23234.

(30) Moutet, J.; Schleinitz, J.; La Droitte, L.; Tricoire, M.; Pointillart, F.; Gendron, F.; Simler, T.; Clavaguéra, C.; Le Guennic, B.; Cador, O.; Nocton, G. Bis-Cyclooctatetraenyl Thulium(II): Highly Reducing Lanthanide Sandwich Single-Molecule Magnets. *Angew. Chem. Int. Ed.* **2021**, *60*, 6042–6046. DOI: 10.1002/anie.202015428.

(31) Clarson, S. J.; Dodgson, K.; Semlyen, J. A. Studies of cyclic and linear poly(dimethylsiloxanes): 19. Glass transition temperatures and crystallization behaviour. *Polymer*, **1985**, *26*, 930–934. DOI: 10.1016/0032-3861(85)90140-5.

(32) Harris, R.K.; Becker, E.D.; Cabral De Menezes, S.M.; Granger, P.; Hoffman, R.E.; Zilm, K.W. Further conventions for NMR shielding and chemical shifts: (IUPAC recommendations 2008). *Pure Appl. Chem.* **2008**, *80*, 59–84.

(33) Bain, G. A.; Berry, J. F. Diamagnetic Corrections and Pascal's Constants. *J. Chem. Educ.* **2008**, *85*, 532–536. DOI: 10.1021/ed085p532.

(34) Ortu, F.; Packer, D.; Liu, J.; Burton, M.; Formanuik, A.; Mills, D. P. Synthesis and structural characterization of lanthanum and cerium substituted cyclopentadienyl borohydride complexes. *J. Organomet. Chem.* **2018**, *857*, 45–51. DOI: 10.1016/j.jorganchem.2017.09.010.

(35) APEX2 Version 2014.11-0, Bruker AXS, Inc.; Madison, WI 2014.

(36) SAINT Version 8.34a, Bruker AXS, Inc.; Madison, WI 2013.

(37) Sheldrick, G. M. SADABS, Version 2014/5, Bruker AXS, Inc.; Madison, WI 2014.

(38) Sheldrick, G. M. SHELXTL, Version 2014/7, Bruker AXS, Inc.; Madison, WI 2014.

(39) International Tables for Crystallography 1992, Vol. C., Dordrecht: Kluwer Academic Publishers.

(40) Spek, A.L. PLATON SQUEEZE: a tool for the calculation of the disordered solvent contribution to the calculated structure factors, *Acta Cryst.* **2015**, *C71*, 9-19. DOI: 10.1107/S2053229614024929.

(41) Spek, A. L. Structure validation in chemical crystallography, *Acta. Cryst.* **2009**, *D65*, 148-155. DOI: 10.1107/S090744490804362X.

Chapter 3:

Reduction of Rare-Earth Metal Complexes Induced by Gamma Irradiation

INTRODUCTION†

As described in Chapter 1, one of the major advances in the chemistry of the rare-earth elements (Ln), i.e., scandium, yttrium, and the lanthanides, was the discovery that the +2 oxidation state was not only accessible for Eu(II), Yb(II), Sm(II), Tm(II), Dy(II), and Nd(II)[1-5] but also for all the other rare-earth metals except radioactive promethium.[6-9] The new Ln(II) ions were frequently generated in trigonal ligand environments in which a d_{z^2} orbital was populated to give $3d^1$ (Sc), $4d^1$ (Y), and $4f^n5d^1$ (lanthanides) electron configurations.[5,9,10] These new Ln(II) species are of interest not only due to their highly reducing reactivity,[11-16] but also due to their physical properties.[17-19] Synthesis of complexes of the new Ln(II) ions generally require sub-ambient temperatures and short reaction times. Although many examples of $4f^n5d^1$ Ln(II) complexes are now known, reduction of some Ln(III) precursors with alkali metals yield only fleeting color changes and the Ln(II) products have evaded definitive characterization.[20-22] Therefore, it was of interest to explore alternative methods for generating Ln(II) complexes.

Alternative reduction methods were also desirable because the discovery of molecular complexes of the new Ln(II) ions raised the question about the potential availability of molecular complexes containing Ln(I) ions.[23,24] Since crystallographically characterized Ln(0) complexes, Ln(3,5–tri–tert–butylbenzene)$_2$ for Ln = Sc, Y, Gd, and Ho are known[25-27] as well as an example of a Sc(I) compound, [{(η^5–$P_3C_2{}^tBu_2$)Sc}$_2$(μ–η^6:η^6–$P_3C_3{}^tBu_3$)],[28] the pursuit of molecular Ln(I) coordination compounds for other rare-earth metals was an intriguing target.

In fact, gamma irradiation was used in 1966 to provide evidence for formation of Sm(I) ions in a KCl matrix. By subjecting single crystals of Sm(II) doped into a KCl matrix grown from a melt phase to

† Portions of this chapter have been published: Moore, W. N. G.; White, J. R. K.; Wedal, J. C.; Furche, F.; Evans, W. J. Reduction of Rare-Earth Metal Complexes Induced by γ Irradiation. *Inorg. Chem.* **2022**, *61*, 17713-17718. DOI: 10.1021/acs.inorgchem.2c02857

gamma irradiation on the order of 2-20 Mrad (20 – 200 Gy), data were collected that suggested reduction of Sm(II) to Sm(I).[29] Specifically, the growth of an absorption in the UV-visible region at 545 nm occurred at an identical rate to the decrease in absorptions at 418 and 620 nm, known to correspond to Sm(II), and the paramagnetic susceptibility decreased from $7.4 \times 10^{-7} + 1.1 \times 10^{-6}/T$ to $5.7 \times 10^{-7} + 1.1 \times 10^{-6}/T$.

In the 1960's, Ln(III) ions doped into MF_2 matrices (M = Ca, Sr, Ba) were also reduced by subjecting them to gamma irradiation; the resulting UV-visible absorption spectra were assigned to Ln(II) ions for the whole lanthanide series.[30,31] Subsequent studies have shown that gamma irradiation of glasses containing Sm(III) ions results in reduction to Sm(II) ions based on UV-visible spectroscopy.[32,33] These glasses are typically prepared using a conventional melt/quench process and use Sm_2O_3 as the samarium starting material. Upon gamma irradiation of the glasses using dosages on the order of 3-20 Mrad (30 – 200 Gy), UV-visible spectroscopy usually shows a single peak around 320 nm corresponding to a 4f–5d transition typical of a Sm(II) ion.[32]

Since these previous crystal lattice and glassy matrix rare-earth metal studies required high temperature melt/quench techniques to prepare the precursors, they were not extendable to molecular species of lower thermal stability. However, gamma irradiation-based cryoreduction had previously been successful in bioinorganic systems[34-39] and thus the extension to molecular rare-earth metal complexes seemed reasonable. In this Chapter, the viability of gamma irradiation of frozen solutions of molecular rare-earth metal species as a method to generate reactive Ln(II) species is described. These preliminary studies demonstrate the viability of the method and identify a new La(II) complex previously inaccessible in solution. Sc ($I = {}^7/_2$), Y ($I = ½$), and La ($I = {}^7/_2$) were the rare-earth metals chosen for this study, since their d^1 Ln(II) ions exhibit definitive EPR spectra due to coupling to their nuclear spins.

EXPERIMENTAL

All manipulations and syntheses described below were conducted with the rigorous exclusion of air and water using standard Schlenk line and glovebox techniques under an argon atmosphere. 2-MeTHF was transferred onto dry 3 Å molecular sieves and degassed *in vacuo* until solvent evaporation was observed. UV-visible absorbance spectra were collected on an Agilent Cary 60 UV-vis. EPR spectra were

collected using the X-band frequency (9.3−9.8 GHz) on a Bruker EMX spectrometer equipped with an ER4119HS-W1 microwave bridge. $Sc^{III}(NR_2)_3$,[40] Cp'_3Y^{III},[7] Cp'_3La^{III},[41] and $La^{III}(NR_2)_3$[40] were synthesized via literature procedures.

General Gamma Irradiation Procedure. In an argon-filled glovebox, 0.3 mL of a 0.05-0.5 M solution of the Ln(III) starting material in 2-methyltetrahydrofuran (2-MeTHF) was transferred by pipet into an EPR tube. The tube was sealed with a rubber septum, removed from the inert atmosphere glove box, and further sealed by wrapping with parafilm. The tube was then *rapidly* (within one second) inserted into a Dewar filled with liquid nitrogen because slow insertion led to poor solvent glassing and inhibited characterization attempts. The Dewar was then exposed to 700 keV gamma irradiation from a ^{137}Cs source in the UCI Nuclear Reactor Facility (see Figure 3.1 for brief workflow diagram). *Caution!* Gamma irradiation is an ionizing form of electromagnetic irradiation that may cause biological damage. Studies must be conducted using appropriate radiological safety equipment and procedures. Following irradiation, continuous wave, X-band EPR spectra were collected at 77 K in perpendicular mode.

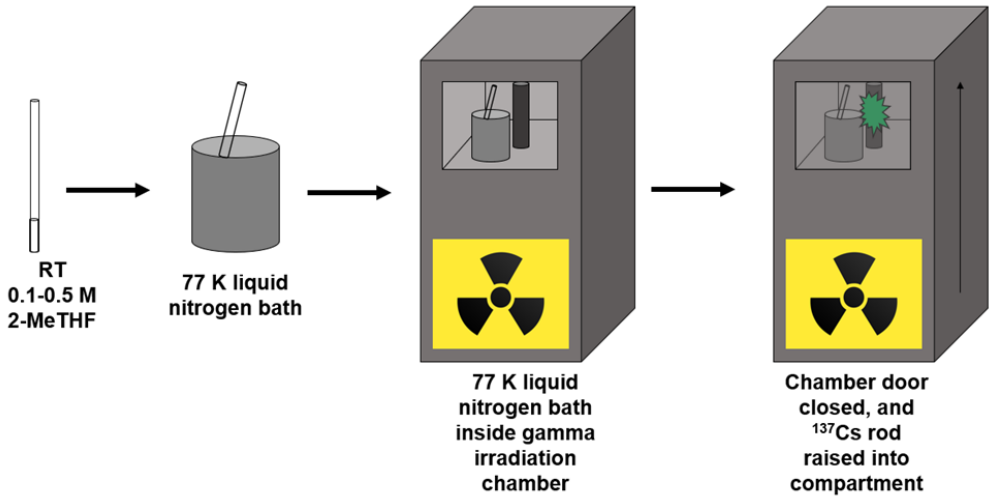

Figure 3.1. Simplified workflow diagram of gamma irradiation procedure.

The following procedure was utilized to collect UV-visible spectra on the irradiated samples. A finger Dewar was half-filled with liquid nitrogen and clamped so that the finger was as close as possible to the detection slit of an Agilent Cary 60 UV-visible spectrophotometer while remaining vertical. The finger

was subjected to a stream of nitrogen gas from a high pressure cylinder to prevent condensation of atmospheric water. The sample EPR tube was inserted into the finger Dewar and a spectrum was collected at a scan rate of 300 nm/min. Two more spectra were collected sequentially using the same rate and the spectra were averaged. The final spectrum was obtained by subtracting the average spectrum of irradiated 2-MeTHF.

RESULTS AND DISCUSSION

Gamma Irradiation of 2-MeTHF. A control sample with no added Ln(III) compound was exposed to 16 h of gamma irradiation (about 2 Mrad or 20 Gy total). EPR spectroscopy at 77 K revealed the intense isotropic signal (g_{iso} = 2.002) associated with irradiated organic solvents.[34-39] UV-visible spectroscopy of the sample showed a broad absorption increasing beyond the 1000 nm limit of the spectrometer, which is consistent with known irradiated samples of 2-MeTHF, λ_{max} = 2150 nm ($\varepsilon = 3.9 \times 10^4\ M^{-1}cm^{-1}$).[42] Attempts to minimize the organic radical EPR signal in irradiated rare-earth metal samples without perturbing the Ln(II) signal (see below) via photobleaching and annealing at 195 K and 174 K were unsuccessful: only a weak organic radical signal was observed and no signal from the Ln(II) ion. Attempts to subtract the EPR spectrum of irradiated 2-MeTHF collected after identical irradiation periods were also unsuccessful. On the other hand, UV-visible absorption spectroscopy allowed for relatively simple background subtraction. Radical absorption could be subtracted in a straightforward manner by irradiating samples of pure 2-MeTHF along with the rare-earth samples of interest for the same amount of time and subtracting the irradiated solvent spectrum.

Gamma Irradiation of Ln(III) Compounds with Known Ln(II) Analogs. The Ln(III) compounds $Sc^{III}(NR_2)_3$, Cp'_3Y^{III}, and Cp'_3La^{III} (R = $SiMe_3$, Cp′ = $C_5H_4SiMe_3$) were chosen to probe the viability of the method, since their corresponding Ln(II) compounds have been chemically isolated, exhibit distinctive EPR spectra, and have UV-visible spectra with distinctive absorptions.[7,10,12,21] The known EPR spectra of $[Sc^{II}(NR_2)_3]^{1-}$ [12] and $[Cp'_3La^{II}]^{1-}$ [10] were clearly discernible even in the presence of the irradiated solvent peak, Figure 3.2, Table 3.1, but the hyperfine coupling (A) of $[Cp'_3Y^{II}]^{1-}$ was unresolved under these conditions. However, the UV-visible spectra for the Ln(II) species generated from gamma irradiation of

these compounds in all cases was consistent with those generated from chemical reduction, Figure 3.3, Table 3.1.

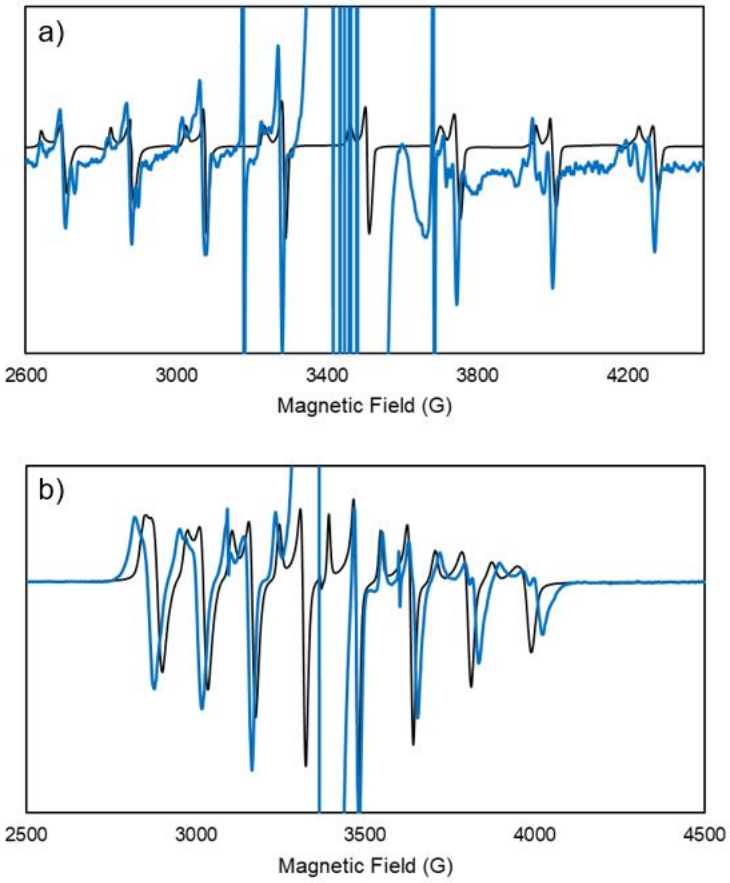

Figure 3.2. Normalized EPR spectroscopic comparison of $[Ln^{II}A_3]^{1-}$ species (A = anion) generated from the gamma irradiation procedure (blue) and chemical reduction (black): (a) $[Sc^{II}(NR_2)_3]^{1-}$; (b) $[Cp'_3La^{II}]^{1-}$.

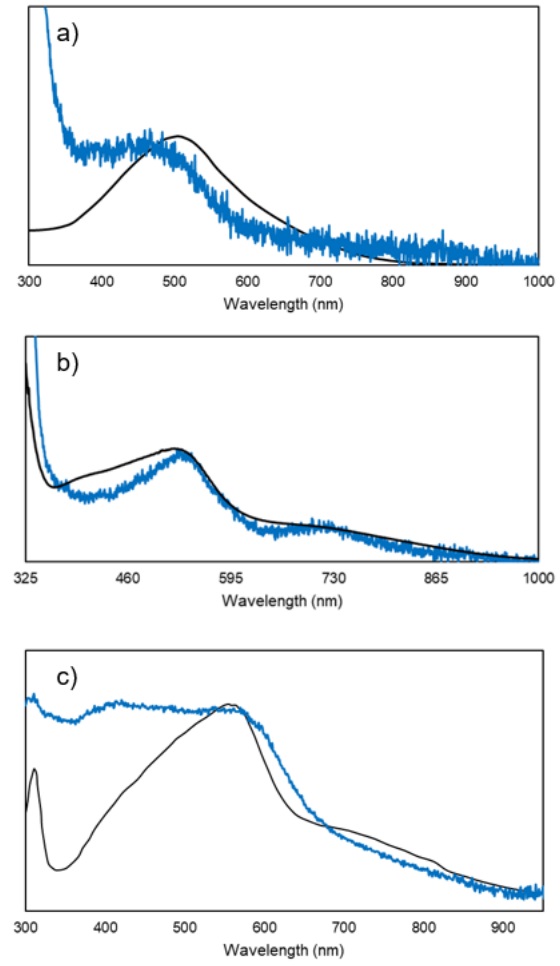

Figure 3.3. Normalized UV-visible spectroscopic comparison of $[Ln^{II}A_3]^{1-}$ species (A = anion) generated from the gamma irradiation procedure (blue) and chemical reduction (black): (a) $[Sc^{II}(NR_2)_3]^{1-}$; (b) $[Cp'_3Y^{II}]^{1-}$; (c) $[Cp'_3La^{II}]^{1-}$.

Table 3.1. Comparison of spectroscopic data of $[Ln^{II}A_3]^{1-}$ species (A = anion) generated from the gamma irradiation procedure (a) and chemical reduction (b), where crypt = 2.2.2-cryptand.

	λ_{max} (nm)	$g_\perp$	g_{II}	A_{ave} (G, MHz)
(a) $[Sc^{II}(NR_2)_3]^{1-}$	500	1.96	2.00	225.7, 625.3
(b) $[K(crypt)][Sc^{II}(NR_2)_3]$ [12]	516	1.964	1.997	225, 622.6
(a) $[Cp'_3Y^{II}]^{1-}$	530, 700	-	-	-
(b) $[Na(crypt)][Cp'_3Y^{II}]$ [21]	390, 530, 700	1.99	2.00	36.6, 100.9

(a) $[Cp'_3La^{II}]^{1-}$	310, 425, 567, 692	1.96	1.98	164.2, 450.9
(b) $[K(crypt)][Cp'_3La^{II}]$ [10]	310, 433, 502, 554, 692	1.96	1.99	155.4, 427.3

Gamma Irradiation of $La^{III}(NR_2)_3$. Given the similarities between spectroscopic data obtained after gamma irradiation and chemical reduction experiments with the compounds above, the characterization of a new Ln(II) species was attempted. Specifically, generation of $[La^{II}(NR_2)_3]^{1-}$ was pursued since it is a species that previously has not been observable in chemical reductions.[22,43,44] Using the general gamma irradiation procedure outlined above, $La^{III}(NR_2)_3$ (69 mg, 0.11 mmol) was dissolved in 0.3 mL 2-MeTHF and exposed to 12 h of gamma irradiation for a total of about 1.5 Mrad (150 Gy). The EPR spectrum of the resulting sample at 77 K exhibited the characteristic isotropic signal for the radical formed by irradiation of 2-MeTHF (g_{iso} = 2.002) as well as an eight line signal ($g_{\perp}$ = 1.98, $g_{\parallel}$ = 2.06, A_{ave} = 504.3 G = 1420.4 MHz) consistent with an unpaired electron in an axial environment coupled to a ^{139}La nucleus (see Figure 3.4). The hyperfine coupling constant is about 3 times greater than that of $[Cp'_3La^{II}]^{1-}$ (A_{ave} = 164.4 G), which is similar in magnitude to the differences observed between $[Y^{II}(NR_2)_3]^{1-}$ (A = 110.0 G)[42] and $[Cp'_3Y^{II}]^{1-}$ (A = 36.6 G)[10,12,43]. The UV-visible spectrum of the sample contains distinct bands at 390 and 670 nm. The UV-visible spectrum is consistent with metal-based 5d → 6p transitions observed for other $[Ln^{II}(NR_2)_3]^{1-}$ complexes with $4f^n5d^1$ electron configurations.[22,43,44]

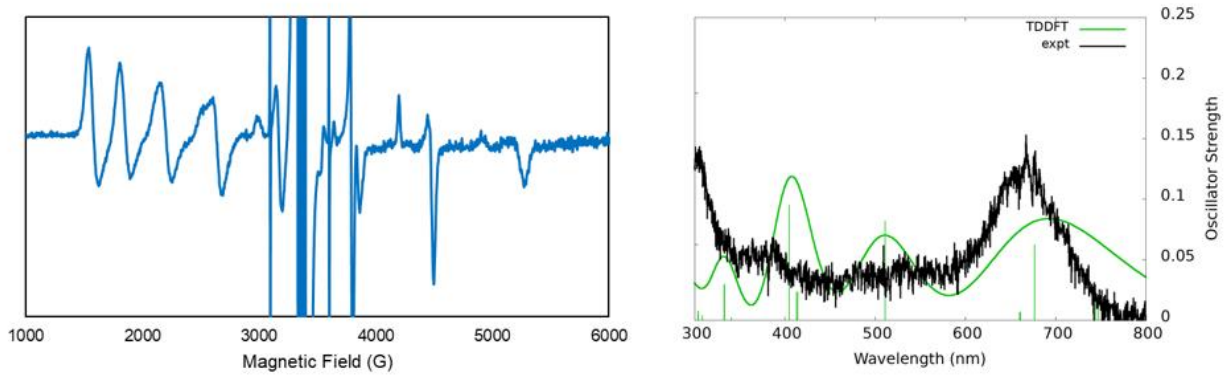

Figure 3.4. EPR (left) and UV-visible absorbance (right) spectroscopic characterization of the species generated upon gamma irradiation of $La^{III}(NR_2)_3$. The simulated UV-visible spectrum is shown in green (right) with computed TDDFT oscillator strengths shown as vertical lines. A Gaussian line broadening of 0.15 eV was applied and the spectrum was empirically blue shifted by 0.30 eV.

Theoretical Studies on $[La^{II}(NR_2)_3]^{1-}$. Electronic structure calculations of the putative La(II) species $[La^{II}(NR_2)_3]^{1-}$ were performed at the density functional level of theory using the TPSSh hybrid meta-generalized gradient density functional[45] with the D3 dispersion correction[46,47] and the resolution of the identity (RI-J) approximation.[48] Scalar relativistic effective core potentials with the def2-TZVP basis set[49] were used for lanthanum and the polarized split-valence basis set def2-SV(P) was used for other atoms.[50] The continuum solvent model COSMO[51] was used with parameters for THF (dielectric constant $\varepsilon = 7.52$, refractive index $R_{ind} = 1.41$).[52] Time-dependent DFT (TDDFT) calculations were performed with an additional diffuse *p* primitive added to the La basis set, which was necessary to accurately simulate the absorption spectrum.[44,53-55] All calculations were performed with the TURBOMOLE package V7.4.1.[56,57]

Structure optimizations were initiated from the optimized structure of $[Gd(NR_2)_3]^{1-}$ [44] by replacing Gd with La. The resulting ground state geometry of $[La^{II}(NR_2)_3]^{1-}$ had C_3 symmetry. The electronic configuration was consistent with a $(5dz^2)^1$ configuration, with the highest occupied molecular orbital (HOMO) having significant $5dz^2$-character with 6s admixture, Figure 3.5. These results are consistent with previous studies on $[Ln^{II}(NR_2)_3]^{1-}$ complexes[22,44] and other $[La^{II}A_3]^{1-}$ species.[9,12,55]

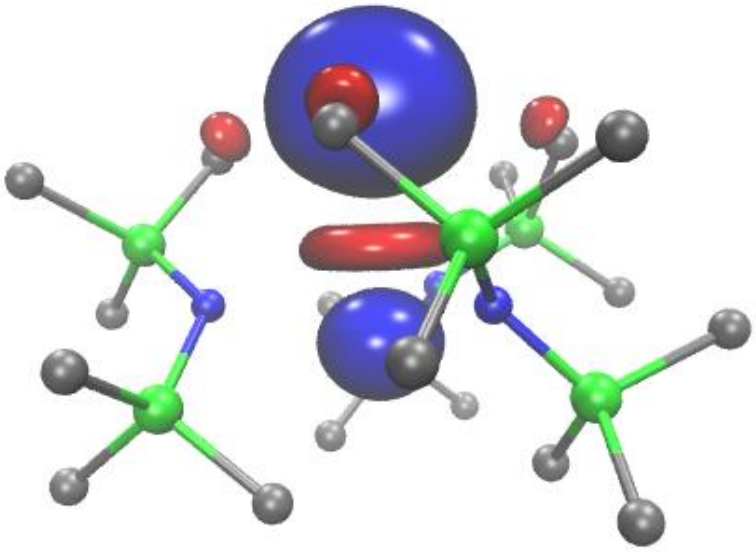

Figure 3.5. Calculated $5dz^2$-like HOMO (ε = −1.439 eV) of $[La^{II}(NR_2)_3]^{1-}$ plotted with a contour value of 0.05.

The simulated UV-visible spectrum of $[La^{II}(NR_2)_3]^{1-}$ qualitatively matches the spectrum obtained by gamma irradiation studies, Figure 3.4. Strong transitions between 650-700 nm are metal-based with 5d → 6p character, consistent with previous studies on $[Gd^{II}(NR_2)_3]^{1-}$.[44] Hence, it appears that gamma irradiation of $La^{III}(NR_2)_3$ generated $[La^{II}(NR_2)_3]^{1-}$, which has been difficult to generate by chemical reduction methods.

Rate of Formation of $[Cp'_3Y^{II}]^{1-}$. Given the particularly good agreement between the electronic absorption spectrum of $[Cp'_3Y^{II}]^{1-}$ prepared by either chemical reduction or gamma irradiation and the fact that the spectra of many different salts of $[Cp'_3Y^{II}]^{1-}$ are identical regardless of the cation present, the absorption at 530 nm of $[Cp'_3Y^{II}]^{1-}$ was used to monitor growth of Y(II) with increasing dosages of gamma irradiation.[7,10,21] A path length of 0.3 cm was determined experimentally using fluorenone as a known standard. Additionally, different starting concentrations (0.075 M vs 0.15 M) of the Y(III) complex Cp'_3Y^{III} were used to determine if this affected the rate of Y(II) formation. The data, recorded in triplicate, are plotted in Figure 3.6. Though the relatively large uncertainties prohibit definitive kinetic analysis, there is clearly growth of Y(II) over time. This concentration study showed that after 6.5 h of irradiation, <1% of Cp'_3Y^{III} has been reduced. Further studies aimed at converting the bulk may benefit from utilizing a higher

dosage setup. Given the uncertainties associated with these growth curves, yields were not calculated for the single measurements conducted above on $[Sc(NR_2)_3]^{1-}$, $[Cp'_3Y]^{1-}$, and $[Cp'_3La]^{1-}$.

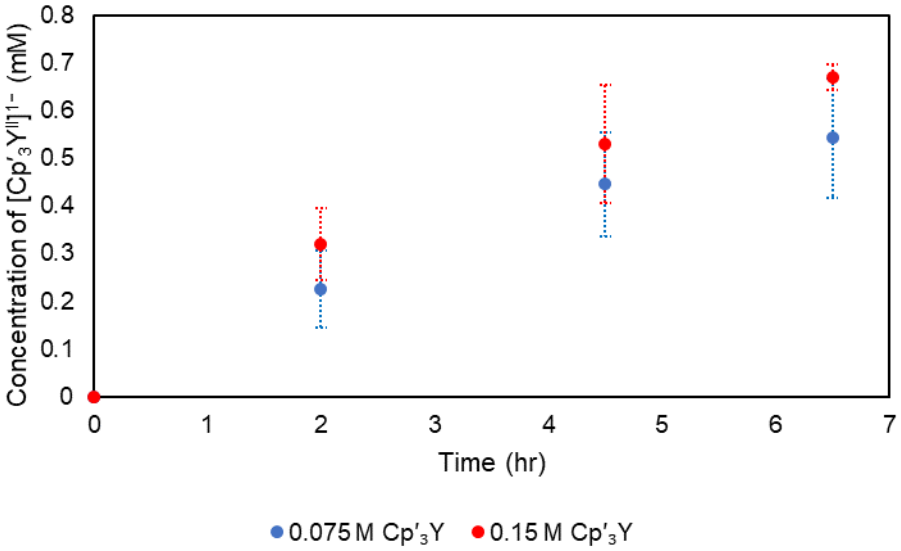

Figure 3.6. Growth of $[Cp'_3Y^{II}]^{1-}$ over time for two different initial concentrations of Cp'_3Y^{III}.

CONCLUSION

Gamma irradiation of $Sc^{III}(NR_2)_3$ and Cp'_3La^{III} yielded 77 K EPR and UV-visible absorption spectra indicative of reduction to the highly reactive Ln(II) complexes, $[Sc^{II}(NR_2)_3]^{1-}$ and $[Cp'_3La^{II}]^{1-}$. A significant obstacle for characterization by EPR spectroscopy is the intense signal associated with the organic radical formed from irradiating 2-MeTHF. This obscured the EPR signal of the Cp'_3Y^{III} irradiation product, but $[Cp'_3Y^{II}]^{1-}$ could be identified by UV-visible spectroscopy. In general, by studying species containing rare-earth metals with large nuclear spins ($I = {}^7/_2$) and large coupling constants, the Ln(II) species formed by irradiation can be detected. This demonstrates the viability of the gamma irradiation reductive technique with molecular rare-earth metal species. Extension of this method to $La^{III}(NR_2)_3$ led to spectroscopic characterization of $[La^{II}(NR_2)_3]^{1-}$ for the first time and shows that this method can be used to demonstrate the existence of species not yet isolable by chemical reduction. Hence, gamma irradiation should be more widely considered for generating highly reactive molecular species when the appropriate spectroscopic assessments can be made.

References

(1) Morss, L. R. Thermochemical Properties of Yttrium, Lanthanum, and the Lanthanide Elements and Ions. *Chem. Rev.* **1976**, *76*, 827–841. DOI: 10.1021/cr60304a007.

(2) Nugent, L. J.; Baybarz, R. D.; Burnett, J. L.; Ryan, J. L. Electron-Transfer and f→d Absorption Bands of Some Lanthanide and Actinide Complexes and the Standard (III-IV) Oxidation Potentials for Each Member of the Lanthanide and Actinide Series. *J. Inorg. Nucl. Chem.* **1971**, *33*, 2503–2530. DOI: 10.1016/0022-1902(71)80226-9.

(3) Bochkarev, M. N. Molecular Compounds of "New" Divalent Lanthanides. *Coord. Chem. Rev.* **2004**, *248*, 835–851. DOI: 10.1016/j.ccr.2004.04.004.

(4) Nief, F. In *Handbook on the Physics and Chemistry of Rare Earths*; Gschneidner, K. A., Jr., Bunzli, J.-C. G., Pecharsky, V. K., Eds.; North-Holland: Amsterdam, **2010**, Vol. 40, Chapter 246.

(5) Woen, D. H.; Evans, W. J. Chapter 293 - Expanding the +2 Oxidation State of the Rare-Earth Metals, Uranium, and Thorium in Molecular Complexes. In *Handbook on the Physics and Chemistry of Rare Earths*; Elsevier B.V., **2016**; Vol. 50, 337–394. DOI: 10.1016/bs.hpcre.2016.08.002.

(6) Hitchcock, P. B.; Lappert, M. F.; Maron, L.; Protchenko, A. V. Lanthanum Does Form Stable Molecular Compounds in the +2 Oxidation State. *Angew. Chem. Int. Ed.* **2008**, *47*, 1488–1491. DOI: 10.1002/anie.200704887.

(7) MacDonald, M. R.; Ziller, J. W.; Evans, W. J. Synthesis of a Crystalline Molecular Complex of Y^{2+}, [(18-Crown-6)K][$(C_5H_4SiMe_3)_3Y$]. *J. Am. Chem. Soc.* **2011**, *133*, 15914–15917. DOI: 10.1021/ja207151y.

(8) MacDonald, M. R.; Bates, J. E.; Fieser, M. E.; Ziller, J. W.; Furche, F.; Evans, W. J. Expanding Rare-Earth Oxidation State Chemistry to Molecular Complexes of Holmium(II) and Erbium(II). *J. Am. Chem. Soc.* **2012**, *134*, 8420–8423. DOI: 10.1021/ja303357w.

(9) Macdonald, M. R.; Bates, J. E.; Ziller, J. W.; Furche, F.; Evans, W. J. Completing the Series of +2 Ions for the Lanthanide Elements: Synthesis of Molecular Complexes of Pr^{2+}, Gd^{2+}, Tb^{2+}, and Lu^{2+}. *J. Am. Chem. Soc.* **2013**, *135*, 9857–9868. DOI: 10.1021/ja403753j.

(10) Fieser, M. E.; Macdonald, M. R.; Krull, B. T.; Bates, J. E.; Ziller, J. W.; Furche, F.; Evans, W. J. Structural, Spectroscopic, and Theoretical Comparison of Traditional vs Recently Discovered Ln^{2+} Ions in the [K(2.2.2-Cryptand)][$(C_5H_4SiMe_3)_3Ln$] Complexes: The Variable Nature of Dy^{2+} and Nd^{2+}. *J. Am. Chem. Soc.* **2015**, *137*, 369–382. DOI: 10.1021/ja510831n.

(11) Kotyk, C. M.; MacDonald, M. R.; Ziller, J. W.; Evans, W. J. Reactivity of the Ln^{2+} Complexes [K(2.2.2-Cryptand)][$(C_5H_4SiMe_3)_3Ln$]: Reduction of Naphthalene and Biphenyl. *Organometallics* **2015**, *34*, 2287–2295. DOI: 10.1021/om501063h.

(12) Woen, D. H.; Chen, G. P.; Ziller, J. W.; Boyle, T. J.; Furche, F.; Evans, W. J. Solution Synthesis, Structure, and CO_2 Reduction Reactivity of a Scandium(II) Complex, $\{Sc[N(SiMe_3)_2]_3\}^-$. *Angew. Chem. Int. Ed.* **2017**, *56*, 2050–2053. DOI: 10.1002/anie.201611758.

(13) Woen, D. H.; Chen, G. P.; Ziller, J. W.; Boyle, T. J.; Furche, F.; Evans, W. J. End-On Bridging Dinitrogen Complex of Scandium. *J. Am. Chem. Soc.* **2017**, *139*, 14861–14864. DOI: 10.1021/jacs.7b08456.

(14) Palumbo, C. T.; Fieser, M. E.; Ziller, J. W.; Evans, W. J. Reactivity of Complexes of $4f^n5d^1$ and $4f^{n+1}$ Ln^{2+} Ions with Cyclooctatetraene. *Organometallics* **2017**, *36*, 3721–3728. DOI: 10.1021/acs.organomet.7b00498.

(15) Trinh, M. T.; Wedal, J. C.; Evans, W. J. Evaluating Electrochemical Accessibility of $4f^n5d^1$and $4f^{n+1}$ Ln(I) Ions in $(C_5H_4SiMe_3)_3Ln$ and $(C_5Me_4H)_3Ln$ Complexes. *Dalton Trans.* **2021**, *50*, 14384–14389. DOI: 10.1039/d1dt02427b.

(16) Wedal, J. C.; Evans, W. J. A Rare-Earth Metal Retrospective to Stimulate All Fields. *J. Am. Chem. Soc.* **2021**, *143*, 18354–18367. DOI: 10.1021/jacs.1c08288.

(17) Meihaus, K. R.; Fieser, M. E.; Corbey, J. F.; Evans, W. J.; Long, J. R. Record High Single-Ion Magnetic Moments Through $4f^n5d^1$ Electron Configurations in the Divalent Lanthanide Complexes $[(C_5H_4SiMe_3)_3Ln]^-$. *J. Am. Chem. Soc.* **2015**, *137*, 9855–9860. DOI: 10.1021/jacs.5b03710.

(18) Ariciu, A. M.; Woen, D. H.; Huh, D. N.; Nodaraki, L. E.; Kostopoulos, A. K.; Goodwin, C. A. P.; Chilton, N. F.; McInnes, E. J. L.; Winpenny, R. E. P.; Evans, W. J.; Tuna, F. Engineering Electronic

Structure to Prolong Relaxation Times in Molecular Qubits by Minimising Orbital Angular Momentum. *Nat. Commun.* **2019**, *10*, 1–8. DOI: 10.1038/s41467-019-11309-3.

(19) Kundu, K.; White, J. R. K.; Moehring, S. A.; Yu, J. M.; Ziller, J. W.; Furche, F.; Evans, W. J.; Hill, S. A 9.2-GHz Clock Transition in a Lu(II) Molecular Spin Qubit Arising from a 3,467-MHz Hyperfine Interaction. *Nat. Chem.* **2022**, *14*, 392–397. DOI: 10.1038/s41557-022-00894-4.

(20) Jenkins, T. F.; Bekoe, S.; Ziller, J. W.; Furche, F.; Evans, W. J. Synthesis of a Heteroleptic Pentamethylcyclopentadienyl Yttrium(II) Complex, [K(2.2.2-Cryptand)]{$(C_5Me_5)_2Y^{II}[N(SiMe_3)_2]$}, and Its C-H Bond Activated Y(III) Derivative. *Organometallics* **2021**, *40*, 3917–3925. DOI: 10.1021/acs.organomet.1c00482.

(21) Moore, W. N. G.; Ziller, J. W.; Evans, W. J. Optimizing Alkali Metal (M) and Chelate (L) Combinations for the Synthesis and Stability of [M(L)][$(C_5H_4SiMe_3)_3Y$] Yttrium(II) Complexes. *Organometallics* **2021**, *40*, 3170–3176. DOI: 10.1021/acs.organomet.1c00379.

(22) Ryan, A. J.; Ziller, J. W.; Evans, W. J. The Importance of the Counter-Cation in Reductive Rare-Earth Metal Chemistry: 18-Crown-6 Instead of 2,2,2-Cryptand Allows Isolation of $[Y^{II}(NR_2)_3]^{1-}$ and Ynediolate and Enediolate Complexes from CO Reactions. *Chem. Sci.* **2020**, *11*, 2006–2014. DOI: 10.1039/c9sc05794c.

(23) Meyer, G. Superbulky Ligands and Trapped Electrons: New Perspectives in Divalent Lanthanide Chemistry. *Angew. Chem. Int. Ed.* **2008**, *47*, 4962–4964. DOI: 10.1002/anie.200801444.

(24) Huh, D. N.; Ciccone, S. R.; Bekoe, S.; Roy, S.; Ziller, J. W.; Furche, F.; Evans, W. J. Synthesis of Ln^{II}-in-Cryptand Complexes by Chemical Reduction of Ln^{III}-in-Cryptand Precursors: Isolation of a Nd^{II}-in-Cryptand Complex. *Angew. Chem. Int. Ed.* **2020**, *59*, 16141–16146. DOI: 10.1002/anie.202006393.

(25) Cloke, F. G. N. Zero Oxidation State Compounds of Scandium, Yttrium, and the Lanthanides. *Chem. Soc. Rev.* **1993**, *22*, 17–24. DOI: 10.1039/CS9932200017.

(26) Brennan, J. G.; Cloke, F. G. N.; Sameh, A. A.; Zalkin, A. Synthesis of Bis(η-1,3,5-Tri-t-Butylbenzene) Sandwich Complexes of Yttrium(0) and Gadolinium(0); The X-Ray Crystal Structure of the

First Authentic Lanthanide(0) Complex, [Gd(η-Bu$^t_3$C$_6$H$_3$)$_2$]. *J. Chem. Soc. Chem. Commun.* **1987**, 1668–1669. DOI: 10.1039/C39870001668.

(27) Anderson, D. M.; Cloke, F. G. N.; Cox, P. A.; Edelstein, N.; Green, J. C.; Pang, T.; Sameh, A. A.; Shalimoff, G. On the Stability and Bonding in Bis(η-Arene)lanthanide Complexes. *J. Chem. Soc. Chem. Commun.* **1989**, 53–55. DOI: 10.1039/C39890000053.

(28) Arnold, P. L.; Cloke, F. G. N.; Hitchcock, P. B.; Nixon, J. F. The First Example of a Formal Scandium(I) Complex: Synthesis and Molecular Structure of the 22-Electron Scandium Triple Decker Incorporating the Novel 1,3,5-Triphosphabenzene Ring. *J. Am. Chem. Soc.* **1996**, *118*, 7630–7631. DOI: 10.1021/ja961253o.

(29) Fong, F. K.; Cape, J. A.; Wong, E. Y. Monovalent Samarium in Potassium Chloride. *Phys. Rev.* **1966**, *151*, 299–303. DOI: 10.1103/PhysRev.151.299.

(30) Dieke, G. H. Chapter 12. Divalent Rare Earth Ions in Crystals. In *Spectra and Energy Levels of Rare Earth Ions in Crystals*; Interscience Publishers, **1968**, 177–188.

(31) McClure, D. S.; Kiss, Z. Survey of the Spectra of the Divalent Rare-Earth Ions in Cubic Crystals. *J. Chem. Phys.* **1963**, *39*, 3251–3257. DOI: 10.1063/1.1734186.

(32) Qiu, J.; Hirao, K. γ-Ray Induced Reduction of Sm^{3+} to Sm^{2+} in Sodium Aluminoborate Glasses. *J. Mater. Sci. Lett.* **2001**, *20*, 691–693. DOI: 10.1023/A:1010998605695.

(33) Madhu, A.; Eraiah, B.; Srinatha, N. Gamma Irradiation Effects on the Structural, Thermal and Optical Properties of Samarium Doped Lanthanum–Lead- Boro-Tellurite Glasses. *J. Lumin.* **2020**, *221*, 117080. DOI: 10.1016/j.jlumin.2020.117080.

(34) Telser, J.; Davydov, R.; Horng, Y. C.; Ragsdale, S. W.; Hoffman, B. M. Cryoreduction of Methyl-Coenzyme M Reductase: EPR Characterization of Forms, MCR_{ox1} and MCR_{red1}. *J. Am. Chem. Soc.* **2001**, *123*, 5853–5860. DOI: 10.1021/ja010428d.

(35) Davydov, R.; Razeghifard, R.; Im, S. C.; Waskell, L.; Hoffman, B. M. Characterization of the Microsomal Cytochrome P450 2B4 O_2 Activation Intermediates by Cryoreduction and Electron Paramagnetic Resonance. *Biochemistry* **2008**, *47*, 9661–9666. DOI: 10.1021/bi800926x.

(36) Davydov, R. M.; Chauhan, N.; Thackray, S. J.; Anderson, J. L. R.; Papadopoulou, N. D.; Mowat, C. G.; Chapman, S. K.; Raven, E. L.; Hoffman, B. M. Probing the Ternary Complexes of Indoleamine and Tryptophan 2,3-Dioxygenases by Cryoreduction EPR and Endor Spectroscopy. *J. Am. Chem. Soc.* **2010**, *132*, 5494–5500. DOI: 10.1021/ja100518z.

(37) Davydov, R. M.; McLaughlin, M. P.; Bill, E.; Hoffman, B. M.; Holland, P. L. Generation of High-Spin Iron(I) in a Protein Environment Using Cryoreduction. *Inorg. Chem.* **2013**, *52*, 7323–7325. DOI: 10.1021/ic4011339.

(38) Dickinson, L. C.; Symons, M. C. R. Electron Spin Resonance Monitoring of Ligand Ejection Reactions Following Solid-State Reduction of Cobalt Globin and Cobalt Protoporphyrin Complexes. *J. Phys. Chem.* **1982**, *86*, 917–921. DOI: 10.1021/j100395a016.

(39) Konishi, S.; Hoshino, M.; Imamura, M. Formation of the Charge-Transfer and Constrained Complexes of Cobalt(II) Tetraphenylporphyrin in Rigid Solution. *J. Phys. Chem.* **1980**, *84*, 3437–3440. DOI: 10.1021/j100462a025.

(40) F. T. Edelmann, in *Synthetic Methods of Organometallics and Inorganic Chemistry*, Vol. 6 (Ed.: W. A. Herrmann), Thieme Verlag Stuttgart, New York, **1997**, pp. 37-40.

(41) Peterson, J. K.; Macdonald, M. R.; Ziller, J. W.; Evans, W. J. Synthetic Aspects of $(C_5H_4SiMe_3)_3Ln$ Rare-Earth Chemistry: Formation of $(C_5H_4SiMe_3)_3Lu$ via $[(C_5H_4SiMe_3)_2Ln]^+$ Metallocene Precursors. *Organometallics* **2013**, *32*, 2625–2631. DOI: 10.1021/om400116d.

(42) Jou, F. Y.; Dorfman, L. M. Pulse Radiolysis Studies. XXI. Optical Absorption Spectrum of the Solvated Electron in Ethers and in Binary Solutions of These Ethers. *J. Chem. Phys.* **1973**, *58*, 4715–4723. DOI: 10.1063/1.1679050.

(43) Fang, M.; Lee, D. S.; Ziller, J. W.; Doedens, R. J.; Bates, J. E.; Furche, F.; Evans, W. J. Synthesis of the $(N_2)^{3-}$ Radical from Y^{2+} and Its Protonolysis Reactivity To Form $(N_2H_2)^{2-}$ via the $Y[N(SiMe_3)_2]_3/KC_8$ Reduction System. *J. Am. Chem. Soc.* **2011**, *133*, 3784–3787. DOI: 10.1021/ja1116827.

(44) Ryan, A. J.; Darago, L. E.; Balasubramani, S. G.; Chen, G. P.; Ziller, J. W.; Furche, F.; Long, J. R.; Evans, W. J. Synthesis, Structure, and Magnetism of Tris(Amide) $[Ln\{N(SiMe_3)_2\}_3]^{1-}$ Complexes of

the Non-Traditional +2 Lanthanide Ions. *Chem. Eur. J.* **2018**, *24*, 7702–7709. DOI: 10.1002/chem.201800610.

(45) Staroverov, V. N.; Scuseria, G. E.; Tao, J.; Perdew, J. P. Comparative Assessment of a New Nonempirical Density Functional: Molecules and Hydrogen-Bonded Complexes. *J. Chem. Phys.* **2003**, *119*, 12129–12137. DOI: 10.1063/1.1626543.

(46) Grimme, S.; Antony, J.; Ehrlich, S.; Krieg, H. A Consistent and Accurate Ab Initio Parametrization of Density Functional Dispersion Correction (DFT-D) for the 94 Elements H-Pu. *J. Chem. Phys.* **2010**, *132*, 154104. DOI: 10.1063/1.3382344.

(47) Grimme, S. Semiempirical GGA-Type Density Functional Constructed with a Long-Range Dispersion Correction. *J. Comput. Chem.* **2006**, *27*, 1787–1799. DOI: 10.1002/jcc.20495.

(48) Weigend, F.; Köhn, A.; Hättig, C. Efficient Use of the Correlation Consistent Basis Sets in Resolution of the Identity MP2 Calculations. *J. Chem. Phys.* **2002**, *116*, 3175–3183. DOI: 10.1063/1.1445115.

(49) Weigend, F.; Ahlrichs, R. Balanced Basis Sets of Split Valence, Triple Zeta Valence and Quadruple Zeta Valence Quality for H to Rn: Design and Assessment of Accuracy. *Phys. Chem. Chem. Phys.* **2005**, *7*, 3297–3305. DOI: 10.1039/b508541a.

(50) Eichkorn, K.; Weigend, F.; Treutler, O.; Ahlrichs, R. Auxiliary Basis Sets for Main Row Atoms and Transition Metals and Their Use to Approximate Coulomb Potentials. *Theor. Chem. Acc.* **1997**, *97*, 119–124. DOI: 10.1007/s002140050244.

(51) Schäfer, A.; Klamt, A.; Sattel, D.; Lohrenz, J. C. W.; Eckert, F. COSMO Implementation in TURBOMOLE: Extension of an Efficient Quantum Chemical Code towards Liquid Systems. *Phys. Chem. Chem. Phys.* **2000**, *2*, 2187–2193. DOI: 10.1039/b000184h.

(52) CRC Handbook of Chemistry and Physics, 97th ed.; Haynes, W. M., Lide, D. R., Bruno, T. J., Eds.; CRC Press, 2016.

(53) Jenkins, T. F.; Woen, D. H.; Mohanam, L. N.; Ziller, J. W.; Furche, F.; Evans, W. J. Tetramethylcyclopentadienyl Ligands Allow Isolation of Ln(II) Ions across the Lanthanide Series in

[K(2.2.2-Cryptand)][($C_5Me_4H)_3$Ln] Complexes. *Organometallics* **2018**, *37*, 3863–3873. DOI: 10.1021/acs.organomet.8b00557.

(54) Wedal, J. C.; Furche, F.; Evans, W. J. Density Functional Theory Analysis of the Importance of Coordination Geometry for $5f^3 6d^1$versus $5f^4$Electron Configurations in U(II) Complexes. *Inorg. Chem.* **2021**, *60*, 16316–16325. DOI: 10.1021/acs.inorgchem.1c02161.

(55) Wedal, J. C.; Ziller, J. W.; Furche, F.; Evans, W. J. Synthesis and Reduction of Heteroleptic Bis(Cyclopentadienyl) Uranium(III) Complexes. *Inorg. Chem.* **2022**, *61*, 7365–7376. DOI: 10.1021/acs.inorgchem.2c00322.

(56) TURBOMOLE V7.4.1 2019, a development of University of Karlsruhe and Forschungszentrum Karlsruhe GmbH, 1989−2007, TURBOMOLE GmbH, since 2007: available from http://www.turbomole.com.

(57) Balasubramani, S. G.; Chen, G. P.; Coriani, S.; Diedenhofen, M.; Frank, M. S.; Franzke, Y. J.; Furche, F.; Grotjahn, R.; Harding, M. E.; Hättig, C.; Hellweg, A.; Helmich-Paris, B.; Holzer, C.; Huniar, U.; Kaupp, M.; Marefat Khah, A.; Karbalaei Khani, S.; Müller, T.; Mack, F.; Nguyen, B. D.; Parker, S. M.; Perlt, E.; Rappoport, D.; Reiter, K.; Roy, S.; Rückert, M.; Schmitz, G.; Sierka, M.; Tapavicza, E.; Tew, D. P.; Van Wüllen, C.; Voora, V. K.; Weigend, F.; Wodyński, A.; Yu, J. M. TURBOMOLE: Modular Program Suite for Ab Initio Quantum-Chemical and Condensed-Matter Simulations. *J. Chem. Phys.* **2020**, *152*, 184107. DOI: 10.1063/5.0004635.

Chapter 4:

Yttrium-mediated Acetylide C–C Bond Formation Yields a Bridging Butatrienylidene Dianion

INTRODUCTION

Detailed studies of rare-earth metal reductive chemistry have provided new oxidation states of simple diatomic molecules like N_2 and NO. For example, the first example of the $(N_2)^{3-}$ radical trianion was observed in $\{[(R_2N)_2(THF)Y]_2(N_2)\}^{1-}$ (R = Me_3Si) which was generated by reduction of the side-on bridged $(N=N)^{2-}$ complex in $[(R_2N)_2(THF)Y]_2(\mu–\eta^2:\eta^2–N_2)$, Figure 4.1.[1-3] This unexpected development led to a new class of single molecule magnets,[4,5] as well as the first example of an $(NO)^{2-}$ complex in $[(R_2N]_2(THF)]\}_2(\mu–\eta^2:\eta^2–NO)$.[6] These results suggest that the rare-earth metals could provide synthetic pathways to other unusual diatomic anions such as $(CN)^{2-}$ and $(CC)^{3-}$.

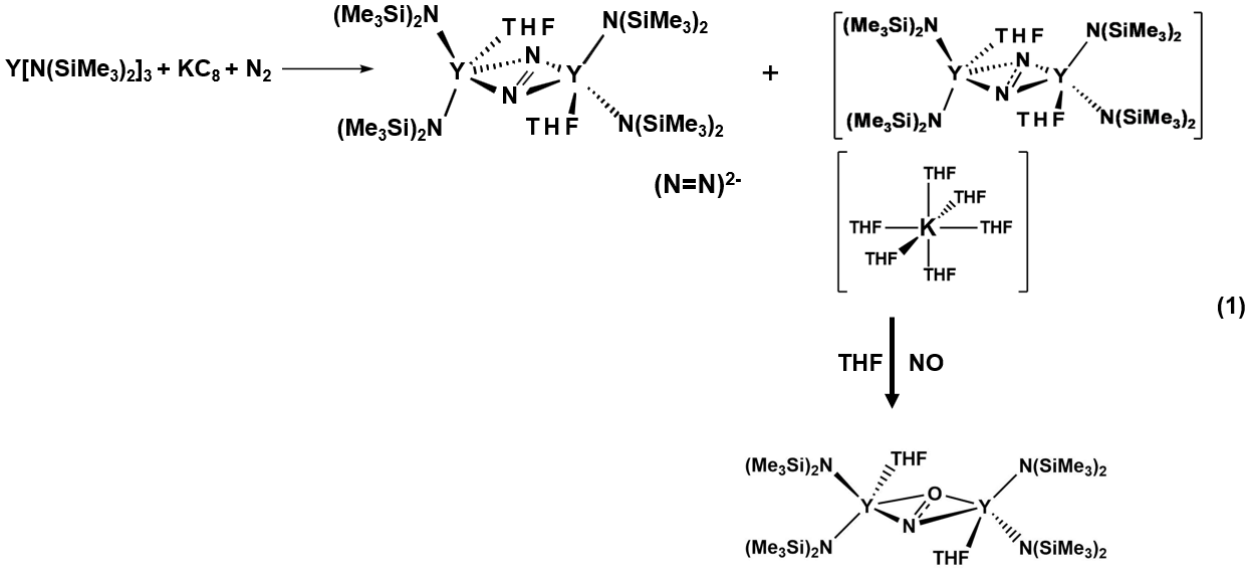

Figure 4.1. Synthesis of the $(N_2)^{3-}$ and $(NO)^{2-}$ bridges in sequence.

Recently, reduced dinitrogen rare earth chemistry has been expanded further by identification of end-on bound $(\mu–\eta^1:\eta^1–N_2)^{2-}$ complexes[7,8] which were found to isomerize to the previously known side-on $(\mu–\eta^2:\eta^2–N_2)^{2-}$ species even in the solid state,[9] Figure 4.2. Since rare-earth metal complexes of the end-on

(μ–η^1:η^1–C_2)$^{2-}$ acetylide dianion are known in $(C_5Me_5)_2Ln(\mu–\eta^1:\eta^1–C_2)Ln(C_5Me_5)_2$ complexes (Ln = Sc, Sm),[10,11] the possibility of reducing these bridges further to $(CC)^{3-}$ is plausible.

Figure 4.2. Solid-state isomerization from (μ–η^1:η^1–N_2)$^{2-}$ to (μ–η^2:η^2–N_2)$^{2-}$ bridge.

To explore further the chemistry of $[Ln(\mu–\eta^1:\eta^1–C_2)Ln]^{4+}$ units and their possible reduction to $(C_2)^{3-}$ species, the reaction of $(C_5Me_5)_2Y(\mu–Ph)_2BPh_2$ with NaC≡CH was explored. This approach was based on results of Cummins et al in 2010[12] and Hayton et al in 2021[13] with U(IV) that demonstrated the reaction of $U(NR_2)_3X$ complexes with NaC≡CH to form the end-on acetylides $[U(NR_2)_3]_2(\mu–\eta^1:\eta^1–C_2)$, as shown in Figure 4.3.[13]

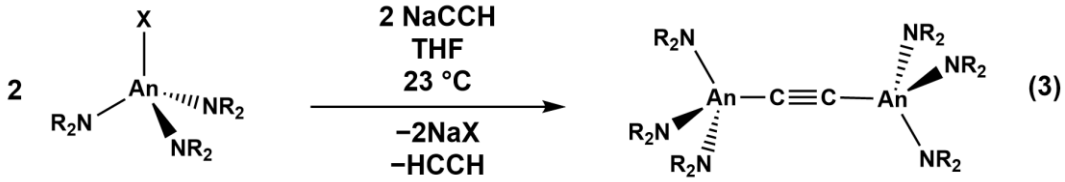

Figure 4.3. Synthesis of $(C_2)^{2-}$ bridges between actinide metals [X = I, NR_2 = N(*t*-Bu)(3,5-$Me_2C_6H_3$), An = U; X = Cl, NR_2 = $N(SiMe_3)_2$, An = U, Th].

Similar chemistry to the reaction in Figure 4.3 seemed conceivable for Y(III) since the $(C_5Me_5)_2Ln(\mu–Ph)_2BPh_2$ complexes readily react with alkali metal organometallic reagents to displace the loosely coordinated $(BPh_4)^{1-}$ anion and form Ln–C bonds.[14-16] However, if an intermediate reaction product such as "$(C_5Me_5)_2YC{\equiv}CH$" formed, it could simply dimerize as was found with $[(C_5H_4Me)_2Sm(\mu–C{\equiv}CCMe_3)]_2$[17] or it could engage in a C–C coupling reaction to form trienediyl complexes of the type $[(C_5Me_5)_2Ln]_2(\mu–\eta^2:\eta^2–PhC{=}C{=}C{=}CPh)$ (Ln = Sm, Y).[18,19] Notably, a potential intermediate like

"$(C_5Me_5)_2YC{\equiv}CH$" may also be isolable if residual coordinating solvent is present,[20] as with the case of $(C_5Me_5)_2Y(C{\equiv}CPh)(THF)$.[21]

In this chapter, yet a different type of reaction is reported in which a bridging butatrienylidene dianion is generated from two $(C{\equiv}CH)^{1-}$ units in a bis(pentamethylcyclopentadienyl) ligand environment. The reaction involves rearrangement of a terminal hydrogen substituent of an acetylide and yields a complex with an unusual bonding mode that has been investigated by density functional theory (DFT). The only previous examples of a butatrienylidene dianion are in the ruthenium clusters, $Ru_5(\mu^5\text{-}CCCCH_2)(\mu^3\text{–}SMe)(\mu\text{–}SMe)(\mu\text{–}PPh_2)_2(CO)_{10}$, **A**, and $Ru_5(\mu^5\text{–}CCCCH_2)(\mu\text{–}SMe)_2(\mu\text{–}PPh_2)_2(CO)_{11}$, **B**, made in a complicated series of transformations starting from $Me_3SiC{\equiv}CSiMe_3$.[22,23]

RESULTS

Dropwise addition of 1 equiv of $(C_5Me_5)_2Y(\mu\text{–}Ph)_2BPh_2$ in a 1:1 toluene:benzene (used to help solubilize the yttrium complex) mixture to a stirred slurry of 1 equiv of $NaC{\equiv}CH$ yields a yellow/orange suspension after stirring overnight. An insoluble white material presumed to be sodium tetraphenylborate was removed by filtration and washed with hexanes leaving the filtrate as a translucent orange solution in the mixed hydrocarbons. The solvent was removed in vacuo to provide yellow-orange solids which were soluble in pentane. Slow evaporation of pentane solutions at room temperature yields crystalline material in 30% yield suitable for single crystal X-ray diffraction studies which was identified by X-ray diffraction as $(C_5Me_5)_2Y(\mu\text{–}\eta^3\text{:}\eta^1\text{–}CCCCH_2)Y(C_5Me_5)_2$, **8-Y**, Figures 4.4 and 4.5.

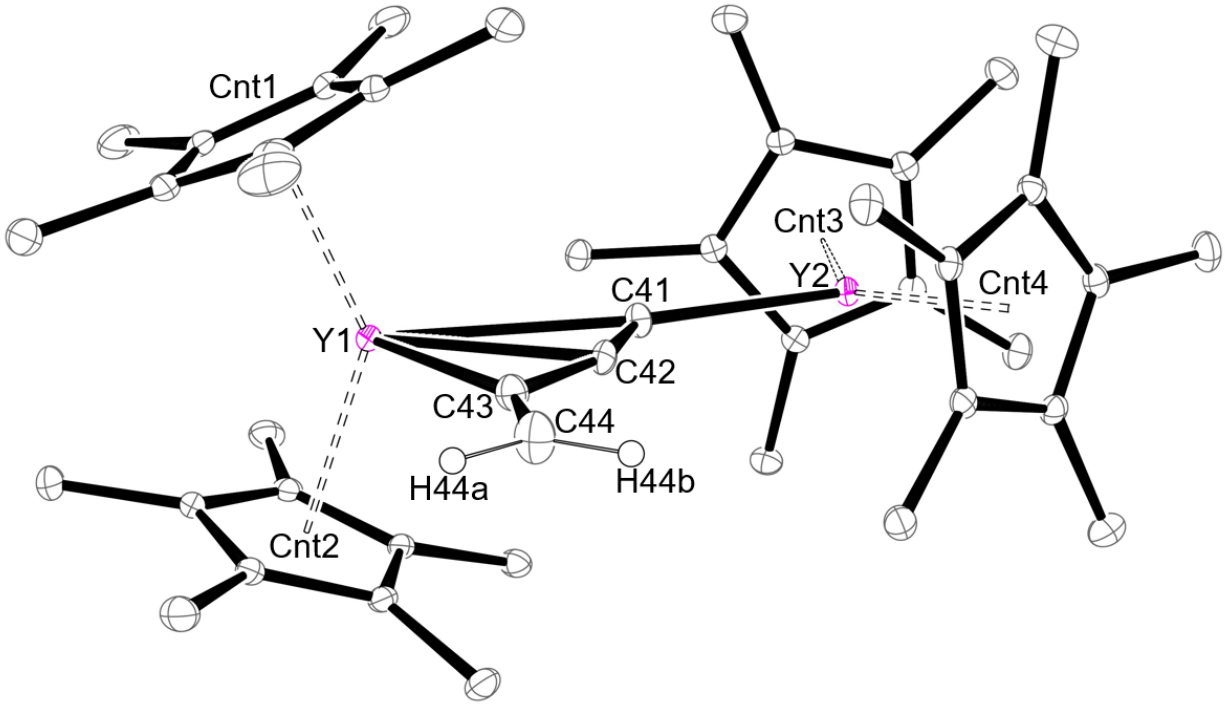

Figure 4.4. ORTEP of $(C_5Me_5)_2Y(\mu\text{–}\eta^3\text{:}\eta^1\text{–}CCCCH_2)Y(C_5Me_5)_2$, **8-Y**, with displacement ellipsoids drawn at 50% probability and all hydrogen atoms except for H44a and H44b eliminated for clarity.

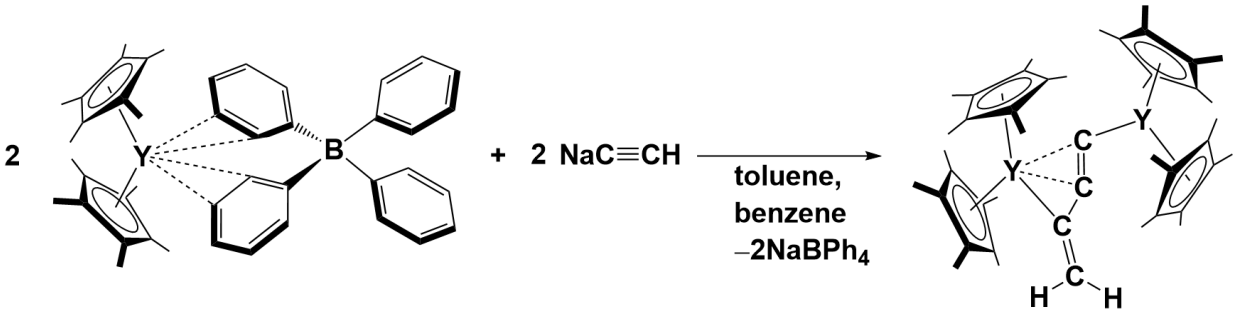

Figure 4.5. Synthesis of **8-Y** described in this work.

Complex **8-Y** contains two $[(C_5Me_5)_2Y]^{1+}$ metallocene units bridged by a C_4 unit with two hydrogen atoms on one terminal carbon, $(CCCCH_2)^{2-}$. The hydrogen atoms on that carbon were located in the X-ray crystal structure. The six atoms in the bridge are co-planar with a root mean squared deviation (RMSD) ω = 0.01 Å. The six atoms plus the two yttrium atoms are coplanar to ω = 0.03 Å. In the previous examples, **A** and **B**, cited above, the three carbon atoms of the C_4H_2 unit twist around the ruthenium clusters to give the six atoms an ω = 0.38 Å for **A** and ω = 0.43 Å for **B**.

In **8-Y**, the C43–C44 distance of 1.331(3) Å is essentially identical to a prototypical C=C bond distance of 1.339 Å measured in ethylene.[24] Conversely, the C41–C42 distance in **1** of 1.240(3) Å is longer than the C≡C triple bond distance of 1.20 Å found for acetylene.[24] This lengthening has also been seen in the formation of complexes containing a formally $[C{\equiv}C]^{2-}$ bridge. For instance, in $[U(N[t\text{-}Bu]Ar)_3]_2(\mu\text{–}\eta^1{:}\eta^1\text{–}C_2)$ and $\{[U[N(SiMe_3)_2]_3\}_2(\mu\text{–}\eta^1{:}\eta^1\text{–}C_2)$, the C≡C distances are 1.227(10) and 1.225(10) Å, respectively. The central C–C bond in the butatrienylidene ligand, C42–C43, is 1.404(3), which is intermediate between a typical C–C single bond and C=C double bond.

The 2.420(2) Å Y2–C41 bond distance in **8-Y** is equivalent to the 2.419(3) Å Y–C(Et) distance in alkyl metallocene, $(C_5Me_5)_2Y(CH_2CH_3)$.[25] The Y1 center is bound to C43 with a similar distance, 2.430(2) Å, and with longer distances to C42 (2.532(2) Å) and C43 (2.779(2) Å). In comparison, $(C_5Me_5)_2Y(allyl)$ has Y–C(allyl) distances of 2.582(2), 2.582(2), and 2.601(2) Å, so the bonding in **1** differs from allyl coordination.[26]

Table 4.1. Selected bond distances and angles in **8-Y**.

Bond	Distance (Å)	Atoms	Angle (°)
Cnt1–Y1	2.366	Cnt1–Y1–Cnt2	137.6
Cnt2–Y1	2.363	Cnt3–Y2–Cnt3	138.6
Cnt3–Y2	2.328	C42–C41–Y2	131.04(14)
Cnt4–Y2	2.342	Y1–C41–Y2	163.30(8)
C41–C42	1.240(3)	C41–C42–C43	157.50(19)
C42–C43	1.404(3)	C42–C43–C44	130.11(19)
C43–C44	1.331(3)	C43–C44–H44a	119.3(14)
C44–H44a	0.97(2)	C43–C44–H44b	123.7(14)
C44–H44b	0.97(2)	H44a–C44–H44b	116.9(19)
Y1–C41	2.779(2)		
Y1–C42	2.532(2)		
Y1–C43	2.430(2)		
Y1–C44	3.660(2)		
Y2–C41	2.420(2)		
Y2–C42	3.367(2)		
Y2–C43	4.754(2)		
Y2–C44	5.588(2)		

The ^1H NMR spectrum of **8-Y** in C_6D_6 displays four separate C_5Me_5 resonances from d 1.97 to 2.16 ppm which suggests that the asymmetric structure is maintained in a solution of a non-coordinating

solvent. Two resonances assignable to the hydrogen atoms on C44 were observed at δ 6.59 and 5.55 ppm with coupling to each other ($J_{H,H}$ = 4.7 Hz), which compares well with the coupling constant for hydrogens on sp^2 carbons of ligands bound to yttrium ($J_{H,H} \approx 4$ Hz).[26] The signal at δ 6.59 ppm also displays a smaller coupling of 1.7 Hz, a magnitude consistent with the yttrium-hydrogen coupling observed for hydrogen atoms bound to the methylene carbon in $(C_5Me_5)_2Y(CH_2CH_3)$ ($J_{Y,H}$ = 2 Hz).[25] The $^{13}C\{^1H\}$ NMR spectrum exhibits a set of four resonances between 11-13 ppm, in the range expected for the methyl groups of C_5Me_5 ligands bound to yttrium. Additionally, four resonances are visible around 117-121 ppm, in the range for the ring carbons of the C_5Me_5 ligands. Three singlet resonances are visible intermediate between these two clusters, with chemical shifts ranging from 14-34 ppm. In order to assess if any of the resonances in the ^{13}C NMR spectrum coupled through bonds to the two signals in the ^1H spectrum apparently corresponding to the C_4H_2 hydrogen atoms, a heteronuclear HMQC experiment was conducted. Two cross peaks are observed corresponding to correlations between the ^1H resonances at δ 5.55 and 6.59 ppm and the ^{13}C resonance at 120.11 ppm.

The IR spectrum of this material displays two weak bands at 2722 and 1870 cm^{-1} that are distinct from the IR spectrum of $(C_5Me_5)_2Y(\mu\text{–}Ph)_2BPh_2$. The higher energy band in particular is consistent with C–H stretching that may arise from the C_4H_2 ligand.

The UV-visible absorption spectrum of yellow/orange **8-Y** contains shoulders on the high energy end of the spectrum with molar absorptivities >1000 $M^{-1}cm^{-1}$ consistent with a charge transfer event.

Reaction of 1 with CO_2. A light yellow/orange solution of **8-Y** (0.057 g, 0.050 mmol) in 2 mL pentane was frozen in a Schlenk flask subjected to 2 atm of CO_2. The flask was warmed to room temperature and stirred for 1 h. An off-white precipitate forms after 5 min. The suspension was filtered in an argon-filled glovebox. Removing the pentane from the filtrate yields 0.03 g of material, indicating that the bulk of **8-Y** reacted to form the precipitate. The precipitate was insoluble in hexanes, toluene, benzene, and THF. An IR of this insoluble material yields the following bands (υ, cm^{-1}): 2949w, 2886w, 1530s, 1438m, 1353m, 1231m, 1098m, 1078w, 1016w, 994w, 972m, 931w, 834m, 748m, 704m.

Theoretical Calculations on 8-Y. Electronic structure calculations of **8-Y** were performed at the density functional level of theory using the TPSSh hybrid meta-generalized gradient density functional[27] with the D3 dispersion correction[28] and the resolution of the identity (RI-J) approximation.[29] Scalar relativistic effective core potentials with the def2-TZVP basis set[30] were used for yttrium and the polarized split-valence basis set def2-SV(P) was used for other atoms.[31] All calculations were performed with the TURBOMOLE package V7.6.[32,33] Geometry optimization of the structure yielded a theoretical model with bond distances and angles that closely represent the structure derived from XRD studies.

Wiberg bond indices (WBI)[34] calculated from the geometry-optimized structure for the $[Y(\mu\text{–}\eta^3\text{:}\eta^1\text{–}CCCCH_2)Y]^{4+}$ unit are included in Table 4.2 below. Notably, the sum of the yttrium–(C41, C42, C43) indices is 2.05, which is consistent with a total of two electron pairs shared with the two yttrium centers, but this sum is not distributed equally. The WBI for Y2–C41 is 0.72 while index sum of Y1 with the C_4 bridge is 1.33. Additionally, the sum of the WBI for the carbon-carbon bonds in the bridge is 4.96, compared to the 6 predicted from a qualitative assessment of the primary resonance structure (see Figure 4.5).

Table 4.2. WBI values for bonds present in the $[Y(C_4H_2)Y]$ portion of **8-Y**.

Bond	Wiberg Bond Index
Y1–C41	0.42
Y2–C41	0.72
Y1–C42	0.32
Y1–C43	0.59
C41–C42	1.95
C42–C43	1.12
C43–C42	1.89

DISCUSSION

The C–C coupling reaction observed in the $(C_5Me_5)_2Y(\mu\text{–}Ph)_2BPh_2$ / NaC≡CH system generates a dinuclear yttrium complex bridged by a C_4H_2 unit where both hydrogen atoms are bound to a single, terminal carbon. The bridge itself is asymmetric with Y1 oriented toward three carbon atoms (C41–C43) and Y2 close to only one carbon, C41. The Y1–C43 and Y2–C41 distances are consistent with Y–C(alkyl) single bond distances.

^{1}H, ^{13}C, and HMQC NMR spectroscopies are consistent with the structural formulation determined by XRD and suggest that the structure remains intact in non-coordinating benzene. In fact, weak coupling can be seen (J = 1.7 Hz) that agrees well with known $J_{Y,H}$ coupling (2 Hz)[25] for a methylene unit in close proximity to an yttrium metal center.

Theoretical calculations were conducted on **8-Y** to elucidate the electronic structure of the complex. The relatively low Wiberg bond index for C41–C42 (1.95) compared with the expected value of 3 based on the triple bond present in the primary resonance structure trends well with the longer bond distance observed in the XRD structure. Furthermore, the WBI for the C_4 unit totals 4.95 which is lower than the expected total of 6 based on the primary resonance structure. Wiberg bond indeces also corroborate the unequal bonding nature between the C_4H_2 bridge and each yttrium metal center. The significantly lower WBI for Y2 suggests that this bond may be more reactive.

CONCLUSION

The reaction of $(C_5Me_5)_2Y(\mu\text{–}Ph)_2BPh_2$ with NaC≡CH was distinct from previous rare-earth metal alkyne reactions as well as the reaction chemistry of $U[NR_2]_3X$ complexes with NaC≡CH. An unusual bridged butatrienylidene, $(C_5Me_5)_2Y(\mu\text{–}\eta^3\text{:}\eta^1\text{–}CCCCH_2)Y(C_5Me_5)_2$, was isolated that shows a new form of hydrocarbyl bonding to rare-earth metallocenes. Though the bonding nature of the C_4H_2 bridge appears to be complicated, both theoretical calculations and spectroscopic characterization indicate the resonance structure in Figure 4.5 is a primary contributor.

EXPERIMENTAL DETAILS

All manipulations and syntheses described below were conducted with the rigorous exclusion of air and water using standard Schlenk line and glovebox techniques under an argon atmosphere free of coordinating solvents. Solvents were transferred onto activated 3 Å molecular sieves and dried *in vacuo* until solvent evaporation was observed. UV-visible absorbance spectra were collected on an Agilent Cary 60 UV-vis. IR spectra were collected on an Agilent Cary 630 equipped with a diamond ATR attachment. ^{1}H, ^{13}C, and 2D NMR experiments were conducted on a CRYO500 NMR spectrometer at room temperature

and referenced internally to residual protio-solvent resonances. $(C_5Me_5)_2Y(\mu\text{–}Ph)_2BPh_2$ was synthesized via literature procedures.[35]

$(C_5Me_5)_2Y(\mu\text{–}\eta^3\text{:}\eta^1\text{–}CCCCH_2)Y(C_5Me_5)_2$, 8-Y. Under an argon atmosphere free of coordinating solvents, a suspension of $(C_5Me_5)_2Y(\mu\text{–}Ph)_2BPh_2$ (0.253 g, 0.400 mmol) in 3 mL of 1:1 toluene/benzene was added dropwise to a slurry of 18% by weight sodium acetylide (0.106 g, 0.400 mmol) in xylenes and 3 mL toluene stirred with a glass-coated stirbar (the reaction proceeds similarly with PTFE stirbars). The pale yellow color darkens and converts to pink/orange over the next 2 hours. Attempts to isolate products from aliquots of the solution during this timeframe were unsuccessful. After stirring overnight, the resulting orange suspension was filtered over a medium frit and washed with hexanes. Solvent was removed from the filtrate under vacuum to yield 0.055 g of crude product. The product was redissolved in pentane and placed in the freezer for 1 hour. After a white precipitate formed, the supernatant was decanted, and recrystallization continued. Upon slow evaporation at room temperature X-ray quality light yellow crystals of $(C_5Me_5)_2Y(\mu\text{–}\eta^3\text{:}\eta^1\text{–}CCCCH_2)Y(C_5Me_5)_2$ were isolated (0.043 g, 30%). ^{1}H NMR (500 MHz, C_6D_6): δ 6.59 (d, 1H, $J_{H,H}$ = 4.7 Hz, $J_{Y,H}$ = 1.7 Hz), δ 5.55 (dd, 1H, $J_{H,H}$ = 4.7 Hz), δ 2.16 (s, 15H), δ 2.08 (s, 15H), δ 2.03 (s, 15H), δ 1.97 (s, 15H) ppm. $^{13}C\{^1H\}$ NMR (125 MHz, C_6D_6): δ 120.11 (s, br), δ 119.16 (s), δ 117.71 (s), δ 117.21(s), δ 34.44 (s), δ 22.73 (s), δ 14.28 (s), δ 12.12 (s), δ 12.10 (s), δ 11.87 (s), δ 11.80 (s) ppm. IR υ, cm^{-1}: 3689w, 3651w, 2951m, 2900s, 2878s, 2722w, 1870w, 1587w, 1569w, 1435s, 1376m, 1360m, 1298w, 1260w, 1132w, 1105m, 1018m, 950w, 871m, 830w, 802w, 747w, 698m. UV-visible λ_{max}, nm (ε, $M^{-1}cm^{-1}$): 325 (2000), 360 (1000).

X-ray Data Collection, Structure Solution and Refinement for $(C_5Me_5)_2Y(\mu\text{–}\eta^3\text{:}\eta^1\text{–}CCCCH_2)Y(C_5Me_5)_2$, 8-Y. A yellow crystal of approximate dimensions 0.140 x 0.159 x 0.180 mm was mounted in a cryoloop and transferred to a Bruker SMART APEX II diffractometer system. The APEX2[36] program package was used to determine the unit-cell parameters and for data collection (90 sec/frame scan time). The raw frame data was processed using SAINT[37] and SADABS[38] to yield the reflection data file. Subsequent calculations were carried out using the SHELXTL[39] program package. The diffraction symmetry was 2/*m* and the systematic absences were consistent with the monoclinic space group $P2_1/c$ that

was later determined to be correct. The structure was solved by direct methods and refined on F^2 by full-matrix least-squares techniques. The analytical scattering factors[40] for neutral atoms were used throughout the analysis. Hydrogen atoms H44A and H44B were located from a difference-Fourier map and refined (x,y,z and U_{iso}). The rest of the hydrogen atoms were included using a riding model. Least-squares analysis yielded wR2 = 0.0751 and Goof = 1.020 for 443 variables refined against 12094 data (0.70 Å), R1 = 0.0336 for those 9443 data with $I > 2.0\sigma(I)$.

References

(1) Evans, W. J.; Fang, M.; Zucchi, G. L.; Furche, F.; Ziller, J. W.; Hoekstra, R. M.; Zink, J. I. Isolation of Dysprosium and Yttrium Complexes of a Three-Electron Reduction Product in the Activation of Dinitrogen, the $(N_2)^{3-}$ Radical. *J. Am. Chem. Soc.* **2009**, *131*, 11195–11202. DOI: 10.1021/ja9036753.

(2) Fang, M.; Bates, J. E.; Lorenz, S. E.; Lee, D. S.; Rego, D. B.; Ziller, J. W.; Furche, F.; Evans, W. J. $(N_2)^{3-}$ Radical Chemistry via Trivalent Lanthanide Salt/Alkali Metal Reduction of Dinitrogen: New Syntheses and Examples of $(N_2)^{2-}$ and $(N_2)^{3-}$ Complexes and Density Functional Theory Comparisons of Closed Shell Sc^{3+}, Y^{3+}, and Lu^{3+} versus $4f^9$ Dy^{3+}. *Inorg. Chem.* **2011**, *50*, 1459–1469. DOI: 10.1021/ic102016k.

(3) Fang, M.; Lee, D. S.; Ziller, J. W.; Doedens, R. J.; Bates, J. E.; Furche, F.; Evans, W. J. Synthesis of the $(N_2)^{3-}$ Radical from Y^{2+} and Its Protonolysis Reactivity to Form $(N_2H_2)^{2-}$ via the $Y[N(SiMe_3)_2]_3/KC_8$ Reduction System. *J. Am. Chem. Soc.* **2011**, *133*, 3784–3787. DOI: 10.1021/ja1116827.

(4) Rinehart, J. D.; Fang, M.; Evans, W. J.; Long, J. R. A N_2^{3-} Radical-Bridged Terbium Complex Exhibiting Magnetic Hysteresis at 14 K. *J. Am. Chem. Soc.* **2011**, *133*, 14236–14239. DOI: 10.1021/ja206286h.

(5) Rinehart, J. D.; Fang, M.; Evans, W. J.; Long, J. R. Strong Exchange and Magnetic Blocking in N_2^{3-} Radical-Bridged Lanthanide Complexes. *Nat. Chem.* **2011**, *3*, 538–542. DOI: 10.1038/nchem.1063.

(6) Farnaby, J. H.; Fang, M.; Ziller, J. W.; Evans, W. J. Expanding Yttrium Bis(Trimethylsilylamide) Chemistry through the Reaction Chemistry of $(N_2)^{2-}$, $(N_2)^{3-}$, and $(NO)^{2-}$ Complexes. *Inorg. Chem.* **2012**, *51*, 11168–11176. DOI: 10.1021/ic301778q.

(7) Woen, D. H.; Chen, G. P.; Ziller, J. W.; Boyle, T. J.; Furche, F.; Evans, W. J. End-On Bridging Dinitrogen Complex of Scandium. *J. Am. Chem. Soc.* **2017**, *139*, 14861–14864. DOI: 10.1021/jacs.7b08456.

(8) Ryan, A. J.; Balasubramani, S. ganesh; Ziller, J. W.; Furche, F.; Evans, W. J. Formation of the End-on Bound Lanthanide Dinitrogen Complexes $[(R_2N)_3Ln–N{=}N–Ln(NR_2)_3]^{2–}$ from Divalent $[(R_2N)_3Ln]^{1–}$ Salts (R = $SiMe_3$). *J. Am. Chem. Soc.* **2020**, *142* (20), 9302–9313. DOI: 10.1021/jacs.0c01021.

(9) Chung, A. B.; Rappoport, D.; Ziller, J. W.; Cramer, R. E.; Furche, F.; Evans, W. J. Solid-State End-On to Side-On Isomerization of $(N{=}N)^{2–}$ in $\{[(R_2N)_3Nd]_2N_2\}^{2–}$ (R = $SiMe_3$) Connects In Situ $Ln^{III}(NR_2)_3$/K and Isolated $[Ln^{II}(NR_2)_3]^{1–}$ Dinitrogen Reduction. *J. Am. Chem. Soc.* **2022**, *144*, 17064–17074. DOI: 10.1021/jacs.2c06716.

(10) St. Clair, M.; Schaefer, W. P.; Bercaw, J. E. Reactivity of Permethylscandocene Derivatives with Acetylene. Structure of Acetylenediylbis(Permethylscandocene), $(\eta^5\text{-}C_5Me_5)_2Sc\text{-}C{\equiv}C\text{-}Sc(\eta^5\text{-}C_5Me_5)_2$. *Organometallics* **1991**, *10*, 525–527. DOI: 10.1021/om00049a001.

(11) Evans, W. J.; Rabe, G. W.; Ziller, J. W. Synthesis and Structure of $[(C_5Me_5)_2Sm(THF)]_2(\mu\text{-}\eta^1{:}\eta^1\text{-}C_2)$. *J. Organomet. Chem.* **1994**, *483*, 21–25. DOI: 10.1016/0022-328X(94)87142-6.

(12) Fox, A. R.; Creutz, S. E.; Cummins, C. C. A Bimetallic Uranium μ-Dicarbide Complex: Synthesis, X-Ray Crystal Structure, and Bonding. *Dalton Trans.* **2010**, *39*, 6632–6634. DOI: 10.1039/c0dt00419.

(13) Kent, G. T.; Yu, X.; Pauly, C.; Wu, G.; Autschbach, J.; Hayton, T. W. Synthesis of Parent Acetylide and Dicarbide Complexes of Thorium and Uranium and an Examination of Their Electronic Structures. *Inorg. Chem.* **2021**, *60*, 15413–15420. DOI: 10.1021/acs.inorgchem.1c02064.

(14) Evans, W. J.; Perotti, J. M.; Ziller, J. W. Synthetic Utility of $[(C_5Me_5)_2Ln][(\mu\text{-}Ph)_2BPh_2]$ in Accessing $[(C_5Me_5)_2LnR]_x$ Unsolvated Alkyl Lanthanide Metallocenes, Complexes with High C-H Activation Reactivity. *J. Am. Chem. Soc.* **2005**, *127*, 3894–3909. DOI: 10.1021/ja045064e.

(15) Evans, W. J.; Perotti, J. M.; Ziller, J. W. Formation of a Bridging Planar Trimethylenemethane Dianion from a Neopentyl Precursor via Sequential β-Alkyl Elimination and C-H Activation. *J. Am. Chem. Soc.* **2005**, *127*, 1068–1069. DOI: 10.1021/ja044529y.

(16) Evans, W. J.; Champagne, T. M.; Ziller, J. W.; Kaltsoyannis, N. Planar Trimethylenemethane Dianion Chemistry of Lanthanide Metallocenes: Synthesis, Structure, Density Functional Theory Analysis, and Reactivity of $[(C_5Me_5)_2Ln]_2[\mu\text{-}\eta^3\text{:}\eta^3\text{-}C(CH_2)_3]$ Complexes. *J. Am. Chem. Soc.* **2006**, *128*, 16178–16189. DOI: 10.1021/ja0645988.

(17) Evans, W. J.; Bloom, I.; Hunter, W. E.; Atwood, J. L. Synthesis of Organosamarium Complexes Containing Sm-C and Sm-P Bonds. Crystallographic Characterization of $[(CH_3C_5H_4)_2SmC{\equiv}CC(CH_3)_3]_2$. *Organometallics* **1983**, *2*, 709–714. DOI: 10.1021/om00078a003.

(18) Evans, W. J.; Keyer, R. A.; Ziller, J. W. Carbon-Carbon Bond Formation by Coupling of Two Phenylethynyl Ligands in an Organolanthanide System. *Organometallics* **1990**, *9*, 2628–2631. DOI: 10.1021/om00159a035.

(19) Evans, W. J.; Keyer, R. A.; Ziller, J. W. Investigation of Organolanthanide-Based Carbon-Carbon Bond Formation: Synthesis, Structure, and Coupling Reactivity of Organolanthanide Alkynide Complexes, Including the Unusual Structures of the Trienediyl Complex $[(C_5Me_5)_2Sm]_2[\mu\text{-}\eta^2\text{:}\eta^2\text{-}Ph(CH_2)2C{=}C{=}C{=}C\text{-}(CH_2)_2Ph]$ and the Unsolvated Alkynide $[(C_5Me_5)_2Sm(C{\equiv}CCMe_3)]_2$. *Organometallics* **1993**, *12*, 2618–2633. DOI: 10.1021/om00031a036.

(20) Cameron, T. M.; Gordon, J. C.; Scott, B. L. Synthesis and Characterization of (Mono)Pentamethylcyclopentadienyl Lutetium Complexes: Formation of Bipyridyl-Stabilized Alkyls, Anilides, and Terminal Acetylides. *Organometallics* **2004**, *23*, 2995–3002. DOI: 10.1021/om0497700.

(21) Casely, I. J.; Ziller, J. W.; Evans, W. J. C-H Activation via Carbodiimide Insertion into Yttrium-Carbon Alkynide Bonds: An Organometallic Alder-ene Reaction. *Organometallics* **2011**, *30*, 4873–4881. DOI: 10.1021/om200419k.

(22) Adams, C. J.; Bruce, M. I.; Skelton, B. W.; White, A. H. A Novel Route to Butatrienylidene Complexes: Stabilisation of $:C{=}C{=}C{=}CH_2$ on Ru_5 Clusters. *Chem. Commun.* **1996**, *32*, 2663–2664. DOI: 10.1039/CC9960002663.

(23) Adams, C. J.; Bruce, M. I.; Skelton, B. W.; White, A. H. Reactions of $Ru_5(\mu_5\text{-}C_2)(\mu\text{-}SMe)_2(\mu\text{-}PPh_2)_2(CO)_{11}$ with Disubstituted Alkynes C_2R_2 (R = Me, Ph). *J. Chem. Soc. Dalton Trans.* **1999**, *584*, 1283–1288. DOI: 10.1039/a809563i.

(24) CRC Handbook of Chemistry and Physics, 88th edition, Section 3.

(25) MacDonald, M. R.; Langeslay, R. R.; Ziller, J. W.; Evans, W. J. Synthesis, Structure, and Reactivity of the Ethyl Yttrium Metallocene, $(C_5Me_5)_2Y(CH_2CH_3)$, Including Activation of Methane. *J. Am. Chem. Soc.* **2015**, *137*, 14716–14725. DOI: 10.1021/jacs.5b08597.

(26) Evans, W. J.; Kozimor, S. A.; Brady, J. C.; Davis, B. L.; Nyce, G. W.; Seibel, C. A.; Ziller, J. W.; Doedens, R. J. Metallocene Allyl Reactivity in the Presence of Alkenes Tethered to Cyclopentadienyl Ligands. *Organometallics* **2005**, *24*, 2269–2278. DOI: 10.1021/om049286x.

(27) Staroverov, V. N.; Scuseria, G. E.; Tao, J.; Perdew, J. P. Comparative Assessment of a New Nonempirical Density Functional: Molecules and Hydrogen-Bonded Complexes. *J. Chem. Phys.* **2003**, *119*, 12129–12137. DOI: 10.1063/1.1626543.

(28) Grimme, S.; Antony, J.; Ehrlich, S.; Krieg, H. A Consistent and Accurate Ab Initio Parametrization of Density Functional Dispersion Correction (DFT-D) for the 94 Elements H-Pu. *J. Chem. Phys.* **2010**, *132*, 154104. DOI: 10.1063/1.3382344.

(29) Grimme, S. Semiempirical GGA-Type Density Functional Constructed with a Long-Range Dispersion Correction. *J. Comput. Chem.* **2006**, *27*, 1787–1799. DOI: 10.1002/jcc.20495.

(30) Weigend, F.; Köhn, A.; Hättig, C. Efficient Use of the Correlation Consistent Basis Sets in Resolution of the Identity MP2 Calculations. *J. Chem. Phys.* **2002**, *116*, 3175–3183. DOI: 10.1063/1.1445115.

(31) Weigend, F.; Ahlrichs, R. Balanced Basis Sets of Split Valence, Triple Zeta Valence and Quadruple Zeta Valence Quality for H to Rn: Design and Assessment of Accuracy. *Phys. Chem. Chem. Phys.* **2005**, *7*, 3297–3305. DOI: 10.1039/b508541a.

(32) TURBOMOLE V7.6 2020, a development of University of Karlsruhe and Forschungszentrum Karlsruhe GmbH, 1989−2007, TURBOMOLE GmbH, since 2007: available from http://www.turbomole.com.

(33) Balasubramani, S. G.; Chen, G. P.; Coriani, S.; Diedenhofen, M.; Frank, M. S.; Franzke, Y. J.; Furche, F.; Grotjahn, R.; Harding, M. E.; Hättig, C.; Hellweg, A.; Helmich-Paris, B.; Holzer, C.; Huniar, U.; Kaupp, M.; Marefat Khah, A.; Karbalaei Khani, S.; Müller, T.; Mack, F.; Nguyen, B. D.; Parker, S. M.; Perlt, E.; Rappoport, D.; Reiter, K.; Roy, S.; Rückert, M.; Schmitz, G.; Sierka, M.; Tapavicza, E.; Tew, D. P.; Van Wüllen, C.; Voora, V. K.; Weigend, F.; Wodyński, A.; Yu, J. M. TURBOMOLE: Modular Program Suite for Ab Initio Quantum-Chemical and Condensed-Matter Simulations. *J. Chem. Phys.* **2020**, *152*, 184107. DOI: 10.1063/5.0004635.

(34) Wiberg, K. B. Application of the Pople-Santry-Segal CNDO Method to the Cyclopropylcarbinyl and Cyclobutyl Cation and to Bicyclobutane. *Tetrahedron* **1968**, *24*, 1083–1096. DOI: 10.1016/0040-4020(68)88057-3.

(35) Evans, W. J.; Davis, B. L.; Champagne, T. M.; Ziller, J. W. C-H Bond Activation through Steric Crowding of Normally Inert Ligands in the Sterically Crowded Gadolinium and Yttrium $(C_5Me_5)_3M$ Complexes. *Proc. Natl. Acad. Sci. U. S. A.* **2006**, *103*, 12678–12683. DOI: 10.1073/pnas.0602672103.

(36) APEX2 Version 2014.11-0, Bruker AXS, Inc.; Madison, WI 2014.

(37) SAINT Version 8.34a, Bruker AXS, Inc.; Madison, WI 2013.

(38) Sheldrick, G. M. SADABS, Version 2014/5, Bruker AXS, Inc.; Madison, WI 2014.

(39) Sheldrick, G. M. SHELXTL, Version 2014/7, Bruker AXS, Inc.; Madison, WI 2014

(40) International Tables for Crystallography 1992, Vol. C., Dordrecht: Kluwer Academic Publishers.

Chapter 5:

Attempts to Reduce Organometallic Rare-earth Metal Precursors Using New Methods: Photoredox Reactions and Barium Powder

INTRODUCTION

The use of potassium and crypt in the chemical reduction of organometallic precursors across the periodic table is well known, generating low oxidation state rare-earth metal, transition metal, actinide metal, and main group metal complexes. Interestingly, transition metal and main group metals are also regularly reduced via other methods, such as photoredox reactions. These reactions involve a more complex electron-transfer process. On a molecular level, a molecule is first excited by light to yield a highly reducing excited state. This excited state should have a reduction potential more negative than the species targeted for reduction. The electron is then transferred to generate the cationic photoreductant in its ground state. In the absence of reactive species present in solution, oftentimes back electron transfer (BET) is observed. In order to preserve the reduced species and regenerate the neutral photoreductant in its ground state, a sacrificial reductant is often included. This is a chemical that serves to reduce the cationic photoreductant and form a stable countercation for the targeted reduced species.

In order to explore the possibility of generating the Ln(II) complexes via photoredox reactions, a relatively strong photoreductant is necessary. The compound, $W(CN_{dipp})_6$, published by Professor Harry Gray and coworkers fits this criterion.[1,2] This complex has a ground state reduction potential of −0.72 V vs $Fc^{+/}0$ (0.5 M $[^nBu_4N][PF_6]$ in CH_2Cl_2), but upon excitation with UV-visible light, the complex enters an excited state, $W(CN_{dipp})_6$*, that has a calculated reduction potential of −3.0 V vs $Fc^{+/0}$ (0.5 M $[^nBu_4N][PF_6]$ in CH_2Cl_2). This is quite near the experimentally measured reduction potentials of non-traditional Cp'_3Ln compounds: −2.9 to −3.1 V vs $Fc^{+/0}$ (0.1 M $[^nBu_4][BPh_4]$).[3] A potential limitation is that the lifetime of the excited state for the tungsten-based complex is reported to be 122 ns in toluene.[1]

Another reduction method that has found success with transition metal and main group complexes is the use of group 2-based reductants. For example, both $[\{(^{Dipp}Nacnac)Mg\}_2]$ and $[\{(^{tBu}Nacnac)Mg\}_2]$

{^{Dipp}Nacnac = [(2,6-diisopropylphenyl)NCMe]$_2$CH and ^{tBu}Nacnac = [(2,6-ditertbutylphenyl)NCMe]$_2$CH} have been used to generate a Ge(0) complex.[4,5] Of the group 2 metals, barium is advantageous in that it has a similar reduction potential to potassium[6,7] ($E_{1/2}(Ba^{+2/0})$ = −2.91 V vs SHE, $E_{1/2}(K^{+/0})$ = −2.93 V vs SHE) which is known to reduce organometallic rare-earth compounds. Furthermore, one metric that aligns with the success of K/crypt for the isolation of reduced complexes is the association constant for the free alkali metal cation and free organic chelate to form the complex cation. The log K_{eq} value for $[K(crypt)]^{1+}$ is 5.3, the highest of all combinations examined in Chapter 1. As Ba^{2+} has a nearly identical ionic radius to K^{1+} and double the charge, its log K_{eq} value is almost double at 9.5.[8] It was therefore of interest to investigate barium as a reductant for the generation of low oxidation state complexes.

This Chapter describes both alternative methods of reducing rare-earth metal complexes: photoredox and barium reduction.

PHOTOREDOX RESULTS AND DISCUSSION

The following experimental framework was utilized to study the efficacy of $W(CN_{dipp})_6$ as a photoreductant for the generation of Ln(II) species. First, an organometallic Ln(III) species, $W(CN_{dipp})_6$, crypt, and a sacrificial reductant were dissolved in a toluene solution under an argon atmosphere, and this was subsequently exposed to high intensity UV-visible light (see Figure 5.1 for reaction scheme and sacrificial reductant variations). In the case of yttrium-based starting Ln(III) species, formation of a Ln(II) salt was assessed by the presence of a darkly colored precipitate. In the case of a lanthanum-based starting material, formation was also assessed by EPR spectroscopy conducted on the solution.

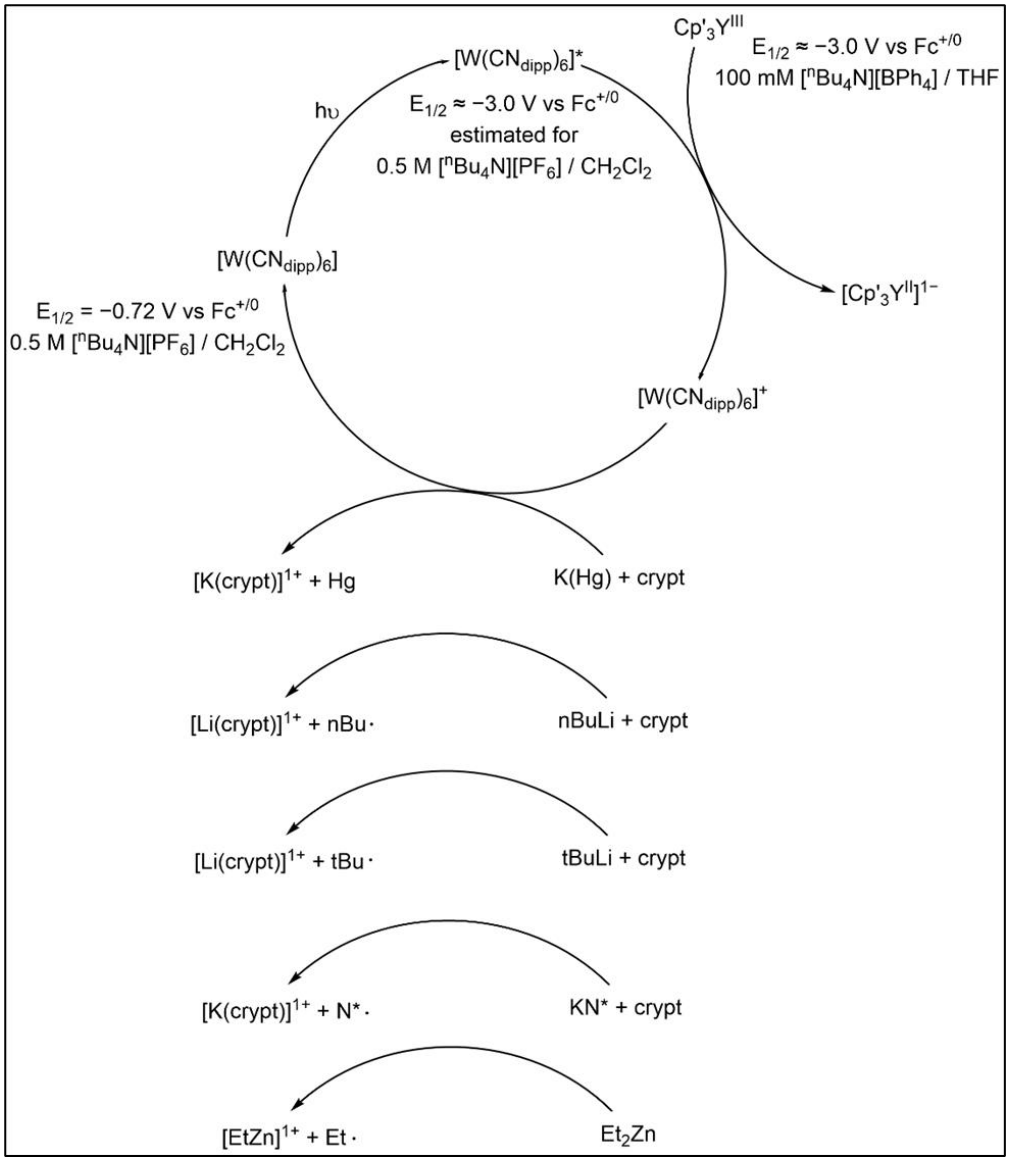

Figure 5.1. Reaction scheme for the photoredox reactions run with Cp′$_3$Y. Variations in sacrificial reductants shown as well, including desired products.

The variable explored most thoroughly was the sacrificial reductant. As shown in Figure 5.1, diethylzinc, potassium bis(trimethylsilyl)amid, tert-butyllithium, *n*-butyllithium, and potassium/mercury amalgam were studied. None of these sacrificial reductants enabled precipitation or isolation of an Y(II) species. A control reaction between Cp′$_3$Y and tBuLi resulted in NMR spectroscopic evidence of 2-methylpropene, consistent with consecutive salt metathesis and β-hydride elimination. The heterogeneous nature of 1% KHg amalgam resulted in no reaction.

In order to explore the possibility that $[Cp'_3Y]^{1-}$ was being generated in situ, but due to BET or some other pathway could not be isolated, EPR spectroscopy of the reaction mixture was attempted. The organic radical present on $W(CN_{dipp})_6$* yielded a large signal that precluded observation of a possible Y(II) species, similar to the characterization of Y(II) generated from the gamma irradiation method in Chapter 3. Therefore, a precursor with a known Ln(II) EPR signal that covers a greater range of magnetic field, Cp'_3La, was employed. Even in this case, no signals consistent with La(II) were observable in the EPR spectrum.

PHOTOREDOX EXPERIMENTAL

Photoredox Reactions. In order to facilitate product separation, toluene was used as a solvent. Reactions involved the addition of Cp'_3Ln (0.011 g, 0.020 mmol), crypt (0.007 g, 0.02 mmol), $W(CN_{dipp})_6$ (0.002 g, 0.002, 5-10% loading), toluene (1 mL), and a sacrificial reductant to an NMR tube that was sealed and exposed to a Hg-vapor lamp (200-400 nm light) for 1 hr. A number of sacrificial reductants were attempted, as exemplified in the reaction scheme in Figure 5.1.

BARIUM RESULTS AND DISCUSSION

Barium is known to be a kinetically slow reductant. Consistent with this, stirring fresh Ba shavings with Cp'_3Ln (Ln = Y, Sm, Tm, Yb) yields no reaction. Therefore, in order to maximize the surface area available and facilitate more rapid kinetics, freshly shaved barium was converted to a powder. About 35 mL of ammonia was condensed over a chunk of sodium to dry the ammonia, and then the ammonia was condensed over fresh barium shavings (2.000 g, 14.50 mmol) in a Schlenk flask cooled in a liquid nitrogen bath. See Figure 5.2 below for setup. A dark blue solution was observed, and then the temperature of the apparatues was raised to room temperature. The ammonia evaporated to leave a gold coating of barium on the flask walls that turned dull grey under vacuum. Collection of the dull grey material in an inert atmosphere glovebox yielded a fine Ba powder.

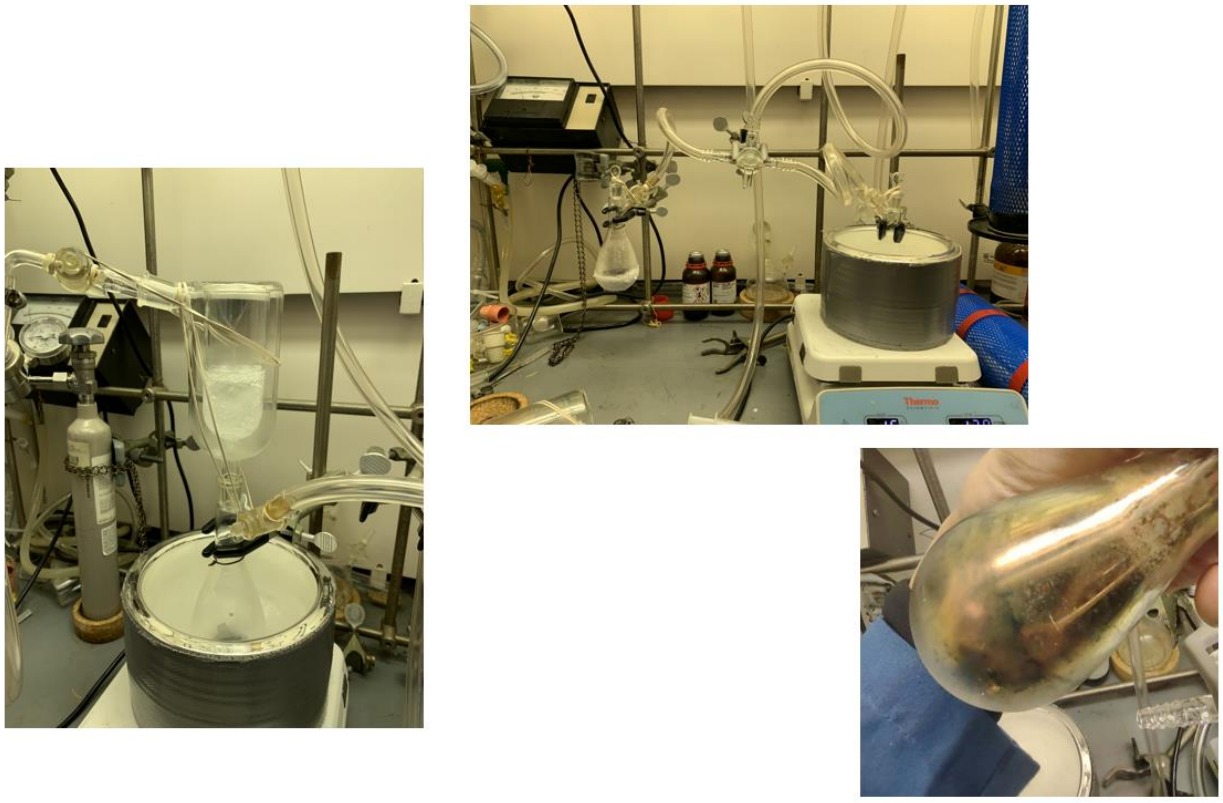

Figure 5.2. Photographs of the experimental setup for condensing the ammonia over sodium (left), transferring the ammonia onto Ba(0) shavings (top), and slow evaporation of the ammonia (right).

Attempts to condense ammonia onto stoichiometric or excess Ba(0) shavings in addition to Cp'_3Y and crypt only yielded the formation of a white precipitate insoluble in hexanes, toluene, diethyl ether, and tetrahydrofuran. This is consistent with previous studies in which the presence of Fe(III) has catalyzed the formation of highly insoluble metal amides.[9,10]

Reactions of the powdered barium with Cp'_3Ln and crypt yielded a variety of results. First of all, Cp'_3Y does not react with the barium powder, even in the presence of crypt, as evidenced by a ^1H NMR showing unreacted starting material. Fortunately, the barium powder does appear to reduce $4f^n$ Cp'_3Ln species with more positive redox potentials that undergo reduction to form traditional electron configurations, $4f^{n+1}$. However, crystals of the putative Ln(II) species were elusive. Crystallization of the Yb(II) species from acetonitrile dried over activated 3 Å molecular sieves yielded dark purple crystals of sufficient quality for XRD analysis. These crystals were thus identified as [Ba(crypt)Cp][$Cp_2Yb(\mu$–

$OSiMe_3)_2YbCp_2$], see Figure 5.3. Use of acetonitrile dried over calcium hydride at reflux and stored over activated sieves have not yielded these or any other crystals yet.

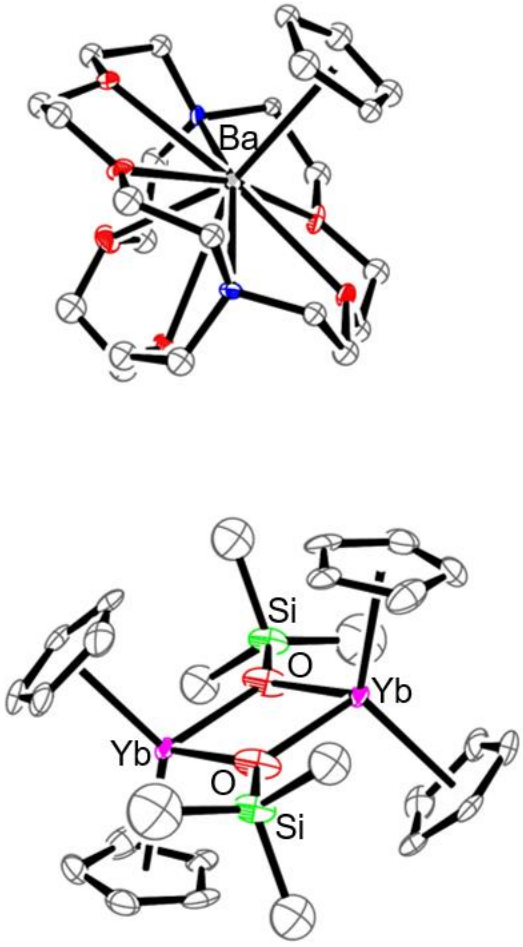

Figure 5.3. ORTEP of [Ba(crypt)Cp][$Cp_2Yb(\mu$–$OSiMe_3)_2YbCp_2$] with ellipsoids drawn at the 50% probability level and hydrogen atoms omitted for clarity.

[Ba(crypt)Cp][$Cp_2Yb(\mu$–$OSiMe_3)_2YbCp_2$]. One half of the bimetallic anion was generated by symmetry operations indicating that each ytterbium ion has an equal oxidation state of +2.5. It is suggested that if this material could be generated in bulk, the presence or lack of an intervalence charge transfer (IVCT) band in the low energy portion of the UV-visible absorbance spectrum may indicate whether it converts to mixed valent in solution. It is unusual that the structure lacks any Cp′ ligands, given their presence in the starting material, which is clean by ^{1}H NMR spectroscopy. The bridging siloxide ligands

are likely a result of activation of the C–Si bond in the Cp′ ligand, facilitated by the presence of water in the acetonitrile.

Also of note in this structure is the presence of barium, encapsulated by crypt, binding to a Cp ligand. The Ba–Cp distance is 2.856 Å, right in the range of the 2.852–2.875 Å distances observed for Ba–Cp′ in the extended structure $[(THF)Cs(\mu\text{–}\eta^5\text{:}\eta^5\text{–}Cp')_3Ba(THF)]_n$.[11] The crypt opens up significantly to accommodate this ligation. By taking the two mean planes of the nitrogen and oxygen atoms of the open arms, the dihedral angle can be calculated at 4.75°. A search of [Ba(crypt)] motifs in the CCDC reveals that in 10/11 (91%) structures, the Ba(II) ion binds to some Lewis base (whether anionic or neutral) aside from just crypt. This suggests that barium is unlikely to be coordinatively and/or electronically saturated in the crypt binding pocket. In order to use this as a synthetic tool, a different precursor was pursued.

In an attempt to leverage this steric preference, stoichiometric Ba(0) powder was combined with crypt and Cp''_3ThBr. Rather than proceed to [Ba(crypt)Br][Cp''_3Th], this reaction remains the deep blue of Cp''_3Th. Using an excess of barium powder yields the teal color associated with $[Cp''_3Th^{II}]^{1-}$. This indicates that rather than the proposed product formulation of [Ba(crypt)Br][Cp''_3Th], the reaction is likely occurring in a stepwise manner to generate $BaBr_2$ and [Ba(crypt)][Cp''_3Th]$_2$.

BARIUM EXPERIMENTAL

Reaction of Cp'_3Y, Ba(powder), and crypt. A vial of Cp'_3Y (0.051 g, 0.1 mmol) and crypt (0.039 g, 0.1 mmol) in about 1 mL THF was pre-cooled to −35 °C and then pipetted over barium (0.008 g, 0.05 mmol). Stirring at room temperature for over 3 h yields an opaque suspension. Filtration of the suspension yields a dark grey precipitate consistent with unreacted barium and a light yellow filtrate. Solvent was removed from the filtrate under vacuum, and ^{1}H NMR spectroscopy confirmed the presence of unreacted Cp'_3Y.

Reaction of Cp'_3Ln (Ln = Sm, Tm, Yb), Ba(powder), and crypt. A vial of Cp'_3Ln (≈ 0.050 g) and crypt (≈ 0.040 g) in about 1 mL THF was pre-cooled to −35 °C and then pipetted over barium (≈ 0.010 g). Stirring at room temperature for 15 minutes yielded dark solutions (Sm = purple, Tm = green, Yb =

green). Removal of the THF under vacuum yielded a sticky solid with UV-visible spectra similar to those of the known [K(crypt)][Cp'_3Ln^{II}] compounds.

Reaction of Cp''_3ThBr, Ba(powder), and crypt. In an attempt to synthesize [Ba(crypt)Br][Cp''_3Th], a solution of Cp''_3ThBr (0.101 g, 0.1 mmol) and crypt (0.039 g, 0.1 mmol) in 1 mL 1:1 THF:Et_2O was pipetted onto barium powder (0.017 g, 0.1 mmol). No color change was observed after 30 min, but stirring at room temperature overnight yields a deep blue color associated with Cp''_3Th. Running the same reaction with an excess of barium yielded a teal color consistent with $[Cp''_3Th]^{1-}$.

X-ray Data Collection, Structure Solution and Refinement for [Ba(crypt)Cp][$Cp_2Yb(\mu$–$OSiMe_3)_2YbCp_2$] . A purple crystal of approximate dimensions 0.122 x 0.253 x 0.319 mm was mounted in a cryoloop and transferred to a Bruker SMART APEX II diffractometer system. The APEX2[12] program package was used to determine the unit-cell parameters and for data collection (30 sec/frame scan time). The raw frame data was processed using SAINT[13] and SADABS[14] to yield the reflection data file. Subsequent calculations were carried out using the SHELXTL[15] program package. The diffraction symmetry was 2/*m* and the systematic absences were consistent with the monoclinic space group $P2_1/n$ that was later determined to be correct. The structure was solved by direct methods and refined on F^2 by full-matrix least-squares techniques. The analytical scattering factors[16] for neutral atoms were used throughout the analysis. Hydrogen atoms were included using a riding model. There were two half-molecules of the dimeric formula-units present, each was located about an inversion center. Disordered atoms were included using multiple components with partial site-occupancy-factors. Anisotropic refinement yielded non-positive-definite displacement parameters for several atoms. Those atoms were refined isotropically. Least-squares analysis yielded wR2 = 0.1999 and Goof = 1.158 for 473 variables refined against 11691 data (0.78 Å), R1 = 0.0818 for those 9557 data with $I > 2.0\sigma(I)$.

CONCLUSION

Despite promising hypotheses concerning the use of photoredox or Ba-based reductions to generate new and/or more stable Ln(II) species, the experiments conducted here suggest otherwise. Regarding the photoredox reactions, no crystallographic or spectroscopic evidence for Ln(II) was observed. Regarding

the use of Ba powder, no reaction was observed with the non-traditional metal complex Cp'_3Y. Fortunately, reduction of some traditional Ln(III) species was observed. Though crystallization proved challenging, the use of wet acetonitrile at room temperature afforded crystals determined to be [Ba(crypt)Cp][$Cp_2Yb(\mu$–$OSiMe_3)_2YbCp_2$] based on XRD studies. These crystals emphasized that although $[Ba(crypt)]^{1+}$ has a significantly higher association constant, its higher electrostatic attraction makes it more likely to interact with the anionic ligands, demonstrated by the binding of cyclopentadienyl in the crystal structure.

References

(1) Sattler, W.; Henling, L. M.; Winkler, J. R.; Gray, H. B. Bespoke Photoreductants: Tungsten Arylisocyanides. *J. Am. Chem. Soc.* **2015**, *137*, 1198–1205. DOI: 10.1021/ja510973h.

(2) Fajardo, J.; Schwan, J.; Kramer, W. W.; Takase, M. K.; Winkler, J. R.; Gray, H. B. Third-Generation $W(CNAr)_6$ Photoreductants (CNAr = Fused-Ring and Alkynyl-Bridged Arylisocyanides). *Inorg. Chem.* **2021**, *60*, 3481–3491. DOI: 10.1021/acs.inorgchem.0c02912.

(3) Trinh, M. T.; Wedal, J. C.; Evans, W. J. Evaluating Electrochemical Accessibility of $4f^n5d^1$ and $4f^{n+1}$ Ln(II) Ions in $(C_5H_4SiMe_3)_3Ln$ and $(C_5Me_4H)_3Ln$ Complexes. *Dalton Trans.* **2021**, *50*, 14384–14389. DOI: 10.1039/d1dt02427b.

(4) Stasch, A.; Jones, C. Stable Dimeric Magnesium(I) Compounds: From Chemical Landmarks to Versatile Reagents. *Dalton Trans.* **2011**, *40*, 5659–5672. DOI: 10.1039/c0dt01831g.

(5) Sidiropoulos, A.; Jones, C.; Stasch, A.; Klein, S.; Frenking, G. N-Heterocyclic Carbene Stabilized Digermanium(0). *Angew. Chem. Int. Ed.* **2009**, *48*, 9701–9704. DOI: 10.1002/anie.200905495.

(6) Bard, A. J.; Parsons, B.; Jordon, J., eds. *Standard Potentials in Aqueous Solutions*, Dekker: New York, **1985**.

(7) Milazzo, G.; Caroli, S.; Sharma, V. K. *Tables of Standard Electrode Potentials*, Wiley: London, **1978**.

(8) Izatt, R. M.; Bradshaw, J. S.; Nielsen, S. A.; Lamb, J. D.; Christensen, J. J.; Sen, D. Thermodynamic and Kinetic Data for Cation-Macrocycle Interaction. *Chem. Rev.* **1985**, *85*, 271–339. DOI: 10.1021/cr00068a003.

(9) Galy, N.; Doucet, H.; Santelli, M. On the Influence of the Nature of the Iron(III) Salt Catalyst Precursor for the Preparation of Sodium Amide. *Comptes Rendus Chim.* **2011**, *14*, 434–436. DOI: 10.1016/j.crci.2010.11.008.

(10) Greenlee, K. W.; Henne, A. L. Sodium Amide. *Inorg. Synth.* **1946**. *2*. 128–135. DOI: 10.1002/9780470132333.ch38.

(11) Huh, D. N.; Ciccone, S. R.; Moore, W. N. G.; Ziller, J. W.; Evans, W. J. Synthesis of Ba(II) Analogs of Ln(II)-in-(2.2.2-Cryptand) and Layered Hexagonal Net Ln(II) Complexes, $[(THF)Cs(\mu–\eta^5:\eta^5–C_5H_4SiMe_3)_3Ln^{II}]_n$. *Polyhedron*, **2021**, *210*, 115393. DOI: 10.1016/j.poly.2021.115493.

(12) APEX2 Version 2014.11-0, Bruker AXS, Inc.; Madison, WI 2014.

(13) SAINT Version 8.34a, Bruker AXS, Inc.; Madison, WI 2013.

(14) Sheldrick, G. M. SADABS, Version 2014/5, Bruker AXS, Inc.; Madison, WI 2014.

(15) Sheldrick, G. M. SHELXTL, Version 2014/7, Bruker AXS, Inc.; Madison, WI 2014.

(16) International Tables for Crystallography 1992, Vol. C., Dordrecht: Kluwer Academic Publishers.

Appendix A:

Fluorescence of [K(2.2.2-cryptand)][$C_5H_4SiMe_3)_3$Eu]

In a broad effort to understand the bonding and spectroscopy associated with the $[Cp'_3Ln]^{1-}$ complexes, visiting scientist Dr. Maria Beltran-Leiva enlisted a collaboration with the specific goal of synthesizing, crystallizing, and obtaining the fluorescence spectrum of [K(crypt)][Cp'_3Eu]. The fluorescence spectrum provides important experimental data regarding the energy difference between the ground and excited state, which can then be compared with values calculated from different methods. In this case, those methods include both high-precision methods (such as LF-DFT and QTAIM) and *ab initio* methods.

Therefore, [K(crypt)][Cp'_3Eu] was synthesized according to literature procedures.[1] The relevant spectra (excitation and emission) were collected on a 1.85 mM solution using a Cary Eclipse fluorescence spectrometer. The spectra provided to Dr. Beltran-Leiva are included below in Figure A.1. The excitation wavelength was found to 405 nm, about 80 nm less than the absorption λmax = 483 nm. The emission wavelength was found to be 449 nm.

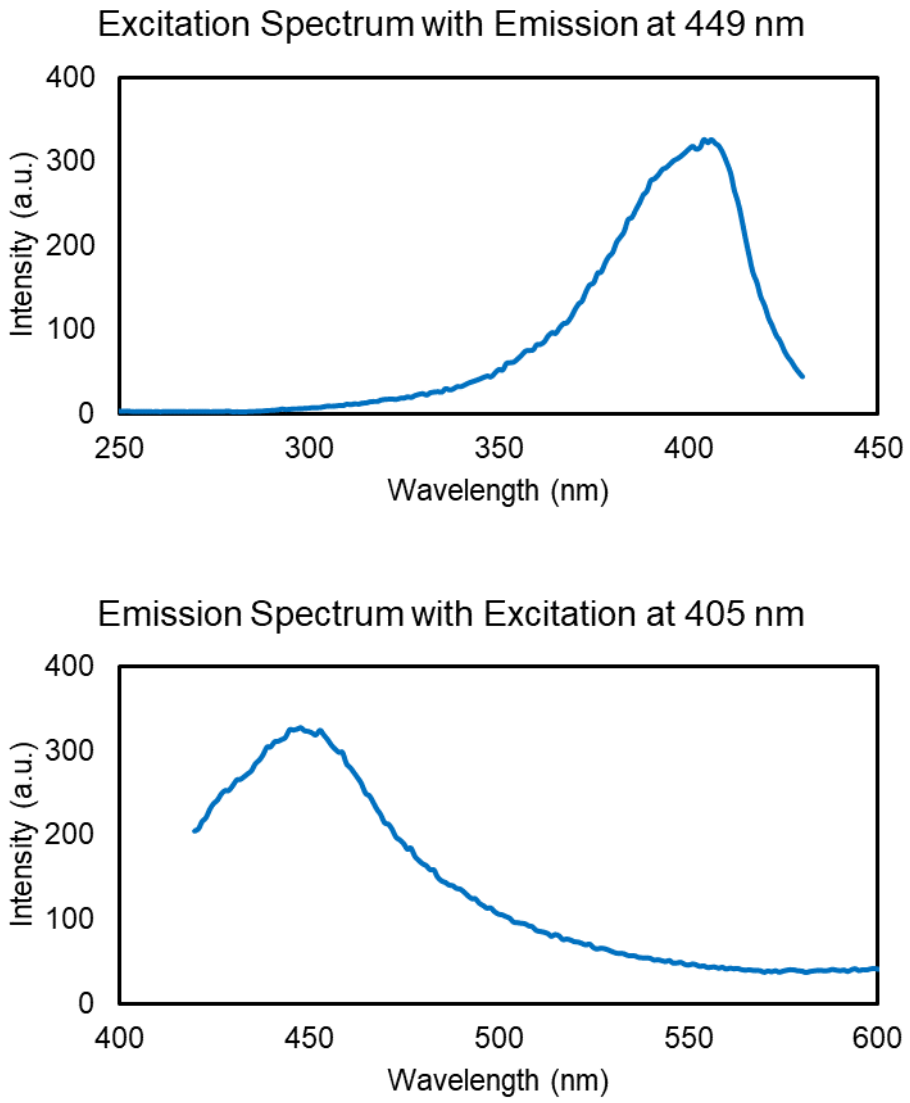

Figure A.1. Excitation (top) and emission (bottom) spectra of [K(crypt)][Cp′$_3$Eu] collected in on a 1.85 mM THF solution at room temperature.

References

(1) Fieser, M. E.; Macdonald, M. R.; Krull, B. T.; Bates, J. E.; Ziller, J. W.; Furche, F.; Evans, W. J. Structural, Spectroscopic, and Theoretical Comparison of Traditional vs Recently Discovered Ln^{2+} Ions in the [K(2.2.2-Cryptand)][($C_5H_4SiMe_3$)$_3$Ln] Complexes: The Variable Nature of Dy^{2+} and Nd^{2+}. *J. Am. Chem. Soc.* **2015**, *137*, 369–382. DOI: 10.1021/ja510831n.

Appendix B:

Spectroscopic Contributions towards the Characterization of Reductive C–O Cleavage Products of Ethereal Solvents and 18-crown-6 in $Ln(NR_2)_3/KC_8$ Reactions ($R = SiMe_3$)

[†]As discussed in the Introduction and Chapter 1 in particular, the decomposition pathways for non-traditional $4f^n5d^1$ and $4d^1$ Ln(II) complexes can be complicated, generating a variety of decomposition products. In an effort to study the decomposition products of the $[Y(NR_2)_3]^{1-}$ Y(II) system ($R = SiMe_3$), my coworker Dr. Amanda Chung crystallized a number of decomposition products in which available C–O bonds (present in ethereal solvents or the 18c6 chelate) were cleaved, including $[K(crypt)][(R_2N)_3Y(OCH_2CH_2OCH_3)]$, $[(R_2N)_2Y(\mu\text{-}OCH_2CH_2OMe\text{-}\kappa O,\kappa O')]_2$, $[K(crypt)][(R_2N)_3Y(OCH_2CH_2CH_2CH_3)]$, $\{[(R_2N)_2]Y[\mu\text{-}O_2(C_{10}H_{20}O_4\text{-}\kappa O,\kappa O')K]\}_2$, and $[K(crypt)]\{(R_2N)_2Y[N(SiMe_3)(SiMe_2CH_2)\text{-}\kappa C,\kappa N]\}$. To examine the spectroscopy (and therefore the product ratios) underpinning the formation of these decomposition products, several targeted experiments were conducted.

Reaction of $Y\{N(SiMe_3)_2\}_3$ with KC_8 and 18c6 in tetrahydrofuran. A vial containing $Y(NR_2)_3$ ($R = SiMe_3$) (0.097 g, 0.17 mmol) and 18c6 (0.046 g, 0.17 mmol) dissolved in about 2 ml THF was cooled to −78 °C, along with a vial containing KC_8 (0.026 g, 0.16 mmol). Using a similarly cold pipette, the THF solution was transferred onto the KC_8 and immediate conversion to a dark blue suspension was observed. After stirring for 2 hr at room temperature, the suspension settled into a clear supernatant and black solid (presumably graphite). The suspension was centrifuged, and the supernatant was decanted. The THF was pumped off, and the resulting white solid was washed with about 3 mL hexanes. The leftover white powder yielded a mass of 0.099 g. The ^{1}H NMR spectrum of this material (see Figure B.1) is consistent with the formation of the cyclometallate $[K(18\text{-crown-6})][\{(Me_3Si)_2N\}_2Y(CH_2SiMe_2NSiMe_3)]$ when compared to

[†] Portions of this appendix have been published: Chung, A. B.; Stennet, C. R.; Moore, W. N. G.; Fang, M.; Ziller, J. Z.; Evans, W. J. Reductive C–O Cleavage of Ethereal Solvents and 18-Crown-6 in $Ln(NR_2)_3/KC_8$ Reactions ($R = SiMe_3$). *Inorg. Chem.* **2023**, *62*, 5854–5862. DOI: 10.1021/acs.inorgchem.3c00689

its previously reported spectrum.[1] ^{1}H NMR (600 MHz, THF-d_8): δ = 3.63 (s, CH_2, 24H, 18-crown-6), 0.12 (s, 36H, NSiMe_3), 0.01 (s, 15H, N(SiMe_3)(SiMe_2CH$_2$)), −0.55 (d, 2H, N(SiMe$_3$)(SiMe$_2$CH_2) $J_{Y,H}$ = 2.6 Hz). In the same sample, additional signals at much lower intensity were observed at δ = 3.94 (t, OCH_2CH$_2$CH$_2$CH$_3$), 1.59 (quint, OCH$_2$CH_2CH$_2$CH$_3$), 1.25 (sext, OCH$_2$CH$_2$CH_2CH$_3$), 0.87 (t, OCH$_2$CH$_2$CH$_2$CH_3), and 0.10 (s, NSiMe_3) in an approximate ratio of 2:2:2:3:54, respectively, in agreement with the formation of [K(18-crown-6)][{(SiMe$_3$)$_2$N}$_3$Y(OCH$_2$CH$_2$CH$_2$CH$_3$)], as a minor product. From these data, it was determined that the cyclometallate and the butoxide are formed in an approximate 4:1 ratio. The percentage yields of the cyclometallate and the butoxide were determined by this molar ratio to be 46% and 12%, respectively. The resonances of the CH$_2$ protons of 18-crown-6 and the methyl protons of the two N(SiMe$_3$)$_2$ ligands of the cyclometallate integrate to a ratio of 30.73:36 versus an anticipated ratio of 24:36 if the cyclometallate had been isolated as the only product. The ratio of the difference between this 'ideal' integration of the 18-crown-6 protons and the ligand N(SiMe$_3$)$_2$ protons of the butoxide complex is 6.73:13.57. This ratio agrees with the assignment of [K(18-crown-6)]$^+$ as the cation of the butoxide complex, as quadrupling the ratio (considering the 4:1 product distribution) gives a value of ca. 24:54, which is expected for the complex [K(18-crown-6)][{(SiMe$_3$)$_2$N}$_3$Y(OCH$_2$CH$_2$CH$_2$CH$_3$)].

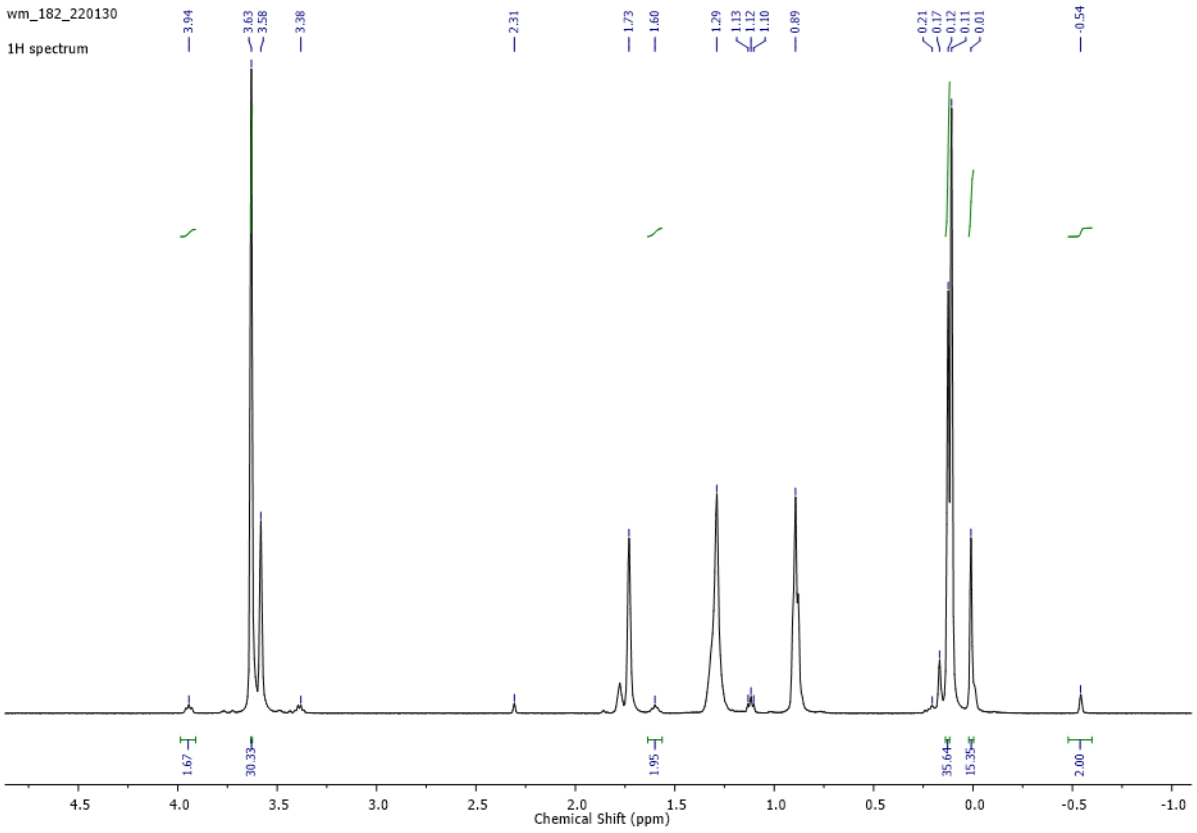

Figure B.1. ^{1}H NMR spectrum of decomposition products following the reaction of $Y\{N(SiMe_3)_2\}_3$ with KC_8 and 18c6 in tetrahydrofuran.

Reaction of $Y\{N(SiMe_3)_2\}_3$ with KC_8 and 18c6 in diethyl ether. A vial containing $Y(NR_2)_3$ (0.102 g, 0.18 mmol) and 18c6 (0.046 g, 0.17 mmol) dissolved in about 2 ml Et_2O was cooled to −78 °C, along with a vial containing KC_8 (0.027 g, 0.16 mmol). Using a similarly cold pipette, the Et_2O solution was transferred onto the KC_8 and immediate conversion to a dark blue suspension was observed. After stirring for 2 hr at room temperature, the suspension settled into a clear supernatant and black solid (presumably graphite). The suspension was centrifuged, and the supernatant was decanted. The Et_2O was pumped off, and the resulting white solid was massed at 0.051 g. The crude product contains peaks in ^{1}H NMR in C_6D_6 (see Figure B.2) that are consistent with the cyclometallate[1]: δ −0.60 (2H, $CH_2SiMe_2NSiMe_3$), 0.64 (>12H, $CH_2SiMe_2NSiMe_3$), 0.65 (>27H, $N(SiMe_3)_2$), 3.06 (>24H, 18c6). Adventitious Et_2O and hexanes were observed as well. Unidentified peaks remain at 0.74, 0.69, 0.67, 0.60, and 0.51 ppm.

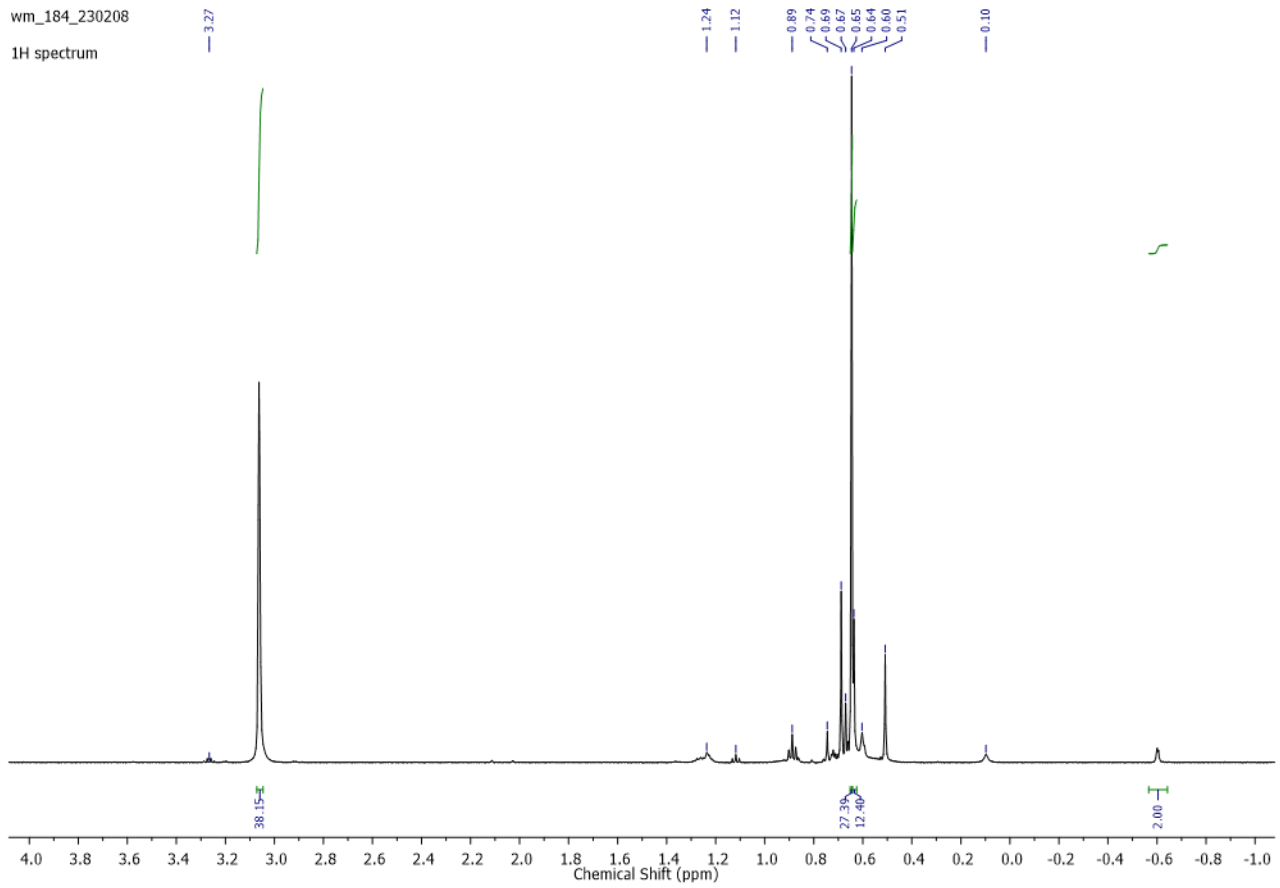

Figure B.2. ^{1}H NMR spectrum of decomposition products following the reaction of $Y\{N(SiMe_3)_2\}_3$ with KC_8 and 18c6 in diethylether.

EPR Spectroscopy of [K(18c6)][Y(NR$_2$)$_3$] (R = SiMe$_3$) combined with DME. A vial containing $Y(NR_2)_3$ (0.055 g, 0.09 mmol) and 18c6 (0.024 g, 0.09 mmol) dissolved in about 0.3 ml Et_2O was cooled to −78 °C, along with a vial containing KC_8 (0.014 g, 0.10 mmol). Using a similarly cold pipette, the Et_2O solution was transferred onto the KC_8 and immediate conversion to a dark blue suspension was observed. The solution was passed through two pipette filters similarly cooled directly into a quartz EPR tube. About 0.1 mL DME cooled to −78 °C was then added directly to the EPR tube. This solution turned clear within 1 s and was immediately capped and transferred out of the box into a Dewar of liquid nitrogen. The X-band, continuous wave, perpendicular mode EPR was collected at 77 K (see Figure B.3) and displays a signal at g_{iso} = 2.0008.

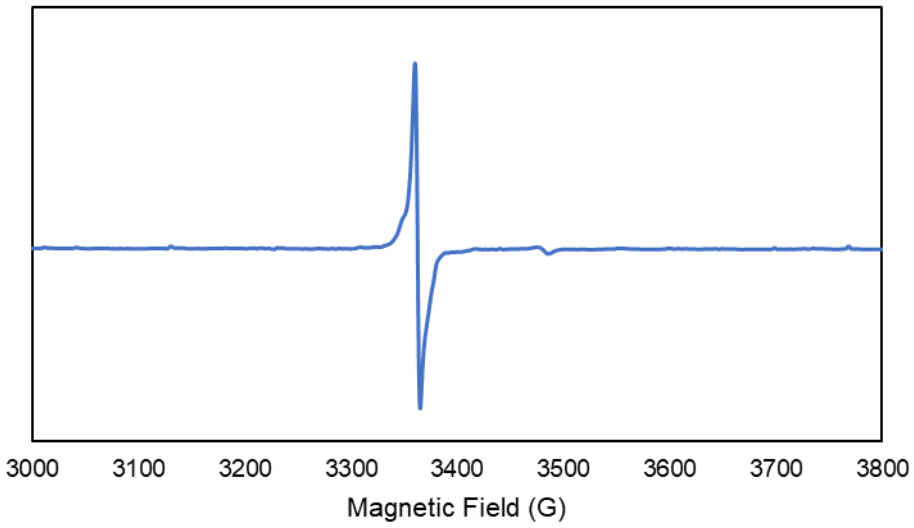

Figure B.3. X-band, continuous wave, perpendicular mode EPR collected at 77 K following the reaction of [K(18c6)][$Y(NR_2)_3$] generated in situ with DME in diethylether.

References

(1) Fang, M.; Bates, J. E.; Lorenz, S. E.; Lee, D. S.; Rego, D. B.; Ziller, J. W.; Furche, F.; Evans, W. J. $(N_2)^{3-}$ Radical Chemistry via Trivalent Lanthanide Salt/Alkali Metal Reduction of Dinitrogen: New Syntheses and Examples of $(N_2)^{2-}$ and $(N_2)^{3-}$ Complexes and Density Functional Theory Comparisons of Closed Shell Sc^{3+}, Y^{3+}, and Lu^{3+} versus $4f^9$ Dy^{3+}. *Inorg. Chem.* **2011**, *50*, 1459–1469. DOI: 10.1021/ic102016k.

Appendix C:

Density Functional Theory Calculations in Contribution to Characterizing the Electronic Nature of $(C_5H_4SiR_3)_3Th$ and $[K(crypt)][(C_5H_4SiR_3)_3Th]$ (R = ^{i}Pr)

†Electronic structure calculations on both $Cp^{TIPS}{}_3Th^{III}$ and $(Cp^{TIPS}{}_3Th^{II})^{1-}$ [Cp^{TIPS} = $C_5H_4Si(^{i}Pr)_3$] were performed using density functional theory (DFT) with the TPSSh hybrid meta-generalized gradient density functional[1] with the D3 dispersion correction[2,3] and the resolution of the identity (RI-J) approximation.[4] Scalar relativistic effective core potentials with the def-TZVP basis set[5] were used for thorium and the polarized split-valence basis set def2-SV(P) was used for other atoms.[6] The continuum solvent model COSMO[7] was used with parameters for THF (dielectric constant $\varepsilon = 7.52$, refractive index $R_{ind} = 1.41$).[8] All calculations were performed with the TURBOMOLE package V7.6.[9,10] Geometry optimizations were computed using coordinates derived from the X-ray diffraction crystal structures for both $Cp^{TIPS}{}_3Th(III)$ and $[Cp^{TIPS}{}_3Th(II)]^{1-}$. All geometry optimizations were calculated with a geometry convergence threshold of 10^{-4} a.u. and energy converge threshold of 10^{-7} a.u. The ground state geometry for $Cp^{TIPS}{}_3Th(III)$ was confirmed by the lack of imaginary frequencies in the vibrational spectrum.[11] The optimized geometry was found to have C_1 symmetry for all species.

The geometry-optimized structures of the neutral $Cp^{TIPS}{}_3Th^{III}$ and the $(Cp^{TIPS}{}_3Th^{II})^{1-}$ anion have average Th–Cnt distances of 2.501 Å and 2.489 Å, which are within 0.03 Å of the experimentally determined Th–Cnt average distances, 2.520 Å and 2.524 Å, respectively. The calculated bond angles are also reproduced within a few degrees for both structures.

The electronic structure suggests $(6d_{z2})^1$ and $(6d_{z2})^2$ electron configurations for $Cp^{TIPS}{}_3Th^{III}$ and $(Cp^{TIPS}{}_3Th^{II})^{1-}$, respectively. These are the same ground state electron configurations assigned to the neutral $Cp''{}_3Th^{III}$ and the anionic $(Cp''{}_3Th^{II})^{1-}$ of the disilyl-substituted cyclopentadienyl analogs.[12] To further verify

† Portions of this appendix have been submitted for publication: Nguyen, J. Q.; Moore, W. N. G.; Anderson-Sanchez, L. M.; Ziller, J. W. Furche, F.; Evans, W. J. Replacing Trimethylsilyl With Triisopropylsilyl Allows Isolation of Stable and Crystalline $(C_5H_4SiR_3)_3Th$ Complexes of Th(III) and Th(II). *Submitted.*

the ground state configuration of $(Cp^{TIPS}{}_3Th^{II})^{1-}$, a geometry optimization was run on the same anion constrained to a triplet state. The total energy was >0.4 eV higher than the singlet ground state. The qualitative $6d_{z2}$ character of the HOMO for $(Cp^{TIPS}{}_3Th^{II})^{1-}$ can be seen in Figure C.1.

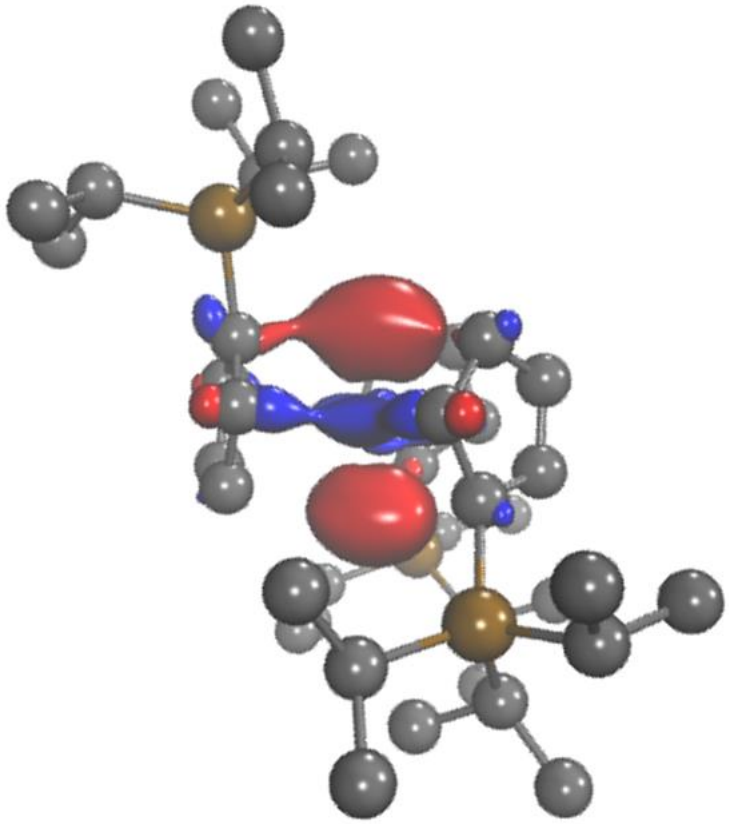

Figure C.1. Calculated HOMO (ε = −1.235) of $(Cp^{TIPS}{}_3Th^{II})^{1-}$ plotted with a contour value of 0.05.

Time-dependent density functional theory calculations were then conducted on the geometry-optimized structures. Additionaly calculations were run where a diffuse *p* primitive was added to the Th basis set for $[Cp^{TIPS}{}_3Th(II)]^{1-}$, but this was not found to improve reproduction of the experimental spectrum, so the spectra shown reflect the unaltered basis set. UV-visible spectra were simulated using Gaussian line profiles with a root mean-square width of 0.15 eV and empirical shifts of 0.30 eV. Molecular orbitals and electronic transition states were analyzed with VMD[21] and Mulliken population analysis. The resulting simulated UV-visible absorption spectra qualitatively reproduce the experimental spectra observed, Figure C.2. For $Cp^{TIPS}{}_3Th^{III}$, the strongest absorptions >550 nm primarily correspond to 6d → 5f transitions. For

$(Cp^{TIPS}{}_3Th^{II})^{1-}$, the three absorptions between 450-650 nm with the greatest oscillator strengths correspond to d → f and/or d → p transitions. See Table C.1 and Table C.2 for all assigned transitions. While further improvement of the agreement between experimental and computational spectra for $Cp^{TIPS}{}_3Th^{III}$ might be possible, the observed deviations are within the expected range for this type of calculation and measurement.

Table C.1. Electronic excitation summary for $Cp^{TIPS}{}_3Th(III)$. All excitations computed are single excitations. Oscillator strengths are reported in the length gauge. Only the dominant contribution to each excitation is given. Wavelengths are given before the empirical shifts.

Wavelength (nm)	Oscillator Strength (len.)	Dominant Contributions			Assignment
		Occupied	Virtual	% Weight	
1331.491	0.002118	200a	201a	99	6d-5f
1146.047	0.000416	200a	202a	99	6d-5f
872.469	0.018094	200a	203a	97	6d-5f
843.977	0.008253	200a	204a	94	6d-6d
804.481	0.015824	200a	205a	91	6d-5f
677.1	0.026727	200a	206a	97	6d-6d
469.252	6.76E-05	200a	207a	99	6d-5f
392.465	0.000466	200a	209a	66	6d-5f/7p
383.342	0.001958	200a	211a	36	6d-7p
378.922	0.000277	200a	208a	77	6p-7s
357.524	0.003224	199a (beta)	200a (beta)	81	ligand-6d
356.794	0.024435	200a	210a	34	6d-7p
349.28	0.020232	200a	212a	19	6d-5f
346.765	0.003313	199a	201a	36	ligand-5f
341.667	0.001892	198a (beta)	200a (beta)	29	ligand-6d
336.391	0.03993	198a (beta)	200a (beta)	52	ligand-6d
332.704	0.000161	199a	202a	45	ligand-5f
329.295	0.011262	200a	215a	24	6d-7p/5f
326.595	0.004668	200a	214a	25	6d-5f/7p
326.278	0.020491	198a	201a	25	ligand-5f
319.37	0.005908	199a (beta)	201a (beta)	42	ligand-5f
318.633	0.005171	200a	216a	53	6d-7p
314.171	0.000716	198a	202a	38	ligand-5f
308.439	0.0018	197a (beta)	200a (beta)	44	ligand-6d
307.558	0.001262	200a	218a	32	6d-5f
305.349	0.002512	200a	217a	77	6d-ligand
302.797	0.000224	196a (beta)	200a (beta)	44	ligand-6d
301.903	0.002958	199a (beta)	202a (beta)	16	ligand-5f
300.2	0.003544	198a (beta)	201a (beta)	47	ligand-5f
299.522	0.001585	199a	203a	29	ligand-5f

Table C.2. Electronic excitation summary for $[Cp^{TIPS}{}_3Th(II)]^{1-}$. All excitations computed are single excitations involving alpha spin to alpha spin transitions. Oscillator strengths are reported in the length gauge. Only the dominant contribution to each excitation is given. Wavelengths are given before the empirical shifts.

Wavelength (nm)	Oscillator Strength (len.)	Dominant Contributions			Assignment
		Occupied	Virtual	% Weight	
1224.814	0.002683	200a	201a	86	6d-5f
1111.132	0.006445	200a	202a	84	6d-5f
745.839	0.012243	200a	204a	68	6d-5f
715.307	0.092606	200a	203a	65	6d-5f
664.755	0.063639	200a	205a	91	6d-5f/7p
581.807	0.001257	200a	206a	99	6d-5f/7s
518.257	0.075669	200a	207a	88	6d-5f/7p
489.455	0.008859	200a	208a	87	6d-5f/7p
470.931	0.004468	200a	209a	83	6d-5f
458.237	0.002657	200a	210a	86	6d-ligand
448.737	0.000637	200a	213a	75	6d-5f/7p
414.247	0.000744	200a	211a	97	6d-ligand
405.863	0.008979	200a	212a	82	6d-5f/ligand
397.085	0.01576	200a	214a	51	6d-ligand
391.431	0.004325	200a	214a	43	6d-ligand
380.064	0.034544	200a	217a	34	6d-ligand
377.865	0.024441	200a	215a	54	6d-ligand
368.028	0.037609	200a	218a	50	6d-ligand
364.719	0.05238	200a	220a	28	6d-ligand
358.642	0.037904	200a	219a	37	6d-ligand
355.528	0.013451	200a	222a	42	6d-ligand
346.756	0.02	200a	221a	71	6d-ligand
341.7	0.056314	200a	223a	68	6d-ligand
335.135	0.011736	200a	224a	50	6d-ligand
327.258	0.001551	200a	225a	70	6d-ligand
320.02	0.013957	200a	226a	82	6d-ligand
318.131	0.002525	200a	227a	43	6d-ligand
316.632	0.004579	200a	227a	49	6d-ligand
309.705	0.025676	200a	230a	92	6d-ligand
309.287	0.001987	200a	229a	91	6d-ligand

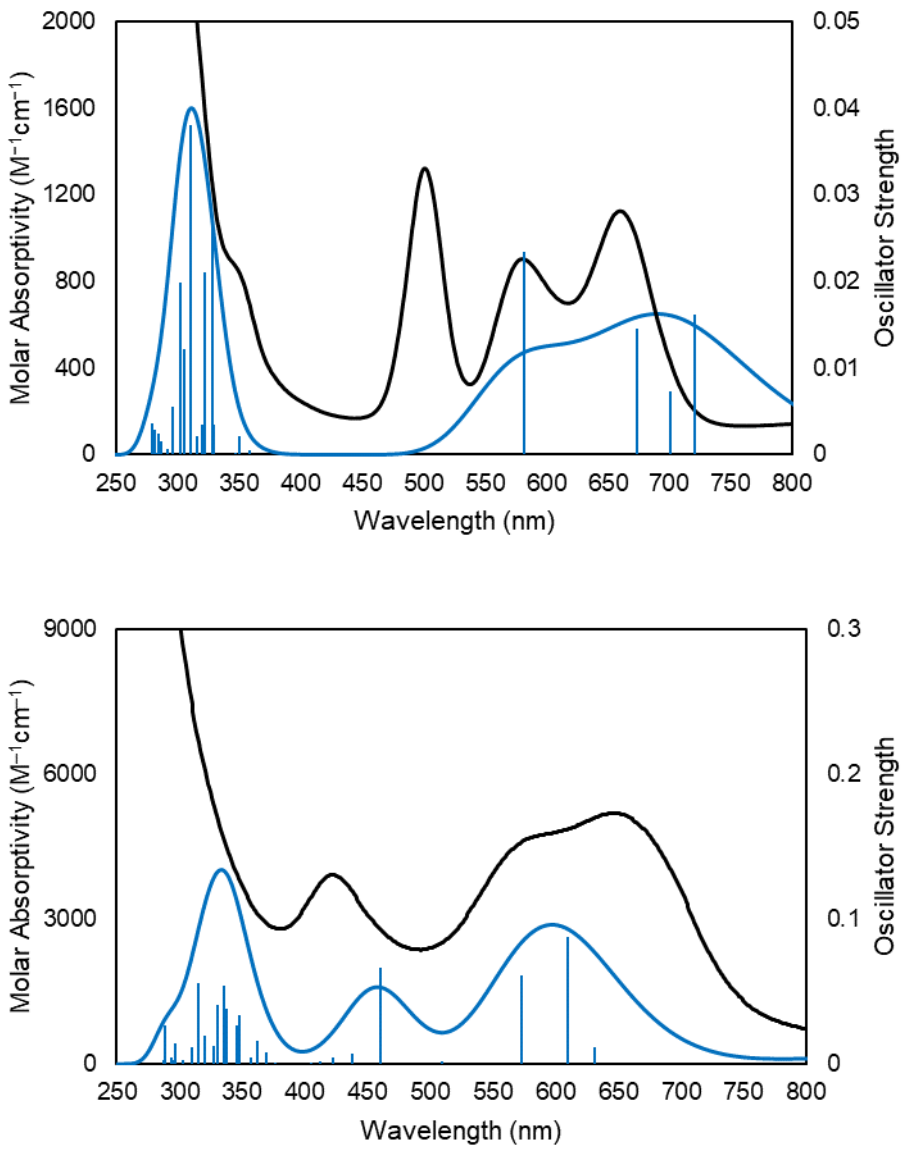

Figure C.2. Simulated (blue) and experimental (black) UV-visible spectra for $Cp^{TIPS}{}_3Th^{III}$ (top), and [K(crypt)][$Cp^{TIPS}{}_3Th^{II}$] (bottom). The computed TDDFT oscillator strengths are shown as blue vertical lines. Each calculated spectrum was empirically blue shifted by 0.30 eV and a Gaussian line broadening of 0.15 eV was applied.

References

(1) Staroverov, V. N.; Scuseria, G. E.; Tao, J.; Perdew, J. P. Comparative Assessment of a New Nonempirical Density Functional: Molecules and Hydrogen-Bonded Complexes. *J. Chem. Phys.* **2003**, *119*, 12129–12137. DOI: 10.1063/1.1626543

(2) Grimme, S.; Antony, J.; Ehrlich, S.; Krieg, H. A Consistent and Accurate Ab Initio Parametrization of Density Functional Dispersion Correction (DFT-D) for the 94 Elements H-Pu. *J. Chem. Phys.* **2010**, *132*, 154104. DOI: 10.1063/1.3382344

(3) Grimme, S. Semiempirical GGA-Type Density Functional Constructed with a Long-Range Dispersion Correction. *J. Comput. Chem.* **2006**, *27*, 1787–1799. DOI: 10.1002/jcc.20495

(4) Weigend, F.; Köhn, A.; Hättig, C. Efficient Use of the Correlation Consistent Basis Sets in Resolution of the Identity MP2 Calculations. *J. Chem. Phys.* **2002**, *116*, 3175–3183. DOI: 10.1063/1.1445115

(5) Cao, X.; Dolg, M. Segmented Contraction Scheme for Small-Core Actinide Pseudopotential Basis Sets. *J. Mol. Struct. THEOCHEM* **2004**, *673*, 203–209. DOI: 10.1016/j.theochem.2003.12.015

(6) Eichkorn, K.; Weigend, F.; Treutler, O.; Ahlrichs, R. Auxiliary Basis Sets for Main Row Atoms and Transition Metals and Their Use to Approximate Coulomb Potentials. *Theor. Chem. Acc.* **1997**, *97*, 119–124. DOI: 10.1007/s002140050244

(7) Schäfer, A.; Klamt, A.; Sattel, D.; Lohrenz, J. C. W.; Eckert, F. COSMO Implementation in TURBOMOLE: Extension of an Efficient Quantum Chemical Code towards Liquid Systems. Phys. *Chem. Chem. Phys.* **2000**, *2*, 2187–2193. DOI: 10.1039/b000184h

(8) CRC Handbook of Chemistry and Physics, 97th ed.; Haynes, W. M., Lide, D. R., Bruno, T. J., Eds.; CRC Press, 2016.

(9) TURBOMOLE V7.6 2020, a development of University of Karlsruhe and Forschungszentrum Karlsruhe GmbH, 1989−2007, TURBOMOLE GmbH, since 2007: available from http://www.turbomole.com.

(10) Balasubramani, S. G.; Chen, G. P.; Coriani, S.; Diedenhofen, M.; Frank, M. S.; Franzke, Y. J.; Furche, F.; Grotjahn, R.; Harding, M. E.; Hättig, C.; Hellweg, A.; Helmich-Paris, B.; Holzer, C.; Huniar, U.; Kaupp, M.; Marefat Khah, A.; Karbalaei Khani, S.; Müller, T.; Mack, F.; Nguyen, B. D.; Parker, S. M.; Perlt, E.; Rappoport, D.; Reiter, K.; Roy, S.; Rückert, M.; Schmitz, G.; Sierka, M.; Tapavicza, E.; Tew, D. P.; Van Wüllen, C.; Voora, V. K.; Weigend, F.; Wodyński, A.; Yu, J. M. TURBOMOLE: Modular Program

Suite for Ab Initio Quantum-Chemical and Condensed-Matter Simulations. *J. Chem. Phys.* **2020**, *152*, 184107. DOI: 10.1063/5.0004635

(11) Deglmann, P.; Furche, F.; Ahlrichs, R. An Efficient Implementation of Second Analytical Derivatives for Density Functional Methods. *Chem. Phys. Lett.* **2002**, *362*, 511–518, DOI: 10.1016/S0009-2614(02)01084-9.

(12) Langeslay, R. R.; Fieser, M. E.; Ziller, J. W.; Furche, F.; Evans, W. J. Synthesis, Structure, and Reactivity of Crystalline Molecular Complexes of the $\{[C_5H_3(SiMe_3)_2]_3Th\}^{1-}$ Anion Containing Thorium in the Formal +2 Oxidation State. *Chem. Sci.* **2015**, *6*, 517–521. DOI: 10.1039/c4sc03033h.

Appendix D:

γ Irradiation of Organometallic Yb(II) Species

Gamma irradiation was first found successful in the generation of Ln(II) ions via reduction of Ln(III) ions by electrons excited from a CaF_2 matrix by γ-irradiation.[1] These ions were characterized by optical spectroscopy for ions across the series. Subsequently, Sm(I) ions were generated via reduction of Sm(II) ions by electrons excited from a KCl matrix by γ-irradiation.[2] In Chapter 3, an approach designed for bioinorganic systems was modified to allow for the γ-irradiation of organometallic Ln(III) precursors in frozen glasses of 2-MeTHF at 77 K. The evidence presented in that Chapter demonstrates that the technique can generate known $[Ln^{II}A_3]^{1-}$ complexes (A = anion) as well as Ln(II) species that have thus far not been isolable chemically.

Given the result showing the formation of Sm(I), it was hypothesized that the method described in Chapter 4 may be able to generate as yet chemically unisolable Ln(I) species as well. Efforts to obtain spectroscopic characterization of species with oxidation states lower than +2 are included in this appendix.

Gamma Irradiation of Yb(II). Ytterbium was the first nucleus chosen for investigation, because in the +2 oxidation state, it has a $4f^{14}$ electron configuration. Since the 4f shell is full, reduction would likely result in the occupation of an orbital reflecting majority Yb 6s- and/or 5d-orbital character. This is important, because anisotropic f-electron configurations typically preclude observation by EPR spectroscopy due to the rapid relaxation from strong spin-orbit coupling. Ytterbium also has two EPR-active isotopes, $I(^{171}\text{Yb}, 14\%) = ½$ and $I(^{173}\text{Yb}, 16\%) = {}^5/_2$. The latter is especially important, as it was found that though Y(II)-containing complexes could be generated by the γ-irradiation method and characterized by UV-visible absorbance spectroscopy, they could not be characterized by EPR spectroscopy since their signals overlapped significantly with the organic radical and free electron signals generated from the irradiated solvent. Hence, the $I = {}^5/_2$ nuclear spin of ^{173}Yb is beneficial because it could spread the EPR signal over a greater magnetic field range due to coupling of the unpaired electron with the non-integer nuclear spin.

First, an Yb(II) salt was examined. Freshly grown crystals of [K(crypt)][Yb(OAr*)$_3$] (OAr* = $^-$C$_6$H$_2$-Ad$_2$-2,6^{t}Bu-4; Ad = 1-adamantyl) obtained with the help of my coworker Lauren Anderson-Sanchez were dissolved in 2-MeTHF at room temperature in an argon-filled glovebox, loaded into a quartz EPR tube, and the tube was capped. After rapidly freezing the tube in a Dewar filled with liquid nitrogen, the system was exposed to ^{137}Cs gamma irradiation for 16 hours. Analysis of the resulting sample with EPR spectroscopy yielded the spectrum shown in Figure D.1.

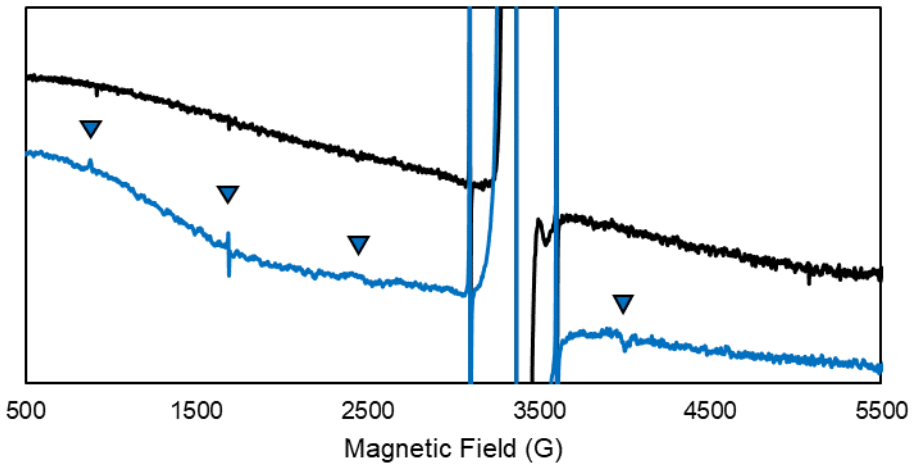

Figure D.1. X-band CW EPR spectra of 2-MeTHF (black) and 0.09 M [K(crypt)][Yb(OAr*)$_3$] in 2-MeTHF (blue) collected in perpendicular mode at 77 K after 16 hr γ-irradiation.

There are clear differences between the two spectra in Figure D.1, with differences located at g = 7.70 (875 G), g = 4.00 (1700 G), g = 2.75 (2450 G), and g = 1.70 (3980 G). The average difference between the low field signals of 787.5 G is similar to half the difference (765 G) between the two higher field signals, indicating a possible signal near g = 2.00 (3215 G) that is hidden by the organic radical and free electride generated from γ-irradiation of 2-MeTHF. These signals are clearly not due to the irradiated solvent or 4f^{14} Yb(II), but their low intensity and ambiguous symmetry environment (isotropic vs axial, vs rhombic) preclude definitive identification.

Since neutral aromatic rings near reduced rare-earth metal centers are also known to undergo partial or full reduction, a second Yb(II) salt was attempted as well. Fresh [K(crypt)][Cp′$_3$Yb] was dissolved in 2-

MeTHF and subjected to the gamma irradiation method described above. The resulting spectra are shown below in Figure D.2.

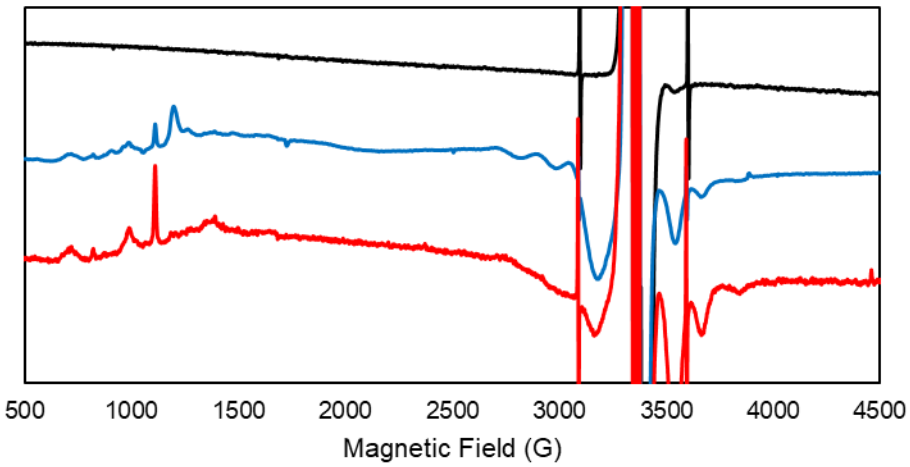

Figure D.2. X-band CW EPR spectra of 2-MeTHF, 7 hrs (black) and 0.26 M [K(crypt)][Cp′$_3$Yb] in 2-MeTHF, 7 hrs (blue), and 0.21 M [K(crypt)][Cp′$_3$Yb] in 2-MeTHF, 6.5 hrs (red), collected in perpendicular mode at 77 K.

Again, there appear to be signals that are distinct from the irradiated 2-MeTHF sample, which also do not correspond to Yb(II): g = 9.64 (730 G), g = 8.15 (830 G), g = 6.80 (990 G), g = 6.03 (1125 G), g = 4.83 (1380 G), g = 3.95 (1705 G), g = 2.50 (2710 G), g = 2.30 (2900 G), g = 2.20 (3060 G), and g = 1.80 (3770 G). These signals are repeatable across different batches of [K(crypt)][Cp′$_3$Yb] as evidenced by the blue and red spectra in Figure D.2.

To investigate the electronic structure of a potential [Cp′$_3$Yb]$^{2-}$ dianion, calculations were performed using density functional theory (DFT) with the TPSSh hybrid meta-generalized gradient density functional[1] with the D3 dispersion correction[2,3] and the resolution of the identity (RI-J) approximation.[4] Scalar relativistic effective core potentials with the def2-TZVP basis set[5] were used for ytterbium and the polarized split-valence basis set def2-SV(P) was used for other atoms.[6] The continuum solvent model COSMO[7] was used with the default parameters, including $\varepsilon = \infty$. All calculations were performed with the TURBOMOLE package V7.6.[8,9]

Calculations were conducted starting from the XRD-derived coordinates for the $[Cp'_3Yb]^{1-}$, adding an electron, and optimizing the geometry. The calculated HOMO is a diffuse orbital with a mix of Yb character (approximately 35% s, 40% p, and 5% d). The qualitative picture can be seen below in Figure D.3, and the orbital is reminiscent of a Rydberg state given the diffuse nature of the electron density. A diffuse orbital may incur weak coupling with the Yb nuclear spin, which would likely result in an EPR signal over a narrower range of magnetic field.

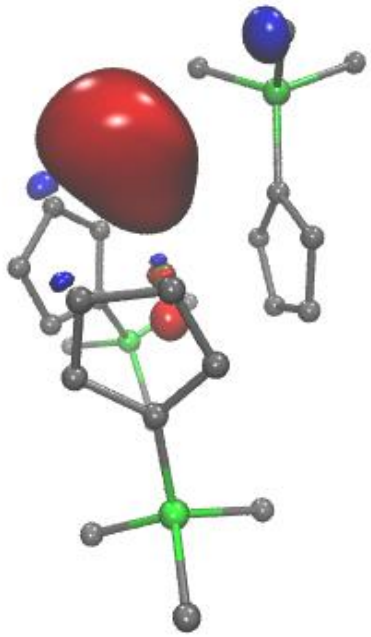

Figure D.3. Calculated HOMO (ε = −0.946 eV) plotted with a contour value of 0.05.

Additionally, the signals, though different from $[Cp'_3Yb]^{1-}$ and irradiated 2-MeTHF, are not necessarily attributable to Yb(I). Since simulation with EasySpin has been unsuccessful in yielding spectra that match the experimental, control studies on a neutral species without another Lewis acidic species present were conducted. Specifically, the species $Cp'''_2Yb(THF)$[10] [$Cp''' = C_5H_2(SiMe_3)_3$] was synthesized. This solvated metallocene was dissolved in 2-MeTHF and irradiated per the procedure above to yield the spectrum below in Figure D.4.

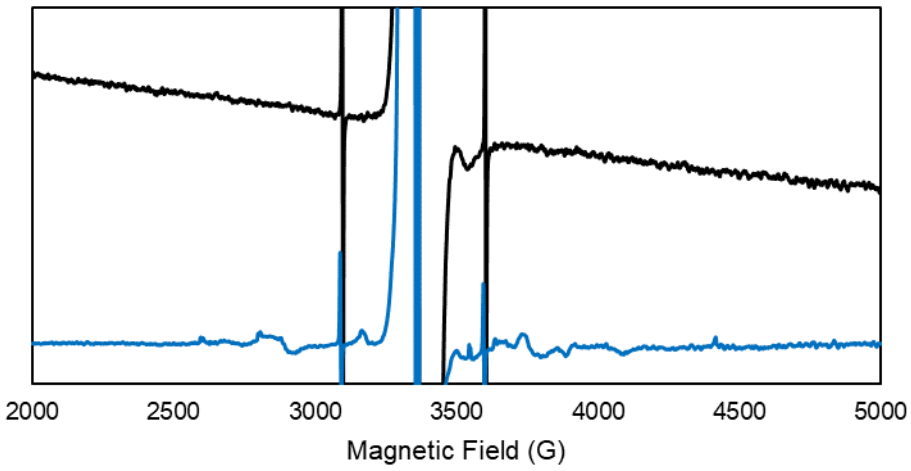

Figure D.4. X-band CW EPR spectra of 2-MeTHF (black) and 0.25 M Cp‴$_2$Yb(THF) in 2-MeTHF (blue) collected in perpendicular mode at 77 K after 6 hr γ-irradiation.

Some signals appear which are not present in the 2-MeTHF solvent control and which do not originate from the Yb(II) starting material, Cp‴$_2$Yb(THF). These signals appear at g = 2.58 (2600 G), g = (2880 G), g = 2.12 (3165 G), g = 1.80 (3750 G), g = 1.72 (3900 G), and g = 1.65 (4065 G). It is unknown what these signals correspond to.

To investigate if alkali metal cations could potentially be reduced from these gamma irradiation setups, two solutions of CsF were prepared. Cs may be advantageous versus K in observing an EPR signal given the greater nuclear spin: $I(^{133}\text{Cs}, 100\%) = {}^{7}/_{2}$ vs $I(^{39}\text{K}, 93\%) = I(^{41}\text{K}, 7\%) = {}^{3}/_{2}$. In one case, CsF (0.055 g, 0.36 mmol) and crypt (0.129 g, 0.34 mmol) were stirred in 2-MeTHF (1.00 mL) overnight to solubilize the salt. In the other case, CsF (0.346 g, 2.3 mol) is dissolved in DI water (0.3 mL). After subjecting these samples to the gamma irradiation procedure described above, the aqueous sample turned bright purple, while the 2-MeTHF sample turned slate blue, see Figure D.5 below. However, both EPR spectra show nothing different than their respective irradiated solvents. This indicates that the $[\text{K(crypt)}]^{1+}$ is likely not getting reduced in the irradiation attempts of [K(crypt)][Yb(II)] salts.

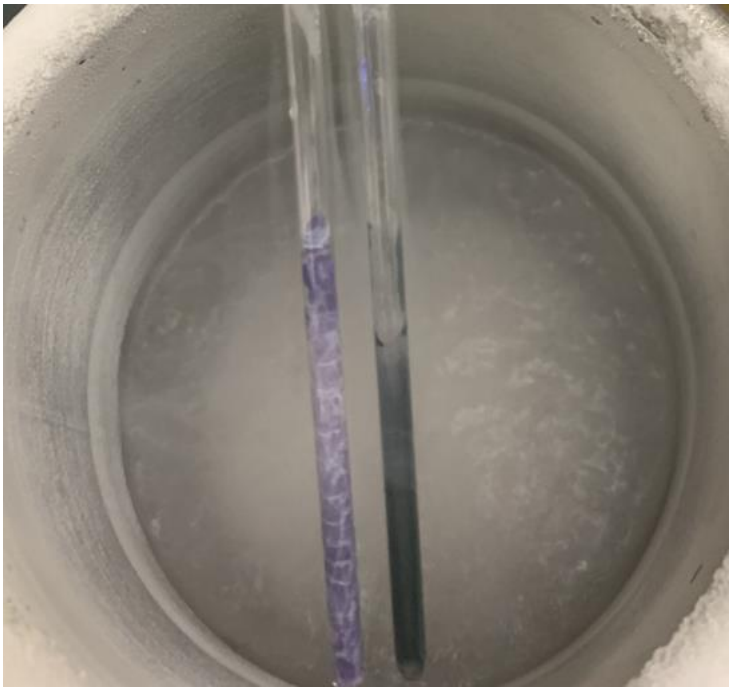

Figure D.5. Photograph of 4.5 M CsF in DI water (left) and 0.34 M Cs(crypt)F in 2-MeTHF (right) following 7 hrs of γ-irradiation.

References

(1) Staroverov, V. N.; Scuseria, G. E.; Tao, J.; Perdew, J. P. Comparative Assessment of a New Nonempirical Density Functional: Molecules and Hydrogen-Bonded Complexes. *J. Chem. Phys.* **2003**, *119*, 12129–12137. DOI: 10.1063/1.1626543

(2) Grimme, S.; Antony, J.; Ehrlich, S.; Krieg, H. A Consistent and Accurate Ab Initio Parametrization of Density Functional Dispersion Correction (DFT-D) for the 94 Elements H-Pu. *J. Chem. Phys.* **2010**, *132*, 154104. DOI: 10.1063/1.3382344

(3) Grimme, S. Semiempirical GGA-Type Density Functional Constructed with a Long-Range Dispersion Correction. *J. Comput. Chem.* **2006**, *27*, 1787–1799. DOI: 10.1002/jcc.20495

(4) Weigend, F.; Köhn, A.; Hättig, C. Efficient Use of the Correlation Consistent Basis Sets in Resolution of the Identity MP2 Calculations. *J. Chem. Phys.* **2002**, *116*, 3175–3183. DOI: 10.1063/1.1445115

(49) Weigend, F.; Ahlrichs, R. Balanced Basis Sets of Split Valence, Triple Zeta Valence and Quadruple Zeta Valence Quality for H to Rn: Design and Assessment of Accuracy. *Phys. Chem. Chem. Phys.* **2005**, *7*, 3297–3305. DOI: 10.1039/b508541a.

(6) Eichkorn, K.; Weigend, F.; Treutler, O.; Ahlrichs, R. Auxiliary Basis Sets for Main Row Atoms and Transition Metals and Their Use to Approximate Coulomb Potentials. *Theor. Chem. Acc.* **1997**, *97*, 119–124. DOI: 10.1007/s002140050244

(7) Schäfer, A.; Klamt, A.; Sattel, D.; Lohrenz, J. C. W.; Eckert, F. COSMO Implementation in TURBOMOLE: Extension of an Efficient Quantum Chemical Code towards Liquid Systems. Phys. *Chem. Chem. Phys.* **2000**, *2*, 2187–2193. DOI: 10.1039/b000184h

(8) TURBOMOLE V7.6 2020, a development of University of Karlsruhe and Forschungszentrum Karlsruhe GmbH, 1989−2007, TURBOMOLE GmbH, since 2007: available from http://www.turbomole.com.

(9) Balasubramani, S. G.; Chen, G. P.; Coriani, S.; Diedenhofen, M.; Frank, M. S.; Franzke, Y. J.; Furche, F.; Grotjahn, R.; Harding, M. E.; Hättig, C.; Hellweg, A.; Helmich-Paris, B.; Holzer, C.; Huniar, U.; Kaupp, M.; Marefat Khah, A.; Karbalaei Khani, S.; Müller, T.; Mack, F.; Nguyen, B. D.; Parker, S. M.; Perlt, E.; Rappoport, D.; Reiter, K.; Roy, S.; Rückert, M.; Schmitz, G.; Sierka, M.; Tapavicza, E.; Tew, D. P.; Van Wüllen, C.; Voora, V. K.; Weigend, F.; Wodyński, A.; Yu, J. M. TURBOMOLE: Modular Program Suite for Ab Initio Quantum-Chemical and Condensed-Matter Simulations. *J. Chem. Phys.* **2020**, *152*, 184107. DOI: 10.1063/5.0004635

(10) Davis, Benjamin L. Ph.D. Dissertation, University of California–Irvine **2006**.

Appendix E:

Exploring the Synthesis of $Th(SAr^{Me})_4$ and $Y(SAr^{Me})_3$ (SAr^{Me} = 2,4,6-trimethylbenzenethiolate)

Organometallic rare-earth and actinide metal complexes are commonly ligated by first row, main group-based ligands, most predominantly are those based on carbon, nitrogen, and oxygen. Some examples of mixed first and second row complexes are known as well as a few examples of complexes bound solely to second row p-block elements, including $Sm(SAr^{tBu})_3$[1] (Ar^{tBu} = 2,4,6-tritertbutylbenzenethiolate) and $Y[P(SiMe_3)_2]_3$[2]. Since the lower rows in the p-block have more diffuse orbitals, they are considered softer ligands versus the smaller, more charge-dense "hard" first row elements. Considering that the reduction of non-traditional Ln(III) complexes to Ln(II) incurs the population of an orbital having largely d character, this makes the metal center a softer Lewis acid. Given the propensity for soft Lewis acids to bind well with soft Lewis bases, it was of interest to synthesize organometallic rare-earth and actinide metal complexes bound by second row p-block ligands.

A commercially available thiolate, SAr^{Me} = 2,4,6-trimethylbenzenethiolate, was chosen for this investigation. Yttrium and thorium were chosen as the target metal ions because they are diamagnetic in their most stable oxidation state (+3 and +4 respectively), allowing for the use of ^{1}H NMR spectroscopy as an informative analytical tool. Furthermore, upon reduction, these complexes have diagnostic EPR spectra that would facilitate characterization of any reduced product.

$Y(SAr^{Me})_3$. Three equivalents of $HSAr^{Me}$ (0.15 mL, 1.0 mmol) were added dropwise to a stirred solution of $Y(NR_2)_3$ (R = $SiMe_3$) (0.202 g, 0.35 mmol) in hexanes. A white precipitate forms nearly immediately, and the suspension was stirred for 1 h at room temperature to ensure completion. The white precipitate was separated by centrifugation, isolated, and dried in vacuo to yield "$Y(SAr^{Me})_3$" (0.113 g, 64%). ^{1}H NMR (THF-d_8, 500 MHz): δ 6.70 (s, 2H), δ 2.34 (s, 6H), δ 2.14 ppm (s, 3H). See Figure E.1 for spectrum.

Three equivalents of $LiSAr^{Me}$ (0.038 g, 0.26 mmol) in 3 mL THF were added to a solution of YCl_3 (0.017 g, 0.09 mmol) in 3 mL THF. The mixture was stirred at 60 °C overnight. Insoluble material was

filtered, and the solvent was removed from the filtrate under vacuum to yield "$Y(SAr^{Me})_3$" (0.044 g, 99%). ^{1}H NMR (THF-d_8, 500 MHz): δ 6.70 (s, 2H), δ 2.34 (s, 6H), δ 2.14 ppm (s, 3H). See Figure E.1 for spectrum.

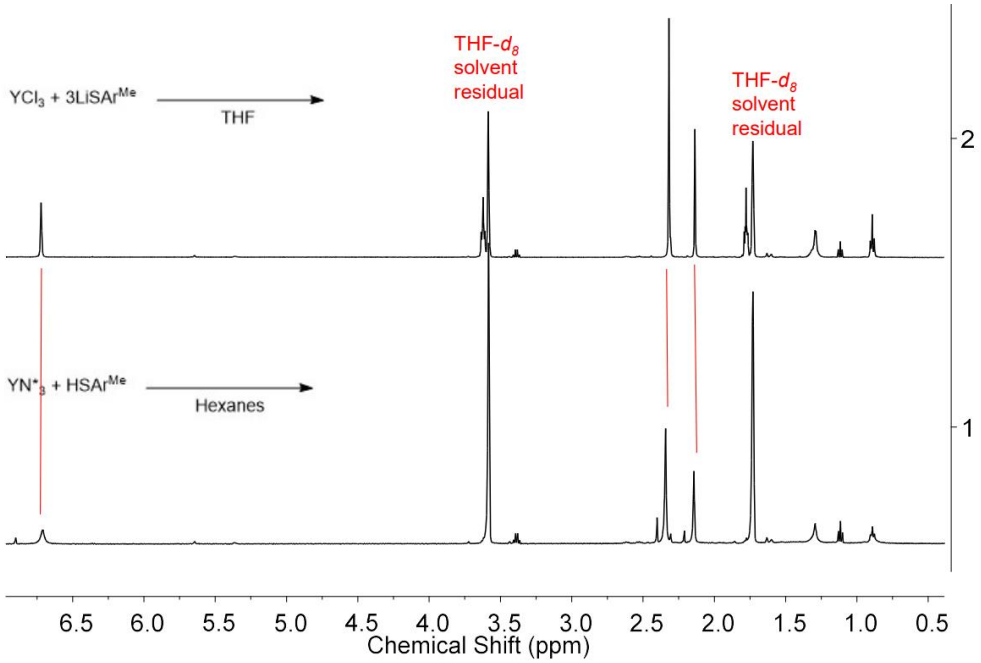

Figure E.1. ^{1}H NMR spectra of the products from multiple synthetic pathways geared towards the generation of $Y(SAr^{Me})_3$.

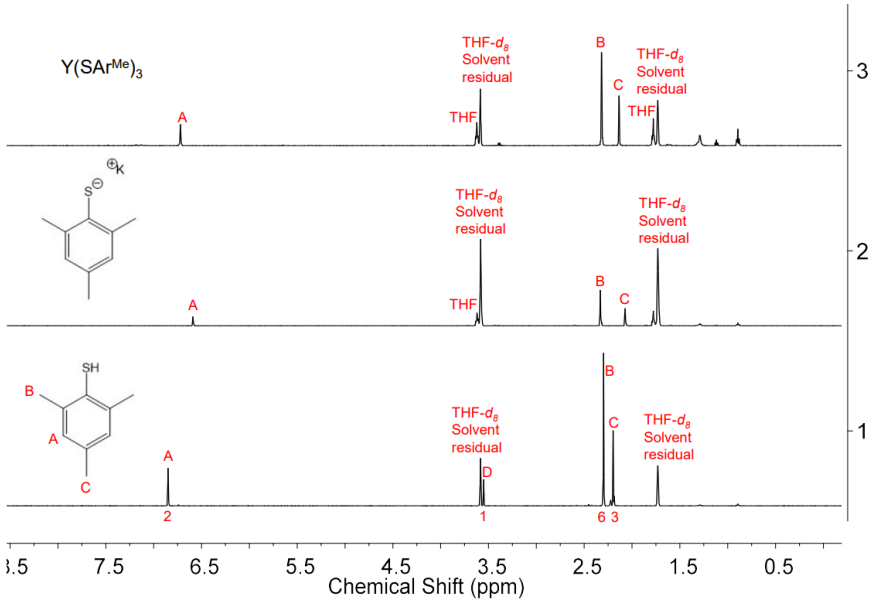

Figure E.2. ^{1}H NMR spectra comparison of protonated ligand ($HSAr^{Me}$), the potassium salt of the ligand (KSArMe), and the product isolated from a reaction of $3KSAr^{Me}$ and YCl_3.

Th(SAr^{Me})$_4$. A volume of 5 mL of THF was pipetted onto an intimate mixture of $ThBr_4(THF)_4$ (0.098 g, 0.12 mmol) and LiSArMe (0.070, 0.49 mmol). The mixture was stirred overnight at room temperature. The suspension was centrifuged, the filtrate was decanted, and the solvent was removed in vacuo to yield "ThSAr$^{Me}_4$" (0.040 g, 44%). ^{1}H NMR (THF-d_8, 500 MHz): δ 6.67 (s, 2H), δ 2.32 (s, 6H), δ 2.12 (s, 3H). See Figure E.3 for spectum.

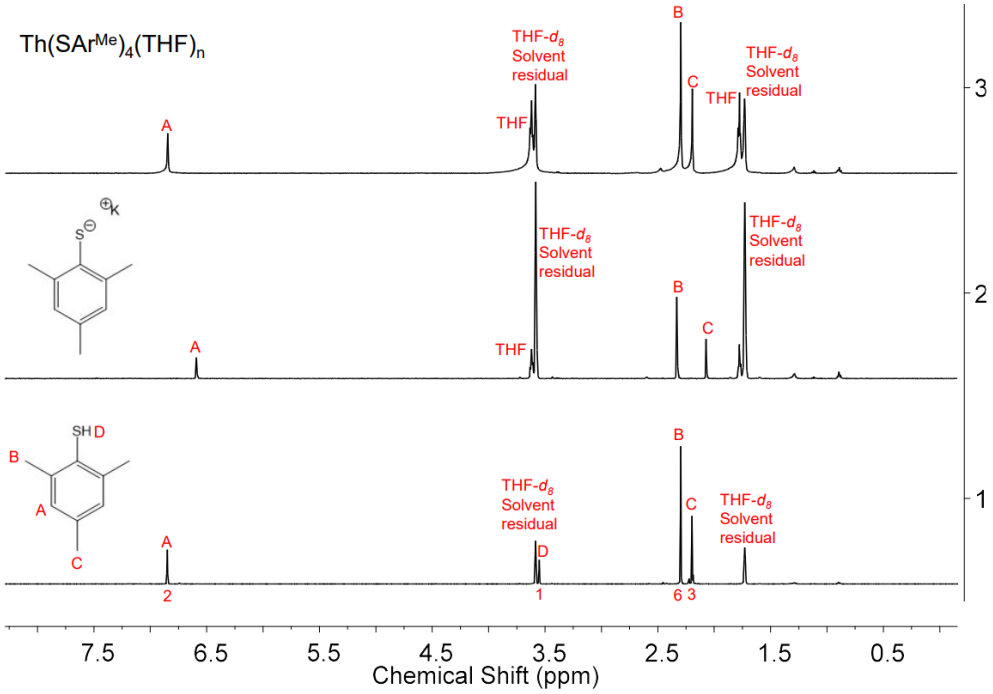

Figure E.3. ^{1}H NMR spectra comparison of protonated ligand (HSAr^{Me}), the potassium salt of the ligand (KSArMe), and the product isolated from a reaction of 4KSAr^{Me} and $ThBr_4THF_4$.

References

(1) Cetinkaya, B.; Hitchcock, P. B.; Lappert, M. F.; Smith, R. G. The First Neutral, Mononuclear 4f Metal Thiolates and New Methods for Corresponding Aryl Oxides and Bis(Trimethylsilyl)Amides. *J. Chem. Soc. Chem. Commun.* **1992**, *1992*, 932–934. DOI: 10.1039/C39920000932.

(2) Westerhausen, M.; Schneiderbauer, S.; Hartmann, M.; Warchhold, M.; Nöth, H. Synthesis and Structures of Yttrium Tris[bis(trimethylsilyl)phosphanide] and 1,1′,3,3′-Tetrakis(trimethylsilyl)yttrocene-tri(tert-butyl)silylphosphanide. *Z. Anorg. Allg. Chem.* **2002**, *628*, 330–332. DOI: 10.1002/1521-3749(200202)628:2<330::AID-ZAAC330>3.0.CO;2-U.

Appendix F

Synthetic and EPR Spectroscopic Contributions to a Project Examining the EPR Signals of U(II) Complexes

†In order to study the EPR spectroscopy of mixed principal quantum number systems, my colleague Dr. Justin Wedal collected EPR spectra for a number of U(II) complexes, some of which have been characterized as having $5f^3 6d^1$ electron configurations and some of which have been characterized as having $5f^4$ electron configurations. All U(II) complexes with the latter $5f^4$ electron configurations including [K(crypt)]{[(^{Ad,Me}ArO)$_3$mes]U} (^{Ad,Me}ArO = 2,6-di-1-adamantyl-4-methylphenoxide) and U(NHAr^{iPr6})$_2$ (NHAr^{iPr6} = 2,6-(2,4,6-^{i}Pr$_3$C$_6$H$_2$)$_2$C$_6$H$_3$) were found to be EPR silent at 5 K, 10 K, and 77 K. The U(II) complexes studied that display the mixed configuration include [K(crown)(THF)$_2$][Cp″$_3$U], [K(crypt)][Cp′$_3$U], [K(crypt)][Cp$^{tet}_3$U] (Cp^{tet} = C$_5$Me$_4$H), [K(crypt)][U(NR$_2$)$_3$] (R = SiMe$_3$), [K(crypt)][(C$_5$Me$_5$)$_2$U(NR$_2$)], [K(crypt)][(C$_5$Me$_5$)U(NR$_2$)$_2$], [K(crypt)][(C$_5$Me$_5$)$_2$U(Cp^{tet})], [K(crypt)][(C$_5$Me$_5$)$_2$U(C$_5$H$_5$)], [K(crypt)][U(OAr)$_3$], and [K(crypt)][(C$_5$Me$_5$)$_2$U(NPh$_2$)]. The first three homoleptic compounds listed were isolated as crystalline solids from reductions with KC$_8$ and crypt, and the rest were generated in situ from reductions with KC$_8$ and crypt. All $5f^3 6d^1$ U(II) complexes unexpectedly display similar two-line axial signals with $g_{\|} = 2.04$ and $g_{\perp} = 2.00$ at 77 K in perpendicular mode collected with an X-band, continuous wave EPR spectrometer. All of the same complexes were silent in parallel mode.

This result was unexpected because it was thought that the coupling between the 5f electrons and 6d electron would be sufficiently strong to preclude observation via EPR spectroscopy, which has been seen for lanthanide complexes retaining an $4f^n 5d^1$ electron configurations. Conversely, if the coupling between the 5f and 6d electrons were sufficiently weak, an EPR signal might be observable for the 5f electrons and/or the 6d electron. Qualitatively, this appeared to be the case given the axial signal observed for all of

† Portions of this appendix have been submitted for publication: Wedal, J. W.; Moore, W. N. G.; Villareal, D.; Fu, W; Lukens, W. W.; Evans, W. J. Perplexing EPR Signals from $5f^3 6d^1$ U(II) Complexes. *Submitted*.

the $5f^3 6d^1$ U(II) complexes. Dr. Wedal also collected spectra on U(III) complexes and determined that the signals near g = 2.00 were not consistent with U(III). For instance, Cp^{tet}_3U exhibits a broad signal near 2100 G.

In order to further evaluate the results obtained by Dr. Wedal and determine whether these apparently axial signals were due to the $5f^3 6d^1$ U(II) complexes or to some other impurity present, several control experiments were conducted. A control experiment was run by passing a cold (−78 °C) solution of crypt in THF (0.24 M) through a column of KC_8 packed above a pipette filter straight into an EPR tube, freezing the tube in liquid nitrogen, and taking an EPR spectrum. The spectrum shows the signal in Figure F.1 below, which clearly does not match the U(II) spectrum, indicating that KC_8/crypt is not solely responsible for the signal observed in the spectrum. Additionally, in order to determine whether a low valent species generated with a small transition metal impurity in the graphite could be responsible for the signal, $[Li(THF)_4][Cp''_3U]$ and $[Cp''U(\mu\text{–}Cp'')_2Cs(THF)_2]_n$ were synthesized according to literature procedures using metal smears rather than graphitic reductants. Both complexes display nearly identical EPR spectra to those observed for the other 10 $5f^3 6d^1$ U(II) complexes (see Figures F.2 and F.3), eliminating the possibility that the signal is arising from a graphite impurity.

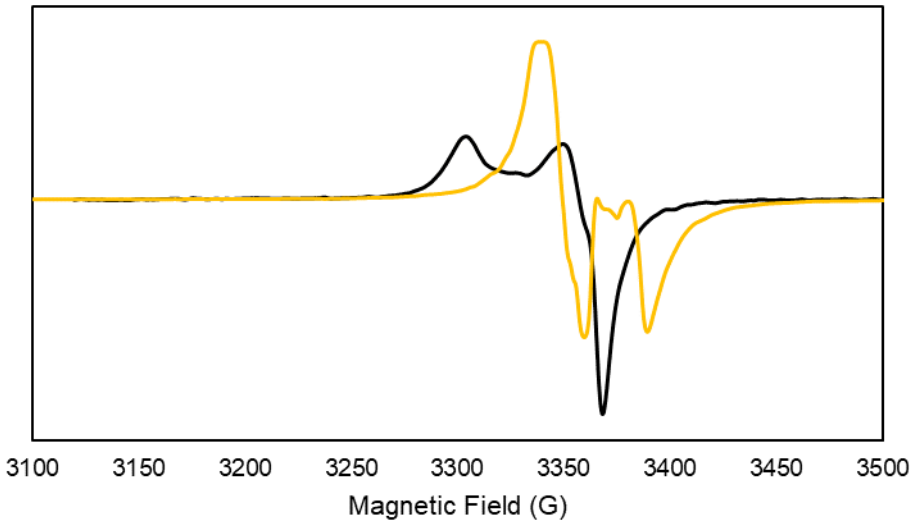

Figure F.1. X-band, CW EPR spectra collected in perpendicular mode at 77 K of the dark blue solution generated by passing a THF solution of crypt (0.24 M) through a pipette column of KC_8 (orange) and crystalline [K(crypt)][Cp″$_3$U] generated from reduction of Cp″$_3$U with KC_8 (**black**).

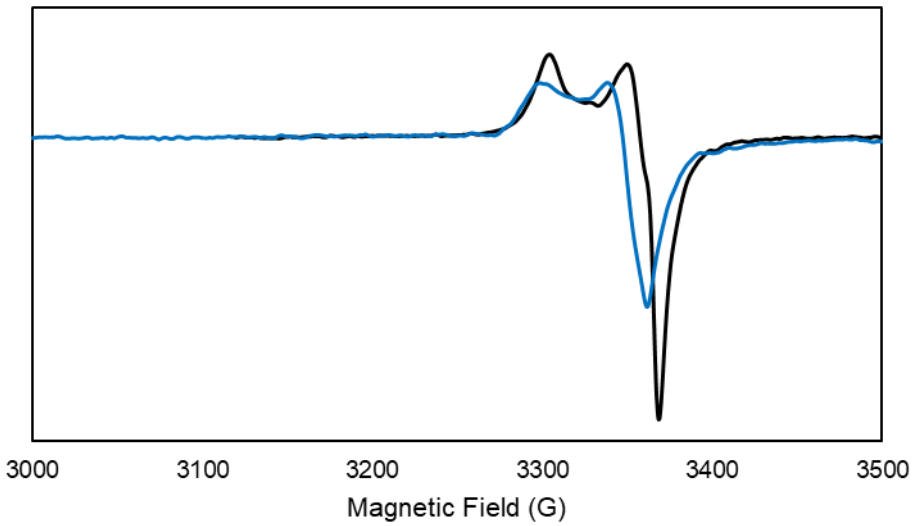

Figure F.2. X-band, CW EPR spectra collected in perpendicular mode at 77 K of crystalline [Cp″U(μ–Cp″)$_2$Cs(THF)$_2$]$_n$ in THF (blue) and crystalline [K(crypt)][Cp″$_3$U] generated from reduction of Cp″$_3$U with KC_8 (**black**).

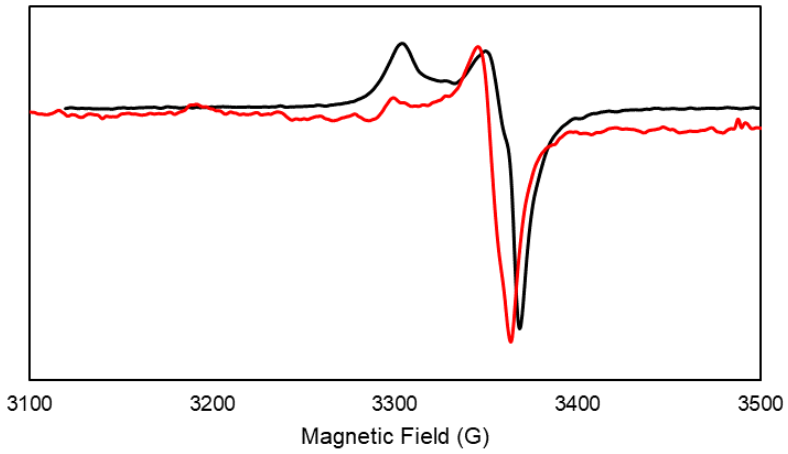

Figure F.3. X-band, CW EPR spectra collected in perpendicular mode at 77 K of crystalline [Li(THF)$_4$][Cp″$_3$U] in THF (blue) and crystalline [K(crypt)][Cp″$_3$U] generated from reduction of Cp″$_3$U with KC_8 (**black**).

Furthermore, a warming experiment was conducted as follows. After collecting a spectrum on [Cp″U(μ–Cp″$_2$Cs(THF)$_2$]$_n$, the sample was warmed to room temperature for 1 minute by submerging the sample tube in DI water. The tube was then dried and refrozen. A spectrum collected on this sample shows that the signal remains present (see Figure F.4), consistent with the conclusion that the signal is not due to an extremely sensitive byproduct of the reaction.

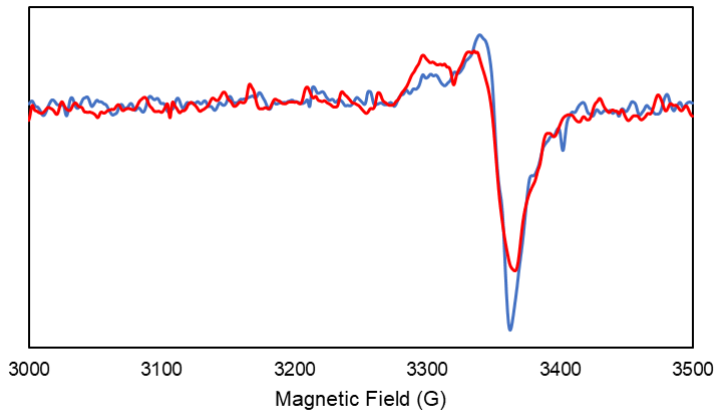

Figure F.4. X-band, CW EPR spectra collected in perpendicular mode at 77 K of crystalline [Cp″U(μ–Cp″)$_2$Cs(THF)$_2$]$_n$ in THF (blue) and the same sample after warming to room temperature for 1 minute and then re-cooling to 77 K (**black**).

Appendix G:

Synthesis of Rare-earth Metal Species Containing the $[C_5H_2(SiMe_3)_3]^{1-}$ Ligand

Cyclopentadienyl ligands, C_5R_5 (R = H, alkyl, aryl, silyl) have been essential to the development of organometallic rare-earth metal and actinide chemistry. Given the large size of these metals, highly substituted cyclopentadienyl ligands have consistently been successful in terms of isolating soluble compounds that can be crystallized for X-ray diffraction studies. C_5Me_5 (Cp^*), C_5Me_4H (Cp^{tet}), $C_5H_4SiMe_3$ (Cp'), $C_5H_3(SiMe_3)_2$ (Cp''), and $C_5H_2(^tBu)_3$ (Cp^{ttt}) have been particularly popular in the f-element area. Additionally the bulky $C_5{}^iPr_5$ ligand has stabilized a number of neutral $(C_5{}^iPr_5)_2Ln(II)$ species.[1,2]

Less studied than these cyclopentadienyls is the $C_5H_2(SiMe_3)_3$ (Cp‴) ligand. Early attempts to make a Sm(II) complex of this ligand provided a crystal structure of the mixed cyclopentadienyl complex, Cp‴Cp″Sm(THF).[3] Although the HCp‴ used in its preparation appeared to be pure by ^1H NMR spectroscopy, conversion to KCp‴ via potassium hydride and reaction with SmI_2THF_2 generated the mixed ligand species that was isolated and characterized by XRD studies and NMR spectroscopy.

Eventually, $Cp'''_2Ln(THF)$ (Ln = Sm, Yb) species[4] were generated and characterized by XRD studies and NMR spectroscopy. These structures are notable in that only one THF molecule coordinates to the metal center. In the case of $(C_5Me_5)_2SmTHF_2$, two THF molecules are bound. The difference of two versus one bound THF indicates that Cp‴ has a significantly larger steric profile than C_5Me_5. Mills and co-workers reported the synthesis of a series of Cp''' complexes that included $Cp'''_2LnCl_2K(THF)_2$, $Cp'''_2Ln(allyl)$, and $Cp'''_2Ln(\mu\text{–}Ph)_2BPh_2$ (Ln = Y and Dy).[5] Even in the case of the final complex, the metal centers coordinate the tetraphenylborate ligand via interactions with two phenyl rings, similar to the C_5Me_5-containing structure $(C_5Me_5)_2Y(\mu\text{–}Ph)_2BPh_2$.

In this Appendix, efforts to desolvate $Cp'''_2Ln(THF)$ (Ln = Sm, Yb) complexes and to form Cp'''_2Nd are described. Initially, the syntheses of $Cp'''_2Ln(THF)$ (Ln = Sm, Yb) were replicated in order to obtain more spectroscopic characterization to help determine if these complexes could be desolvated. Characterization of the $Cp'''_2Ln(THF)$ complexes by IR spectroscopy was conducted first, see Figure G.1.

Furthermore, desolvation of Cp‴$_2$Sm(THF) was attempted by placing the complex in a sublimation tube under vacuum at 10^{-3} Torr. The complex sublimes at ≈ 70 °C and retains the dark purple color characteristic of the solvated species. An IR of the sublimed product was obtained and is compared with that of Cp‴$_2$Sm(THF) below. Few, if any, differences are observable. In fact, two extra bands are visible at approximately 980 and 920 cm^{-1}. It is possible that under these conditions, the complex decomposes by cyclometallation of a trimethylsilyl group in the Cp‴ ligand or by some other mechanism.

Cp‴$_2$Sm(THF); IR υ, cm^{-1}: 3040w, 2949m, 2892w, 1428w, 1400w, 1341w, 1312w, 1242s, 1178w, 1139w, 1090m, 1077m, 1020w, 1002m, 937m, 922m, 817s, 745s, 680m

Cp‴$_2$Sm(THF) after sublimation; IR υ, cm^{-1}: 3684w, 3684w, 3044w, 2951m, 2895w, 1522w, 1432w, 1403w, 1344w, 1315w, 1245s, 1141w, 1115w, 1091m, 1078m, 1003w, 977w, 938w, 924w, 905w, 824s, 749s, 686s

Cp‴$_2$Yb(THF); IR υ, cm^{-1}: 3044w, 2950m, 2892w, 1424w, 1401w, 1342w, 1314w, 1240s, 1139w, 1087m, 1074m, 1023w, 1002m, 939w, 923w, 820s, 745s, 681s

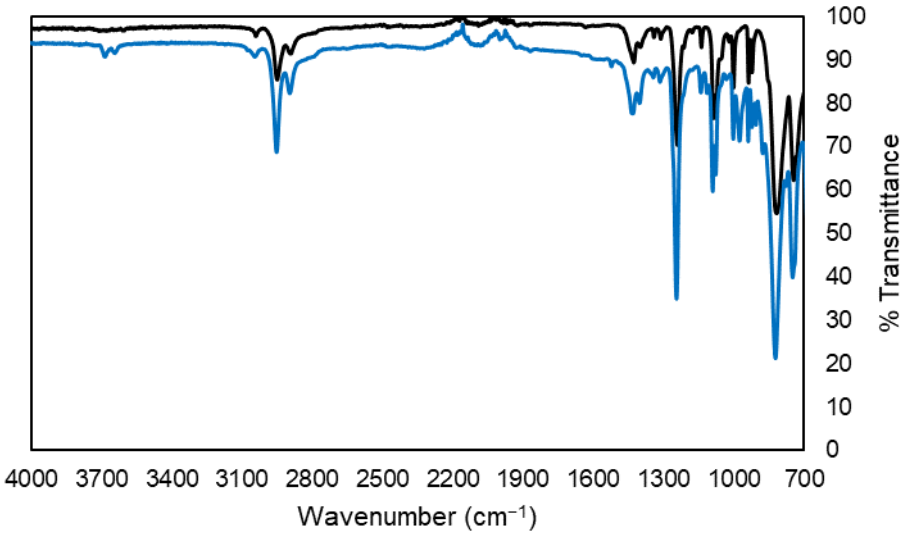

Figure G.1. IR spectral overlay of Cp‴$_2$Sm(THF) before (**black**) and after (blue) sublimation.

Given the difficulty of desolvating rare-earth metal metallocenes, the synthesis of these complexes with starting material free of coordinating solvent was pursued. Therefore, unsolvated NdI_3 was synthesized by modifying a procedure published by Prof. Gerd Meyer.[6]

NdI_3. In an argon-filled glovebox, freshly shaved Nd metal (5.0 g, 35 mmol) and freshly cleaned ammonium iodide (31.0 g, 214 mmol) were ground together with a mortar and pestle. The mixture was dispersed evenly along a heavy-walled sublimation tube (7 cm diameter, 30 cm length). The sublimation tube was closed via a 24/40 adapter, and the apparatus was removed from the glovebox. The apparatus was then placed in a horizontal tube furnace and attached with Tygon tubing to a three way joint with an argon inlet and a bubbler release. The line was purged with argon for 30 min. The tube was then opened to Ar and heated to 300 °C in increments of 50 °C per hour, and then left under dynamic Ar overnight at 280 °C. The apparatus was then evacuated while the temperature was maintained at 280 °C, and excess NH_4I was readily removed via sublimation. The resulting dark green powder was brought into the glovebox and examined by IR spectroscopy. No signal for an N–H stretching vibration was visible in the IR spectrum.

Cp‴$_2$NdI(THF). Solid KCp‴ (0.750 g, 2 mmol) was tapped into a vial of NdI_3 (0.604 g, 1 mmol) stirring in 15 mL of diethylether. The light green solution turned light blue after 1 hr stirring. The diethyl ether was removed under reduced pressure after 2 hr. The material was then dissolved in toluene and heated at reflux for 72 hr. The toluene was then removed under reduced pressure, hexanes were added, and the suspension was stirred overnight. Centrifugation reveals a greyish-white precipitate and a yellow-brown solution. The solution was decanted, and the hexanes were removed under vacuum to yield crude Cp‴$_2$NdI(THF) (0.654 g, 0.8 mmol, 68%). Slow evaporation of a concentrated hexanes solution yielded light blue crystals Cp‴$_2$NdI(THF) suitable for XRD studies. A concentrated hexanes solution left at −35 °C over two nights yielded crystals of an impurity: [Cp‴Cp″Nd(μ–Cl)]$_2$.

Crystal Analysis. The crystal structure of Cp‴$_2$NdI(THF) indicates that despite not using THF explicitly during the synthesis of this complex, it is coordinatively unsaturated enough that it will bind adventitious THF present in the glovebox atmosphere. It is suggested that future syntheses occur in a glovebox free of coordinating solvents.

The crystal structure of [Cp‴Cp″Nd(μ–Cl)]$_2$ indicates that a free ligand purity of ≈ 80% (by ^{1}H NMR spectroscopy) is insufficient to yield pure Nd-containing product sans the Cp″ ligand. This is consistent with prior studies using the Cp‴ ligand. Additionally, the presence of the bridging chloride

ligands suggests that aside from KCp″, another impurity likely derives from the trimethylsilyl chloride used in the synthesis of the HCp‴ intermediate. In this structure, it is interesting that the larger Cp‴ ligands are cis to one another rather than trans, given their greater steric requirement than Cp″. It was investigated whether dispersion forces could be playing a role in the formation of this isomer by determining the number of H…H contacts within 2.4 Å. It was found that there are a total of 2 such contacts, with the number rising to 6 if the limit is expanded to 2.7 Å.

Table G.1. Metrical comparison between the two [Cp‴Nd] species crystallized.

Bond	[Cp‴Cp″Nd(μ–Cl)]$_2$ (Å)	Cp‴$_2$NdI(THF) (Å)
Nd–Cp‴(cent)	2.455	2.481
	2.487	2.489
Nd–Cp″(cent)	2.487	-
	2.464	
Nd–I	3.144(11)	3.0647(6)
	3.145(6)	
	3.103(6)	
	3.136(11)	
Nd–Cl	2.797(2)	2.695(6)
	2.800(3)	
	2.795(3)	
	2.799(2)	
Nd–THF	-	2.4581(18)

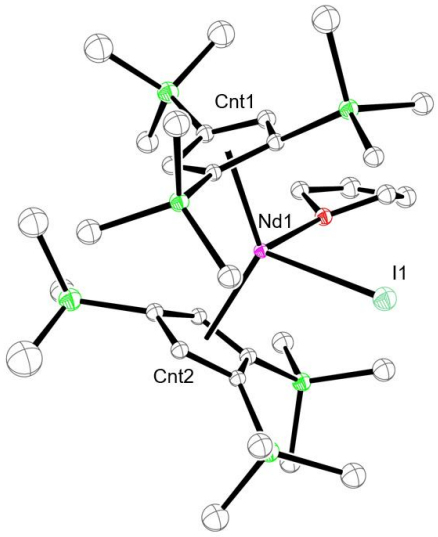

Figure G.2. ORTEP of Cp‴$_2$NdI(THF) with ellipsoids drawn at the 50% probability level and hydrogen atoms omitted for clarity.

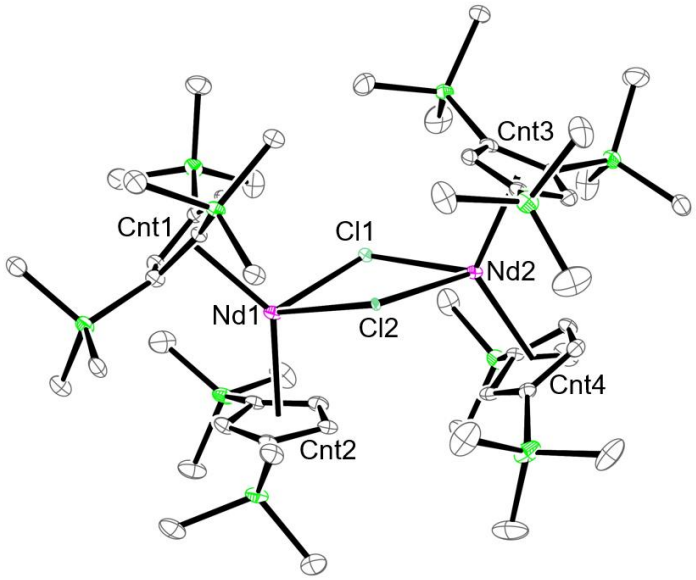

Figure G.3. ORTEP of $[Cp'''Cp''Nd(\mu–Cl)]_2$ with ellipsoids drawn at the 50% probability level and hydrogen atoms omitted for clarity.

Desolvation of $Cp'''_2Ln(THF)$ species via sublimation to generate unsolvated metallocenes has been unsuccessful so far. The use of an unsolvated lanthanide halide starting material does function to generate complexes with the Cp‴ ligand bound, namely $[Cp'''Cp''Nd(\mu–Cl)]_2$ and $Cp'''_2NdI(THF)$. However, the latter indicates that the Nd metal center (larger than Sm and Yb) is sterically unsaturated even with two Cp‴ ligands and an iodide bound. Thus, attempts to synthesize unsolvated Cp'''_2Ln species should occur in gloveboxes or Schlenk lines free of atmospheric coordinating solvents in the atmosphere. Furthermore, as has been shown in prior studies with the Cp‴, ligand purification is essential to obtain bulk purity based on the bridging chloride crystal structure incorporating Cp″ ligands.

X-ray Data Collection, Structure Solution and Refinement for $[Cp'''Cp''Nd(\mu–Cl)]_2$. A blue crystal of approximate dimensions 0.123 x 0.183 x 0.194 mm was mounted in a cryoloop and transferred to a Bruker SMART APEX II diffractometer system. The APEX2[6] program package was used to determine the unit-cell parameters and for data collection (90 sec/frame scan time). The raw frame data was processed using SAINT[7] and SADABS[8] to yield the reflection data file. Subsequent calculations were carried out using the SHELXTL[9] program package. The diffraction symmetry was 2/*m* and the systematic absences

were consistent with the monoclinic space group $P2_1/c$ that was later determined to be correct. The structure was solved by direct methods and refined on F^2 by full-matrix least-squares techniques. The analytical scattering factors[10] for neutral atoms were used throughout the analysis. Hydrogen atoms were included using a riding model. The chlorine and iodine atoms were disordered and were included using multiple components and partial site-occupancy-factors as 95:5 Cl1:I1 and 90:10 Cl2:I2. Least-squares analysis yielded wR2 = 0.1126 and Goof = 1.083 for 625 variables refined against 21021 data (0.70 Å), R1 = 0.0581 for those 14170 data with I > 2.0σ(I).

X-ray Data Collection, Structure Solution and Refinement for Cp‴$_2$NdI(THF). A green crystal of approximate dimensions 0.096 x 0.115 x 0.242 mm was mounted in a cryoloop and transferred to a Bruker SMART APEX II diffractometer system. The APEX2[7] program package was used to determine the unit-cell parameters and for data collection (30 sec/frame scan time). The raw frame data was processed using SAINT[8] and SADABS[9] to yield the reflection data file. Subsequent calculations were carried out using the SHELXTL[10] program package. The diffraction symmetry was 2/*m* and the systematic absences were consistent with the monoclinic space group $P2_1/c$ that was later determined to be correct. The structure was solved by direct methods and refined on F^2 by full-matrix least-squares techniques. The analytical scattering factors[11] for neutral atoms were used throughout the analysis. Hydrogen atoms were included using a riding model. Several atoms were disordered and included using multiple components and partial site-occupancy-factors, and geometric and displacement constraints (SADI, SIMU). The disorder for the iodine and chlorine atoms was modeled as 75:25 iodine:chlorine. Least-squares analysis yielded wR2 = 0.0732 and Goof = 1.032 for 475 variables refined against 12060 data (0.73 Å), R1 = 0.0319 for those 9626 data with I > 2.0σ(I).

References

(1) Gould, C. A.; McClain, K. R.; Yu, J. M.; Groshens, T. J.; Furche, F.; Harvey, B. G.; Long, J. R. Synthesis and Magnetism of Neutral, Linear Metallocene Complexes of Terbium(II) and Dysprosium(II). *J. Am. Chem. Soc.* **2019**, *141*, 12967–12973. DOI: 10.1021/jacs.9b05816.

(2) McClain, K. R.; Gould, C. A.; Marchiori, D. A.; Kwon, H.; Nguyen, T. T.; Rosenkoetter, K. E.; Kuzmina, D.; Tuna, F.; Britt, R. D.; Long, J. R.; Harvey, B. G. Divalent Lanthanide Metallocene Complexes with a Linear Coordination Geometry and Pronounced 6s-5d Orbital Mixing. *J. Am. Chem. Soc.* **2022**, *144*, 22193–22201. DOI: 10.1021/jacs.2c09880.

(3) Evans, W. J.; Kociok-Köhn, G.; Foster, S. E.; Ziller, J. W.; Doedens, R. J. Synthesis and Structure of Mono-THF Solvates of Bis(Cyclopentadienyl)Samarium(II) Complexes: $(C_5Me_5)_2Sm(THF)$ and $[C_5H_2(SiMe_3)_3][C_5H_3(SiMe_3)_2]Sm(THF)$. *J. Organomet. Chem.* **1993**, *444*, 61–66. DOI: 10.1016/0022-328X(93)83055-Z.

(4) Davis, Benjamin L. Ph.D. Dissertation, University of California–Irvine **2006**.

(5) Corner S. C.; Goodwin C. A. P.; Ortu F.; Evans P.; Zhang H.; Gransbury G. K.; Whitehead G. F. S.; Mills D. P. Synthesis of heteroleptic yttrium and dysprosium 1,2,4-tris(trimethylsilyl)cyclopentadienyl complexes. *Aust. J. of Chem.* **2022**, *75*, 684-697. DOI: 10.1071/CH21314.

(6) Meyer, G.; Morss, L. R.; Synthesis of Lanthanide and Actinide Compounds.

(7) APEX2 Version 2014.11-0, Bruker AXS, Inc.; Madison, WI 2014.

(8) SAINT Version 8.34a, Bruker AXS, Inc.; Madison, WI 2013.

(9) Sheldrick, G. M. SADABS, Version 2014/5, Bruker AXS, Inc.; Madison, WI 2014.

(10) Sheldrick, G. M. SHELXTL, Version 2014/7, Bruker AXS, Inc.; Madison, WI 2014.

(11) International Tables for Crystallography 1992, Vol. C., Dordrecht: Kluwer Academic Publishers.

Appendix H:

Crystallographic and Computational Details

Code	Formula	a	b	c	α	β	γ	Volume
wgm1	$Cp'_2Yb(THF)_2$	11.2	11.9	20.2	90.0	90.0	90.0	2699
wgm2	$[(THF)Cs(\mu–\eta^5:\eta^5–Cp')_3Tm]_n$	9.4	16.8	21.0	90.0	91.9	90.0	3347
wgm3	[(18c6)Cs][Cp′]	16.7	17.2	8.7	90.0	90.0	90.0	2500
wgm4	$[Cs(\mu–\eta^5:\eta^5–Cp')_3Yb]_n$	9.5	19.6	17.0	90.0	90.7	90.0	3179
wgm5	$[(THF)Na_2(18c6)_2][Cp'_3Y]_2$	11.8	27.1	27.9	90.0	99.3	90.0	8853
wgm7	$[Na(crypt)][Cp'_3Y]$	16.2	13.2	26.0	90.0	100.4	90.0	5485
wgm11*	$[Ba(crypt)Cp][Cp_2Yb(\mu–OSiMe_3)_2YbCp_2]$	15.6	21.6	15.8	90.0	97.9	90.0	5296
wgm13	$(C_5Me_5)_2Y(\mu–\eta^3:\eta^1–CCCCH_2)Y(C_5Me_5)_2$	16.0	14.7	17.2	90.0	100.7	90.0	3972
wgm15	$Cp^*_2Y–O–YCp^*_2$	11.5	11.5	14.2	90.0	90.0	90.0	1878
wgm16	$[Cp'''Cp''NdCl]_2$	22.0	25.9	12.3	90.0	102.8	90.0	6871
wgm17	$Cp'''_2NdI(THF)$	16.7	13.1	20.5	90.0	93.3	90.0	4471

* Structure is connectivity only.